U.PORTO

FEUP FACULDADE DE ENGENHARIA
UNIVERSIDADE DO PORTO

INTEGRATED MASTER IN ENVIRONMENTAL ENGINEERING
2017/2018

INTENSIFYING HETEROGENEOUS PHOTOCATALYSIS FOR BROMATES REDUCTION USING THE NETMIX PHOTOREACTOR

SARA GABRIELA DA SILVA E SANTOS

Dissertation submitted for the degree of
MASTER ON ENVIRONMENTAL ENGINEERING

Developed in

Associate Laboratory LSRE-LCM – Laboratory of Separation and Reaction Engineering - Laboratory of Catalysis and Materials, Faculty of Engineering of University of Porto

President of the jury: Manuel Fernando Ribeiro Pereira
Associated Professor in the Department of Chemical Engineering at Faculty of Engineering of University of Porto

---

Supervisor: Tânia Filomena Castro Valente Silva
Postdoctoral Researcher at the Associate Laboratory LSRE-LCM

Co-Supervisor: Vítor Jorge Pais Vilar
Principal Researcher at the Associate Laboratory LSRE-LCM

Co-Supervisor: Rui Alfredo da Rocha Boaventura
Principal Researcher at the Associate Laboratory LSRE-LCM

October 2018

ACKNOWLEDGMENTS

First of all, I would like to thank my supervisor, Dr. Tânia Silva, for the guidance and support provided throughout this dissertation. I am sincerely grateful for all the patience, counseling in the moments of greater anxiety and motivation to surpass the obstacles we faced during this work. I would also like to thank my co-supervisor, Dr. Vítor Vilar, for giving me the opportunity to perform this dissertation with his team, for all the support, for believing in my capabilities and always encouraging me to go a little further in my work. Not least, I would like to express my gratitude to my co-supervisor, Dr. Rui Boaventura, for his knowledge, support and all the valuable comments on this dissertation

My sincere gratitude also goes to my co-worker Larissa, for always being available and supportive and for her kind words and optimism in the most difficult times. An especial thank you also goes to my dear friend and co-worker Daniela, for her friendship, for accompanying me throughout these five years and always being supportive and motivational. I would also like to acknowledge all the team of the E404a laboratory from LSRE for all the support and stress-relieving moments during our breaks.

Last but not least, I would like to express my heartfelt gratitude to my beloved parents, my mother Joaquina and my father Ilídio, and to my dear sister Marta, who were always so supportive in my decisions and allowed me to pursue my dreams, and without whom this work would not have been possible.

This work is a result of project "AIProcMat@N2020 - Advanced Industrial Processes and Materials for a Sustainable Northern Region of Portugal 2020", with the reference NORTE-01-0145-FEDER-000006, supported by Norte Portugal Regional Operational Programme (NORTE 2020), under the Portugal 2020 Partnership Agreement, through the European Regional Development Fund (ERDF), and of Project POCI-01-0145-FEDER-006984 – Associate Laboratory LSRE-LCM funded by ERDF through COMPETE2020 - Programa Operacional Competitividade e Internacionalização (POCI) – and by national funds through FCT - Fundação para a Ciência e a Tecnologia.

ABSTRACT

Substances like bromate (BrO_3^-), an oxidized contaminant that can be found in post-ozonation waters, can have a noxious effect in human health even at low concentrations and are not easily eliminated. Therefore, advanced treatment processes for BrO_3^- removal from waters intended for human consumption are required.

The present dissertation focuses on BrO_3^- (200 µg L^{-1}) reduction by heterogeneous photocatalysis, using a mili-photoreactor, based on the NETmix technology, and UVA light-emitting diodes (LEDs). The photoreactor was assembled in two configurations, allowing the study of front-side (FSI) and back-side (BSI) irradiation mechanisms, by coating the catalyst nanoparticles on the channels and chambers of a back stainless steel slab (SSS) or on a front borosilicate slab (BS), respectively. The BrO_3^- reduction rate was assessed as a function of: i) catalyst type; ii) solution pH; iii) dissolved oxygen (DO) content; iv) addition of formic acid (CH_2O_2) as a sacrificial agent (SA); v) catalyst film thickness; vi) illumination mechanism (BSI and FSI); vii) irradiation intensity; viii) solution temperature; and ix) fresh water matrix.

Preliminary experiments showed that: i) at pH 3.0, bromate reduction was promoted by acid hydrolysis of the reactor acrylic structure; ii) Fe_2O_3 did not present photocatalytic reactivity, in opposition to TiO_2; and iii) a controlled environment is required to a proper results comparison.

Higher BrO_3^- reduction rates were obtained: i) using the FSI mechanism, associated with a 3-fold increase of catalyst surface area per reactor volume, when compared to BSI; and ii) at pH 5.5, since above the TiO_2-P25 pH of zero charge (~6.4) the BrO_3^- molecules are weakly adsorbed onto the negatively charged catalyst surface. Nitrogen injection (to eliminate DO) did not significantly improve the reaction rate since it was not possible to completely purge the oxygen from the system due to the many NETmix photoreactor inlet points. The addition of CH_2O_2 as SA had a negative effect on the BrO_3^- reduction at pH 6.5, either in the presence or absence of high amounts of DO, possibly, due to higher competition between CHO_2^- and BrO_3^- for the adsorption sites. Neither temperature nor an irradiance increase showed a considerable improvement on the reduction rate. Moreover, TiO_2 film remain stable for at least 13 consecutive reactions.

When compared with the synthetic water (SW) experiments, under the best conditions (SSS: pH=5.5, 15 mL of 2% wt. TiO_2 suspension, 25ºC, SA absence, [DO] = 232 – 263 µM), the fresh water (FW) matrix had a negative effect on the reaction rate. This can be associated with the presence of both inorganic and organic matter in FW at much higher concentrations than BrO_3^- leading to lower reaction rates since they can compete with BrO_3^- for the catalyst surface. Heterogeneous TiO_2 photocatalysis, using a NETmix photoreactor, was successfully applied to a chemically pre-treated FW, achieving a $[BrO_3^-] < 10$ µg L^{-1} (guideline value) after 2-hour.

Keywords: Heterogeneous photocatalysis; Bromate reduction; Titanium dioxide, NETmix photoreactor; Microscale illumination; Process intensification.

RESUMO

O pré-tratamento de águas destinadas ao consumo humano por processos de ozonização podem conduzir à formação do ião bromato (BrO_3^-), um contaminante de difícil eliminação e que, mesmo em baixas concentrações, pode ter um efeito nocivo para a saúde humana. Assim, processos avançados de tratamento são necessários para a sua degradação.

A presente dissertação foca-se na redução de BrO_3^- (200 µg L^{-1}) via fotocatálise heterogénea, usando um mili-fotoreator, baseado na tecnologia NETmix, e UVA-LEDs. O fotoreator foi montado segundo duas configurações, permitindo o estudo dos mecanismos de iluminação posterior (BSI) e frontal (FSI), através da deposição de catalisador na placa frontal de borossilicato (BS) ou nos canais e câmaras da placa posterior de aço inoxidável (SSS), respetivamente. A cinética de redução do BrO_3^- foi avaliada em função: i) do tipo de catalisador; ii) do pH da solução; iii) do teor de oxigénio dissolvido (DO); iv) da adição de ácido fórmico (CH_2O_2) como agente sacrificante; v) da espessura de filme de catalisador; vi) do mecanismo de iluminação; vii) da irradiância; viii) da temperatura; e ix) da matriz de uma água real (FW).

Os testes preliminares mostraram que: i) a pH 3,0, a redução de BrO_3^- foi promovida pela hidrólise ácida do acrílico do reator; ii) contrariamente ao TiO_2, o Fe_2O_3 não apresentou atividade fotocatalítica; e iii) é essencial um ambiente controlado para a devida comparação dos resultados.

Velocidades de redução maiores foram obtidas: i) usando o mecanismo de FSI, devido ao aumento da área da superfície do catalisador por volume de reator; e ii) a pH 5,5, uma vez que acima do pH do ponto de carga zero (6,4) do TiO_2 o BrO_3^- é fracamente adsorvido na superfície negativamente carregada do catalisador. A injeção de azoto (para eliminação do DO) praticamente não melhorou a velocidade de reação, pois não foi possível a purga completa do oxigénio devido ao elevado número de entradas que o reator possui. A adição de CH_2O_2 teve efeito negativo a pH 6,5, tanto na presença como na ausência de DO, possivelmente, devido à maior competição entre os iões CHO_2^- e BrO_3^- pelos locais de adsorção. Nem o aumento da temperatura nem da irradiância mostraram uma melhoria considerável na velocidade de redução. Além disso, o filme de TiO_2 permaneceu estável após, pelo menos, 13 reações consecutivas.

Quando comparados à água sintética, sob as melhores condições (SSS: pH 5,5, 15 mL de uma suspensão de TiO_2, a 2%, 25 ºC, sem CH_2O_2, [DO] = 232 – 263 µM), os testes com a FW conduziram a velocidades de reação mais baixas. Este comportamento pode ser associado à presença de matéria orgânica e inorgânica, em concentrações muito maiores que as do BrO_3^-, que vão competir pela superfície do catalisador. A fotocatálise heterogénea mediada pelo TiO_2, usando o fotoreator NETmix, foi aplicada sucesso a uma FW quimicamente pré-tratada, atingindo-se uma $[BrO_3^-] < 10$ µg L^{-1} (valor de referência) após 2 horas de reação.

Palavras-chave: Fotocatálise heterogénea; Redução de bromatos; Dióxido de titânio; NETmix fotoreator; Iluminação em microescala; Intensificação do processo.

DECLARATION

I hereby declare, on my word of honor, that this work is original and that all non-original contributions were properly referenced with source identification.

Sara Gabriela da Silva e Santos

Porto, ___ of ________________, 2018

INDEX

1 Introduction ... 1
  1.1 Background and motivation ... 1
  1.2 Objectives ... 2
  1.3 Structure of the thesis ... 3
2 Context and State of the art ... 5
  2.1 Bromate ... 5
  2.2 Advanced Oxidation/Reduction Processes ... 6
  2.3 Heterogeneous photocatalysis ... 7
    2.3.1 Photocatalysts ... 10
      2.3.1.1 Iron oxide ... 10
      2.3.1.2 Titanium dioxide ... 10
    2.3.2 Effect of operational parameters in heterogeneous photocatalysis ... 11
      2.3.2.1 Photocatalyst dose ... 13
      2.3.2.2 Initial contaminant concentration ... 14
      2.3.2.3 Illumination source and intensity ... 14
      2.3.2.4 Solution pH ... 14
      2.3.2.5 Temperature ... 15
      2.3.2.6 Dissolved oxygen ... 15
      2.3.2.7 Inorganic compounds ... 16
      2.3.2.8 Natural organic matter ... 16
  2.4 Photocatalytic Reactors ... 16
    2.4.1 Photoreactors limitations ... 16
      2.4.1.1 Photon transfer limitations ... 16
      2.4.1.2 Mass transfer limitations ... 17
    2.4.2 Micro and mili-photoreactors ... 18
3 Materials and Methods ... 21
  3.1 Chemicals and materials ... 21
    3.1.1 Fresh water sample from a Water Treatment Plant ... 23
  3.2 Photoreactor experimental setup ... 23
  3.3 Preparation of catalyst films ... 26

3.4 Photocatalytic experiments procedure 28
3.5 Analytical methods 29
3.6 kinetic models 30
4 Results and discussion 31
4.1 Preliminary results 31
4.1.1 Influence of pH using iron oxide (Fe_2O_3) as photocatalyst 31
4.1.2 Influence of dissolved oxygen content and addition of a sacrificial agent using TiO_2-P25 as photocatalyst 34
4.2 Borosilicate glass slab experiments 37
4.2.1 Influence of pH, dissolved oxygen content, sacrificial agent addition and catalyst film reusability 37
4.2.2 Influence of catalyst film thickness 42
4.3 Stainless steel slab experiments 44
4.3.1 Influence of solution pH and dissolved oxygen content 44
4.3.2 Influence of the catalyst film thickness and illumination intensity 48
4.3.3 Influence of temperature 51
4.3.4 Influence of a fresh water matrix 52
5 Conclusions 55
6 Limitations and future work 57
7 References 59

LIST OF FIGURES

Figure 1. 1 – BrO_3^- formation mechanisms in ozonation processes of water containing Br^- ions. Adapted from [9, 10]. 2

Figure 2. 1 – Number of documents published with the term “Photocatalysis” and “Heterogeneous photocatalysis” in the period of 2008 – 2017. Data retrieved from Scopus (http://www.scopus.com/) in September 2018. 8

Figure 2. 2 – Schematic illustration of the basic mechanism of a heterogeneous photocatalytic process on the catalyst surface. 9

Figure 2. 3 – NETmix photoreactor: a) network of channels and chambers; b) detailed chamber and respective channels. 19

Figure 3. 1 – Schematic representation of the experimental installation setup. 25

Figure 3. 2 – Photograph of the experimental apparatus. 25

Figure 3. 3 – Spray deposition system. 27

Figure 3. 4 – Photograph of the (a) BS and (b) SSS: (.1) before and (.2) after the TiO_2-P25 aqueous suspension deposition. 27

Figure 4. 1 – Influence of pH on BrO_3^- reduction mediated by Fe_2O_3 photocatalyst coated onto the BS. Open symbols: 20 mg Fe_2O_2, no light. Solid symbols: 20 mg Fe_2O_2, UVA-LEDs. No symbol (dashed line): no catalyst, no light. pH 3 (□, ■, - - -), solution pH (○, ●). Experimental conditions: $[BrO_3^-]_0$ = 1.56 μM, Q = 75 L h^{-1}, T = 25 °C, [DO]: 232-263 μM. 33

Figure 4. 2 – Influence of DO content and addition of CH_2O_2 as a SA on the BrO_3^- reduction by TiO_2-P25 photocatalyst deposited on the BS. Solid symbols: (e) first reactions. Open symbols: (f) second reactions. (a) With DO, without CH_2O_2 (■, □); (b) without DO, without CH_2O_2 (●, ○); (c) with DO, with CH_2O_2 (▲, △); (d) without DO, with CH_2O_2 (◆, ◇). Experimental conditions: $[BrO_3^-]$ = 1.56 μM, pH 5.5, Q = 75 L h^{-1}, T = 25 ºC, UVA-LEDs 270 mW, 20 mg of TiO_2-P25. 35

Figure 4. 3 – (a) Influence of pH, DO content and CH_2O_2 addition on the BrO_3^- reduction by TiO_2-P25 photocatalyst deposited on the BS. (b), (c) Replicates: 1st (———), 2nd (- - - - -), 3rd (· · · · ·), 4th (· · – · ·). Solid symbols: pH 6.5. Open symbols: pH 5.5. With DO, without CH_2O_2 (■, □); without DO, without CH_2O_2 (●); with DO, with CH_2O_2 (▲); without DO, with CH_2O_2 (◆). Experimental conditions: $[BrO_3^-]$ = 1.56 μM, Q = 75 L h^{-1}, T = 25 ºC, UVA-LEDs 270 mW, 20 mg of TiO_2-P25. 37

Figure 4. 4 – Influence of catalyst film thickness on the BrO_3^- reduction by TiO_2-P25 photocatalyst deposited on the BS. Mass of catalyst: 10 mg (■); 20 mg (●); 40 mg (▲). Experimental conditions: $[BrO_3^-]$ = 1.56 μM, pH 5.5, Q = 75 L h^{-1}, T = 25 ºC, [DO]: 232-263 μM, UVA-LEDs 270 mW. 43

Figure 4. 5 – Influence of pH and DO content on the BrO_3^- reduction by TiO_2-P25 photocatalyst deposited on the SSS. Reactor: NETmix photoreactor (———); Batch photoreactor (- - - - -). Solid symbols: [DO]: 232-263 μM (without N_2 injection). Open symbols: [DO] < 3.1 μM (with N_2 injection). Solution pH: 5.5 (■, □), 6.5 (●), 7.5 (▲). Experimental conditions: [BrO_3^-] = 1.56 μM, Q = 75 L h^{-1}, T = 25 ºC, UVA-LEDs 270 mW, 15 mL of a 2% wt. TiO_2-P25 aqueous suspension. 45

Figure 4. 6 – Influence of the catalyst film thickness and illumination intensity on the BrO_3^- reduction by TiO_2-P25 photocatalyst deposited on the SSS and comparison with the BS (★) best result (40 mg of TiO_2, pH 5.5, [BrO_3^-] = 1.56 μM, Q = 75 L h^{-1}, T = 25 ºC, [DO]: 232-263 μM, without CH_2O_2). Solid symbols: with catalyst, UVA-LEDs 270 mW. Open symbols: with catalyst, UVA-LEDs 1400 mW. Crossed symbols: no light. TiO_2-P25 deposited on the SSS: 0 mL (◆, ◈), 10 mL (●), 15 mL (■, □, ☒), 20 mL (▲, △). Experimental conditions: [BrO_3^-] = 1.56 μM, pH 5.5, Q = 75 L h^{-1}, T = 25 ºC, [DO]: 232-263 μM. 49

Figure 4. 7 – Influence of temperature on the BrO_3^- reduction by TiO_2-P25 photocatalyst deposited on the SSS. Temperature: 15 ºC (■); 20 ºC (●); 25 ºC (▲); 30 ºC (◆). Experimental conditions: [BrO_3^-] = 1.56 μM, pH 5.5, Q = 75 L h^{-1}, UVA-LEDs 270 mW, [DO]: 232-263 μM, 15 mL of a 2% wt. TiO_2-P25 aqueous suspension. 51

Figure 4. 8 – Influence of the fresh water matrix on the BrO_3^- reduction by TiO_2-P25 photocatalyst deposited on the SSS. Solid symbols: synthetic water. Open symbols: chemically treated fresh water. pH: 5.5 (■, □); 6.5 (●, ○); 7.5 (▲, △). Experimental conditions: [BrO_3^-] = 1.56 μM, Q = 75 L h^{-1}, T = 25 ºC, UVA-LEDs 270 mW, [DO]: 232-263 μM, 15 mL of a 2% wt. TiO_2-P25 aqueous suspension. 52

LIST OF TABLES

Table 2. 1 – Summary of BrO_3^- photocatalytic reduction studies. 12

Table 3. 1 – Sodium bromate physicochemical properties. 21

Table 3. 2 – Physicochemical properties of the chemicals used in this work. 22

Table 3. 3 – Physicochemical characterization of the FW from a WTP. 23

Table 3. 4 – Summary of the NETmix photoreactor design dimensions. 24

Table 3. 5 – Analytical methods. 29

Table 4. 1 – Operational conditions and pseudo-first-order kinetic constants for bromate reduction (*k*), calculated for the preliminary tests performed, along with the corresponding coefficient of determination (R^2) and residual variance (S^2_R). 32

Table 4. 2 – Operational conditions and pseudo-first-order kinetic constants for bromate reduction (*k*), calculated for the borosilicate glass slab experiments, along with the corresponding coefficient of determination (R^2) and residual variance (S^2_R). 39

Table 4. 3 – Operational conditions and pseudo-first-order kinetic constants for bromate reduction (*k*), calculated for the stainless steel slab experiments performed, along with the corresponding coefficient of determination (R^2) and residual variance (S^2_R). 46

NOTATION

A_{BS}	Borosilicate glass slab area	cm^2
e^-	Electron of the conduction band	
E_{bg}	Bandgap energy	eV
E^o	Standard electrode potential	V
h^+	Hole of the valence band	
I	Irradiated power	$W\ m^{-2}$
k	Pseudo-first-order kinetic constant	min^{-1}
$m_{deposited}$	Mass of catalyst deposited	mg
Q	Flow rate	$L\ h^{-1}$
R^2	Coefficient of determination	
Re	Reynolds number	
S^2_R	Residual variance	
t	Time	min
T	Temperature	ºC/K
$V_{deposited}$	Volume of catalyst deposited	mL
V_i	Initial volume of the BrO_3^- solution	mL

Greek Letters

ε	Emissivity	
σ	Stefan-Boltzmann constant	$W\ m^{-2}\ K^{-4}$
λ	Wavelength	nm

List of Acronyms

AOP	Advanced oxidation process
ARP	Advanced reduction process
BS	Borosilicate glass slab
BSI	Back side irradiation
CB	Conduction band
COS	Carbon oxidation state
DIC	Dissolved inorganic carbon
DO	Dissolved oxygen
DOC	Dissolved organic carbon
FA	Fulvic acid
FAO	Food and Agriculture Organization
FSI	Front side irradiation
FW	Fresh water
HA	Humic acid
IARC	International Agency for Research on Cancer
IC	Ion chromatography
LED	Light emitting diode
MW	Molecular weight
NHE	Normal hydrogen electrode
NOM	Natural organic matter
PMMA	Polymethyl methacrylate
PTFE	Polytetrafluoroethylene
PW	Pure water
PZC	Point of zero charge
ROS	Reactive oxidizing species
SA	Sacrificial agent
SHE	Standard hydrogen electrode

SM	Static mixer
SSS	Stainless steel slab
SW	Synthetic water
TDC	Total dissolved carbon
TDI	Total dissolved iron
TSS	Total suspended solids
UPW	Ultrapure water
UV	Ultraviolet
VB	Valence band
VSS	Volatile suspended solids
WHO	World Health Organization
WTP	Water treatment plant

Chemical names

${}^{\bullet}CO_2^-$	Carboxylate radical anion
Br^-	Bromide
$Br^{\bullet}$	Bromine radical
BrO_3^-	Bromate
CdS	Cadmium sulphide
CH_2O_2	Formic acid
Cl^-	Chloride Ion
CO_2	Carbon dioxide
CO_3^{2-}	Carbonate ion
Cr (VI)	Hexavalent chromium
Cu^{2+}	Cupric ion
Fe^{2+}	Ferrous ion
Fe_2O_3	Iron oxide
α–Fe_2O_3	Hematite
γ–Fe_2O_3	Maghemite
Fe_3O_4	Magnetite
FeO	Wüstite
H^+	Hydrogen ion
$H^{\bullet}$	Hydrogen atom radical
H_2O	Water
H_2O_2	Hydrogen peroxide
HCO_3^-	Bicarbonate ion
HO^-	Hydroxide ion
$HO^{\bullet}$	Hydroxyl radical
$HOO^{\bullet}$	Hydroperoxyl radical
$KBrO_3$	Potassium bromate
N_2	Nitrogen
$NaBrO_3$	Sodium bromate
O_2	Oxygen
$O_2^{\bullet-}$	Superoxide radical
O_3	Ozone
PO_4^{3-}	Phosphate ion
$R^{\bullet}$	Highly reducing specie
SnO_2	Tin (IV) oxide
$SO_3^{\bullet-}$	Sulfite anion radical
SO_4^{2-}	Sulfate ion
TiO_2	Titanium oxide
WO_3	Tungsten trioxide
ZnO	Zinc oxide

1 INTRODUCTION

1.1 BACKGROUND AND MOTIVATION

One of the most important natural resources for the survival of the ecosystems in our planet is water. It plays a crucial role in our social and economic activities and therefore it’s a matter of great concern for the policymakers on a global scale. In 2015, at the United Nations summit, the world leaders adopted the 2030 Sustainable Development Agenda, which defined a series of goals and targets for all the countries in order to protect humanity and the planet, through a balance between the social, economic and environmental dimensions. Out of all the 17 goals, the goal 6 is specifically related with the access to water and sanitation for everyone, which presupposes, among others, the access to safe drinking water and an improvement of its quality by, for example, reducing the pollution in water resources [1].

Climate change and its consequences on the water-cycle along with the accelerated urbanization and population growth worldwide (allied to an increase in water consumption) have drawn attention for the problematic of water scarcity. However, this problem is aggravated when the available water resources end up being contaminated by untreated wastewaters, through leaching from contaminated soils, runoff from agriculture or by industrial discharges. This problematic requires a more efficient management of the resource, in order to reach a balance between the demand and the water availability [2].

The presence of the so-called “emerging pollutants”, which have increased and diversified through the years due to the development of new chemicals and materials for industries combined with the constant innovations in most of the sectors, like the pharmaceutical and medical sectors for example, have caused the appearance of new compounds that cannot be naturally removed in the ecosystems or treated by conventional treatment processes [3]. Therefore, it has been mandatory to develop new techniques and invest in the advancement of existing technologies targeting cost-efficient water treatments [4]. Also, policies related to water for human consumption are becoming increasingly restrictive regarding the presence of certain substances in water. Thus, the addition of an advanced technology after the conventional treatment step can be an effective way to remove those contaminants [5].

In the past few years, the advanced oxidation/reduction processes (AOPs/ARPs) as efficient methods to remove contaminants from water, have gained a lot of interest from the scientific community. The production of highly reactive species, like strong chemical oxidants or electron-rich free radicals, allows to efficiently remove toxic compounds from water [6, 7]. Substances like bromate, an oxidized contaminant (Figure 1.1) that can be found in post-ozonation waters, can have a noxious effect in human health at low concentrations and are not easily eliminated [8].

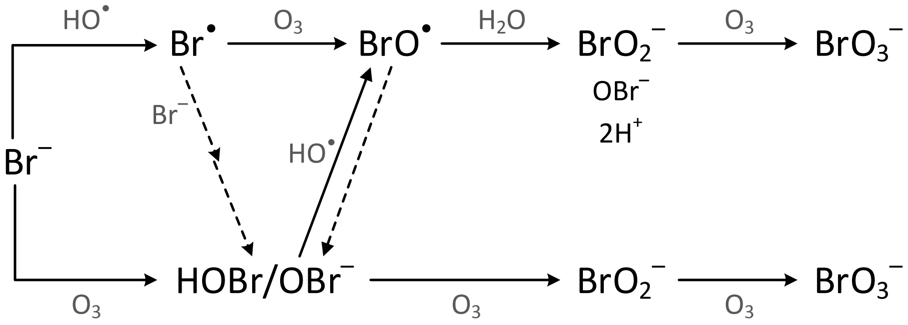

Figure 1. 1 – BrO_3^- formation mechanisms in ozonation processes of water containing Br^- ions. Adapted from [9, 10].

Therefore, the application of UV-driven heterogeneous ARPs to remove them from water seems to be a promising option but still requires further studies in order to overcome the mass and photon transfer limitations inherent to this kind of processes.

1.2 OBJECTIVES

The present dissertation focuses on the intensification of heterogeneous photocatalytic process for bromate (BrO_3^-) removal from aqueous solutions, using a mili-photoreactor, based on the NETmix technology, and microscale illumination. The photoreactor consists of a network of cylindrical chambers interconnected through a series of rectangular channels that allows a high degree of mixing under laminar regime. The combination of a mili-photoreactor with a microscale illumination system, such as ultraviolet light emitting diodes (LEDs), allows to simultaneously overcome photon and mass transfer limitations. Two photoreactor configurations were assessed: i) an acrylic structure containing a stainless steel slab (SSS) imprinted with a network of channels and chambers where the catalyst was deposited and then covered with a borosilicate slab (BS) without catalyst, corresponding to a front-side illumination (FSI) mechanism; and ii) an acrylic base imprinted with the network of channels and chambers (with no catalyst) and covered with a BS coated with a determined mass of catalyst, corresponding to a back-side illumination (BSI) mechanism. The bottom and upper slabs of both photoreactors were sealed together by mechanical compression and O-rings.

The main purpose of this study was to evaluate the BrO_3^- photocatalytic reduction under different operational conditions, using a synthetic aqueous solution containing 200 $\mu g\ L^{-1}$ of BrO_3^- in ultrapure water. In the best conditions, a chemically treated fresh water spiked with the same amount of BrO_3^- was also used. The efficiency of the photocatalytic reduction reactions was assessed by measuring the BrO_3^- and bromide (Br^-) concentrations during the reaction through ion chromatography. The influence of the following operational variables on BrO_3^- photocatalytic reduction was evaluated: i) catalyst type (Fe_2O_3 and TiO_2); ii) solution pH (5.5, 6.5 and 7.5); iii) presence/absence of dissolved oxygen; iv) addition of formic acid as a sacrificial agent ($[BrO_3^-]:[CH_2O_2]$ molar ratio of 1:3); v) catalyst film thickness (10, 20 or 40 mg of catalyst on the BS and 10, 15 and 20 mL of a 2% wt. catalyst suspension on the SSS); vi) illumination mechanism (BSI and FSI); vii) irradiation intensity (270 and 1400 mW); viii) solution temperature (15 ºC, 20 ºC, 25 ºC and 30 ºC). The influence of a fresh water matrix on $BrO_3^–$ reduction and the reusability of the photocatalytic films were also appraised.

1.3 STRUCTURE OF THE THESIS

This work is structured in six main chapters: Introduction, State of the Art, Materials and Methods, Results and Discussion, Conclusions and Limitations and Future Work.

The first chapter provides a brief introduction to the problematic of water contamination and to the reasons that motivated us to pursue this work. It also presents the objectives and the structure of the dissertation.

The second chapter introduces the contaminant under study and gives a description of the most relevant aspects about the advanced reduction processes, especially the photocatalytic removal of oxyanions in water, with emphasis on the $BrO_3^–$ reduction. The catalyst support medium and the photoreactor are also approached in this chapter.

The third chapter presents a description of all the chemicals used in the experimental work, describes the preparation of the support media and the catalyst deposition technique, and presents the experimental installation and procedures. The analytical determinations and the kinetic models used are also included in this section.

The fourth chapter presents and discusses the main results obtained in the experimental work, as well as the preliminary tests performed. The influence of the catalyst type, solution pH, dissolved oxygen content, addition of a sacrificial agent, catalyst film thickness, illumination mechanism, irradiation intensity, solution temperature, water matrix and catalyst reusability on $BrO_3^–$ reduction are discussed in this chapter.

The fifth and sixth chapters summarize all the conclusions obtained throughout this study and the limitations encountered and perspectives for future work, respectively.

2 CONTEXT AND STATE OF THE ART

2.1 BROMATE

Bromate ion (BrO_3^-) is an oxyanion that has a central bromine atom bonded to three oxygens and can also be found in the form of salt, like potassium bromate ($KBrO_3$) or sodium bromate ($NaBrO_3$). They are commonly found in the dyeing of textiles due to its oxidizing power [11]. $KBrO_3$ was used in the past in flour maturation processes and as a food additive but the Joint Food and Agriculture Organization (FAO)/World Health Organization (WHO) Expert Committee on Food Additives considered that the use of $KBrO_3$ in food processing was not acceptable and that bromate, in general, should not be present in food [12]. Both compounds are easily dissolved in water ($KBrO_3$ solubility: 7.55 g/100 mL at 25 ºC, $NaBrO_3$ solubility: 28.28 g/100 mL at 25ºC [13]), which facilitates the contamination of water bodies. Once in solution BrO_3^- is very stable, does not volatilize and practically does not adsorb to the soil or sediments, thus it is not easily removed from water [12].

During the drinking water treatment, the pre-oxidation of waters containing bromide (Br^-) ions by ozonation, chlorination or hypochlorination processes, can result in the formation of disinfection by-products like BrO_3^- (Figure 1.1) [8]. The formation of these by-products depends on the Br^- concentration, water pH, organic matter content, oxidant dosage, among other factors [8, 14]. Although Br^- may be naturally present in the majority of water bodies within a range of 15-200 µg L^{-1} (especially in areas with salt intrusions, sedimentary rock dissolution, effluent discharge or road runoff), BrO_3^- is not usually found in surface or groundwater used for drinking water production. However, when pre-oxidation processes are used, BrO_3^- concentrations can range from of 0.4-60 µg L^{-1} [8].

According to the International Agency for Research on Cancer (IARC), a department of the World Health Organization (WHO), the exposure to BrO_3^- is possibly carcinogenic to humans (group 2B) [15], which led to the establishment of a guideline value of 10 µg BrO_3^- L^{-1} in water for human consumption, both in the United States (US) [16] and the European Union (EU) [17] corresponding to an upper-bound excess lifetime cancer risk of 1 in 10 000 [12, 18]. This parametric value, defined for the Member States of the European Community through the Council Directive 98/83/EC, was transposed into Portuguese national law by the law decree no. 243/2001, subsequently amended by the law decree no. 306/2007 and, most recently, by the law decree no. 152/2017.

In order to comply with those requirements, it is mandatory to reduce the BrO_3^- concentration in the water. This can be achieved in three different ways [14]:

(i) Decreasing the Br^- concentration in the water by removing the Br^- ions prior to the pre-oxidation stage in the water treatment process;

(ii) Reducing the amount of BrO_3^- produced during the pre-oxidation stage;

(iii) Removing BrO_3^- from post-ozonation water.

The first method consists in reducing the Br^- concentration in water, not allowing it to be oxidized to BrO_3^-, and can be performed through membrane techniques, electrochemical processes or adsorption [10]. Another alternative is to prevent the BrO_3^- formation during the water treatment, which usually involves scavenging or decreasing the concentration of some intermediate products like $HOBr/BrO^-$, by ammonia or hydrogen peroxide addition, reducing the exposure of bromine radicals ($Br^\bullet$) to ozone (O_3) [9, 10], or lowering the concentration of hydroxyl radical ($HO^\bullet$) trough pH dropping [19]. These techniques aim to minimize the concentration of BrO_3^- formed during the pre-oxidation process, however, they present several limitations since they use high disinfectant dosages and have very high costs. In order to overcome those limitations, there is a third method that aims to remove BrO_3^- ions from post-oxidation waters using advanced technologies such as photolysis, catalysis and photocatalysis, that will allow the reduction of BrO_3^- to Br^- ions. These technologies are widely used as they let the conversion of oxyanions into harmless by-products [20].

2.2 ADVANCED OXIDATION/REDUCTION PROCESSES

The Advanced Oxidation Processes (AOPs) are a treatment methodology, frequently applied to water decontamination, which is defined by the *in-situ* generation of highly reactive oxidizing species (ROS), more specifically hydroxyl radicals ($HO^\bullet$). With a very strong oxidizing power, these species are able to react with most organic molecules, even recalcitrant compounds, either completely mineralizing them or transforming them into less complex and preferably harmless by-products [21, 22]. This radical is one of the strongest oxidizing agent, with a standard redox potential of $E^o(HO^\bullet/H_2O) = +(2.73 \pm 0.02)$ V *vs* NHE [23], and usually attack organic compounds with reaction rate constants in the order of 10^9 M^{-1} s^{-1} [24].

AOPs can be used to remove organic contaminants from water by complete mineralization, generating CO_2, H_2O and inorganic acids, or to improve the contaminant degradability if possible, thereby enabling the implementation of a post-treatment when the complete mineralization is not achieved [5]. These processes include the use of ultraviolet (UV) radiation, ozone, hydrogen peroxide (H_2O_2), catalysts such as titanium dioxide (TiO_2), ultrasounds (sonolysis), among others. Some examples of those systems are: UV/H_2O_2, UV/O_3, $UV/H_2O_2/O_3$, O_3/H_2O_2, Fe^{2+}/H_2O_2 (Fenton reaction), $UV/Fe^{2+}/H_2O_2$ (Photo-Fenton), UV/TiO_2, $UV/H_2O_2/TiO_2$ [25, 26].

When the contaminants are already in an oxidized form, a new type of treatment called Advanced Reduction Processes (ARPs) arises.

The ARPs are very similar to the AOPs mentioned before, however, instead of using oxidizing radicals they combine reagents and activation methods in order to produce highly reactive reducing radicals. Contrary to the more conventional techniques like reverse osmosis, ion exchange, ultra/nanofiltration, that only concentrate or transfer the contaminant to another phase, the ARPs allow the elimination of the pollutants or their transformation into harmless compounds, minimizing the waste production [27].

Both ARPs and AOPs can be divided into homogeneous or heterogeneous processes. The homogeneous processes occur in a single phase and are dependent on chemical interactions between the reagents and the target substances. The processes that showed a greater potential are the UV/Sulfite systems due to the simultaneous formation of reactive reducing species, such as electrons (e^-), hydrogen atom radicals ($H^\bullet$) and sulfite anion radicals ($SO_3^{\bullet -}$) [28]. Some authors have studied the removal of BrO_3^- ions through this process and concluded, depending on the experimental conditions, that there are two main mechanisms present in BrO_3^- removal: i) direct photolysis and ii) reaction with the reducing radicals [20, 29, 30].

On the other hand, the heterogeneous processes occur in the presence of a catalyst (slurry or immobilized in an inert support) through the adsorption of the reactant molecules on the active sites at its surface and desorption of the products after the chemical reaction occurred, leaving the active sites available for the adsorption of new reactant molecules [31]. The use of a catalyst in suspension improves mass transfer due to a higher surface area in contact with the bulk solution but creates the necessity of an additional step to remove the catalyst from solution, which is expensive and time consuming [32]. Therefore, a supported catalyst is preferred. Since this study is going to be focused in heterogeneous processes, they will be explored more extensively in this chapter.

2.3 HETEROGENEOUS PHOTOCATALYSIS

Photocatalysis and the phenomena associated with it are a well-known process that have been widely studied in the past decade (Figure 2.1), due to its effective approach to destroy toxic substances.

Heterogeneous photocatalysis is a photoinduced reaction accelerated by the presence of a catalyst. Once the catalyst is activated by incident light, the photocatalytic process can be summed up to the following steps [33-35]:

1. Transport of the reactants from the liquid medium (bulk) to the catalyst surface;
2. Adsorption of the reactants at the catalyst surface;
3. Photocatalytic reaction in the catalyst surface;
4. Desorption of the reaction products;
5. Transport of the reaction products from the catalyst surface to the bulk.

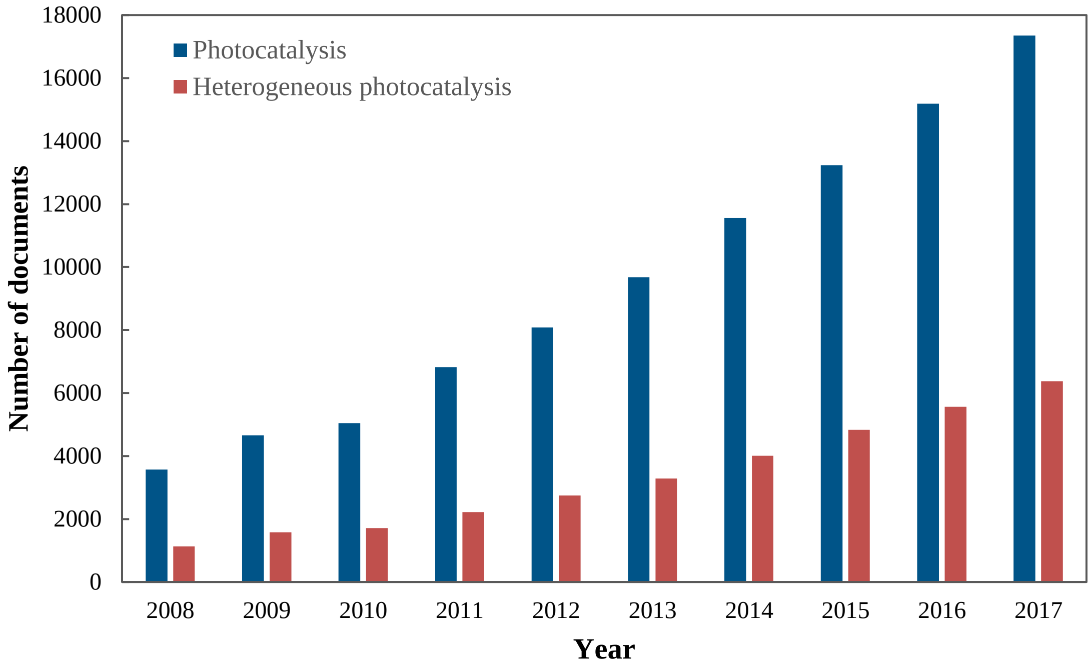

Figure 2. 1 – Number of documents published with the term “Photocatalysis” and “Heterogeneous photocatalysis” in the period of 2008 – 2017. Data retrieved from Scopus (http://www.scopus.com/) in September 2018.

In heterogeneous photocatalysis, the catalyst is a semiconductor material (e.g. Titanium dioxide – TiO_2, Cadmium sulphide – CdS, Zinc oxide – ZnO, Iron (III) oxide – Fe_2O_3, Tin (IV) oxide – SnO_2, Tungsten trioxide – WO_3 [36, 37]), which is activated by absorption of a photon ($h\upsilon$) with an energy equal or higher than the semiconductor’s band-gap energy (E_{bg}), inducing the transference of a negative electron (e^-) with reducing capacity from the valence band (VB) to the conduction band (CB) of the catalyst, thus generating a positive hole (h^+) in the valence band with oxidative properties. Thermodynamically, when an electron acceptor A has a redox potential more positive than that of the e_{CB}^-, it can be photocatalytic reduced in the CB. On the other hand, the electron donors D can react with the h_{VB}^+ in the VB when its redox potential in more negative than the potential of the h_{VB}^+ [38]. The photocatalytic process can be represented as follows [36, 39]:

$$A_{ads}+D_{ads} \xrightarrow[h\upsilon > E_{bg}]{\text{semiconductor}} A^{-}+D^{+} \tag{1}$$

where A_{ads} and D_{ads} represent the electron acceptors and donors, respectively, adsorbed on the catalyst surface. Figure 2.2 outlines the photocatalytic process mentioned above.

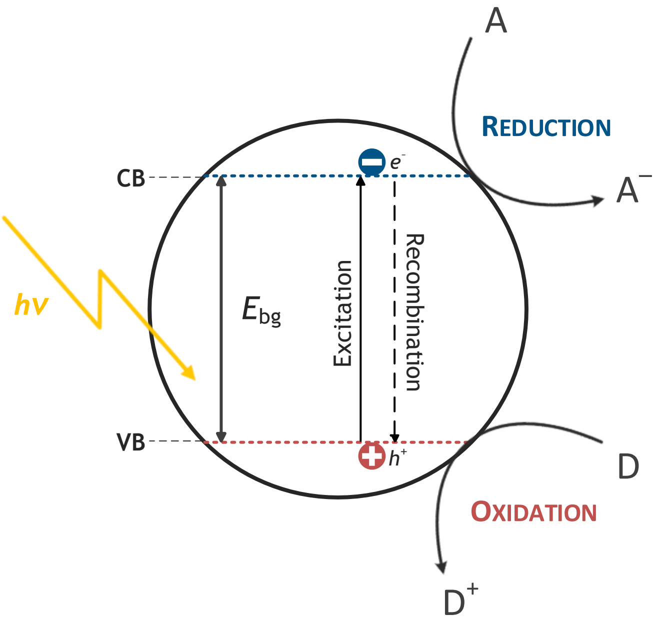

Figure 2. 2 – Schematic illustration of the basic mechanism of a heterogeneous photocatalytic process on the catalyst surface.

Inorganic species can be removed by photocatalytic processes through three main mechanisms [38]: i) direct reduction of the target compounds by the photogenerated e_{CB}^-; ii) indirect reduction of the substances by intermediate species generated via h_{VB}^+ or $HO^\bullet$ oxidation of electron donors; and iii) oxidative removal by h_{VB}^+ or $HO^\bullet$.

For example, BrO_3^- molecules reduction into Br^- occurs through the reaction with the photogenerated e_{CB}^- ($E^o = +1.423$ V *vs* SHE), according to Eq. (2) [40]:

$$BrO_3^- + 6H^+ + 6e^- \rightarrow Br^- + 3H_2O \tag{2}$$

On the other hand, the photogenerated h_{VB}^+ (Eq. (3)) can react with water (that dissociates in H^+ and HO^-) and produce the highly oxidizing $HO^\bullet$, as represented in Eqs. (3) – (5). Both h_{VB}^+ and $HO^\bullet$ are able to re-oxidize the reduced species to its original form, conducting to a short-circuiting of the entire process [38].

$$\text{semiconductor} + hv \rightarrow e_{CB}^- + h_{VB}^+ \tag{3}$$

$$H_2O \rightarrow H^+ + HO^- \tag{4}$$

$$HO^- + h_{VB}^+ \rightarrow HO^\bullet \tag{5}$$

Furthermore, the electron/hole pairs (e_{CB}^-/h_{VB}^+) formed can, eventually, recombine and inhibit the photocatalytic reaction to occur, being necessary to prevent the recombination of the charge carriers [22, 41].

Another concern, is the presence of oxygen, since the photogenerated electrons can react with the O_2 molecules and reduce them to the superoxide radical ($O_2^{\bullet-}$), which can further be protonated to form $HOO^\bullet$ and at the end produce H_2O_2 (Eq. (6) – (8)) [38, 42]. Therefore, those electrons are no longer available to reduce the desired contaminant.

$$(O_2)_{ads} + e_{CB}^- \rightarrow O_2^{\bullet -} \tag{6}$$

$$O_2^{\bullet -} + H^+ \rightarrow HOO^\bullet \tag{7}$$

$$2HOO^\bullet \rightarrow (H_2O_2)_{ads} + O_2 \tag{8}$$

Sacrificial agents (SA) are organic or inorganic substances that can be used in photocatalysis as an electron donor or acceptor. When the goal is to degrade a pollutant trough photocatalytic reduction reactions, adding a sacrificial electron donor agent, such as: i) alcohols; ii) carboxylic acids; iii) aldehydes; or iv) organic matter, to scavenge the h^+ or other oxidizing species (e.g. $HO^\bullet$), might improve significantly the reaction efficiency [38]. The following reaction (Eq. (9)) illustrates the oxidation of a SA (e.g. carboxylic acid – RH) by the holes in VB, which might generate a highly reducing specie ($R^\bullet$) that can further be used to reduce the target pollutants [38].

$$RH + h_{VB}^+ \rightarrow R^\bullet + H^+/H_2O \tag{9}$$

Therefore, the use of a SA can avoid, at the same time, the recombination of e_{CB}^-/h_{VB}^+ pairs, the re-oxidation of the pollutants that we are trying to remove through photocatalytic reduction reactions and generate highly reducing species.

2.3.1 Photocatalysts

2.3.1.1 Iron oxide

Iron oxide is a metal oxide that has different crystalline structures, such as hematite (α–Fe_2O_3), maghemite (γ–Fe_2O_3), wüstite (FeO) and magnetite (Fe_3O_4), being hematite the most thermodynamically stable state under ambient conditions [43]. Due to its narrow bandgap energy, about 2.0 – 2.2 eV, when it comes to light absorption, Fe_2O_3 is a good photocatalyst since it can absorb light in the UV and visible range of the spectrum (up to 600 nm, which corresponds to 40% of the solar spectrum), unlike TiO_2 that can only absorb UV radiation ($\lambda < 380$ nm) [43, 44]. Hematite is a promising semiconductor material since it is cheaper, very stable in water, environmental compatible, non-toxic and it is an abundant compound [45]. Nevertheless, the utilization of hematite as a photocatalytic material can have some disadvantages such as higher recombination of the e^-/h^+ pairs, worse photocatalytic activity when compared with TiO_2, lower charge carrier diffusion and slight conductivity [43, 46]. The use of smaller Fe_2O_3 particles, like micro or nanoparticles, showed better degradation efficiencies since they allow a higher specific surface area [43].

2.3.1.2 Titanium dioxide

The most common catalyst used in heterogeneous photocatalysis is titanium dioxide (TiO_2), a light sensitive semiconductor from the family of transition metal oxides that absorbs electromagnetic radiation in the near UV region. It can occur in minerals like rutile (most stable form of TiO_2), anatase, brookite, perovskite, among others [36]. TiO_2 practical applications include photovoltaic cells, environmental decontamination through photocatalytic degradation of the pollutants, as a sensor and in biomedicine [36, 47]. Since TiO_2 is a stable compound with high photoactivity, biologically and chemically inert, relatively cheap and easy to produce, it's frequently used as a semiconductor photocatalyst [14, 34].

Anatase and rutile have differences in their lattice structures, leading to different electronic band structures and density, which is responsible for the differences in their band gaps: 3.20 eV for anatase and 3.02 eV for rutile [36]. Also, despite of only being able to use a small percentage of the solar spectrum (~ 5%), TiO_2 is the most photoactive catalyst in a wavelength $\lambda < 384$ nm for anatase and $\lambda < 420$ nm for rutile [34, 36].

Among different TiO_2 based catalysts (e.g. TiO_2-P25, TiO_2-PC500, TiO_2-PC105, among others), TiO_2-P25 consists of 80% anatase and 20 % rutile phases, while TiO_2-PC500 and TiO_2-PC105 consists only in anatase phase. Even though anatase has a larger surface area and higher activity in water treatment compared to rutile, when these two phases are mixed together, they seem to create a synergic effect that enhances the photocatalytic reaction, possibly due to an effective charge-carrier separation induced by the different crystalline phases junction [38, 48]. As a result, TiO_2-P25 has been extensively used for photocatalytic applications due to its high activity when compared to other TiO_2 based catalysts.

2.3.2 Effect of operational parameters in heterogeneous photocatalysis

There are several parameters that may affect the photocatalytic processes, as described below, such as: i) photocatalyst type and dose; ii) nature and initial concentration of the contaminant; iii)) illumination source and intensity; iv) solution pH; v) temperature; vi) presence/absence of dissolved oxygen (DO); vii) presence of interfering species in the solution, like typical inorganic ions such as carbonates/bicarbonates (CO_3^{2-}/HCO_3^{-}), sulfates (SO_4^{2-}), phosphates (PO_4^{3-}), among others; and viii) presence of natural organic matter (NOM) [20, 33, 49]. Table 2.1 shows a compilation of some studies reported by several authors regarding the influence of some of the previous parameters on the BrO_3^- photocatalytic reduction using TiO_2 as catalyst.

Table 2. 1 – Summary of BrO_3^- photocatalytic reduction studies

$[BrO_3^-]_0$	Operational conditions	Efficiency	Ref.
100 mg L^{-1}	TiO_2: 0.1, 0.3 and 0.5 g (suspended in a batch reactor); UVA light (Philips, 32 W); pH: 3, 7 and 11; [Methanol]: 0, 10, 15, 20, 40, 60% (v/v); T: 20, 40 and 60 ºC; [HA]: 0, 5, 30 and 50 mg L^{-1}; Total volume = 200 mL.	0.302 min$^{-1\,a}$ (pH 3) 0.040 min$^{-1\,a}$ (pH 7) 0.019 min$^{-1\,b}$ (pH 7) 0.007 min$^{-1\,a}$ (pH 11)	[50]
0.050 mg L^{-1}	Platinised TiO_2 (0.5% Pt w/w) in dispersion; Cylindrical photoreactor: two half cylinders, each containing six germicidal lamps (8 W, 254 nm); pH: 6.5, 7.8, 7.9, 8.1; T = 20 ºC;	(0.045 ± 0.004) min$^{-1\,c}$ (pH 8.1); (0.200 ± 0.006) min$^{-1\,d}$ (pH 7.9); (0.030 ± 0.002) min$^{-1\,d}$ (pH 7.8); (3.20 ± 0.01) min$^{-1\,e}$ (pH 6.5)	[14]
0.075 mg L^{-1}	Thin film of 50 mg of Pt/TiO_2 coated on the quartz tube of the photoreactor; Commercial UV sterilizer flow reactor (AquaUV model: UV 605); 40 W low-pressure Hg lamp.	$(1.6 \pm 0.1) \times 10^{-2}$ s^{-1}	
12.8 mg L^{-1}	100 mg TiO_2-P25 from Degussa (ca. 75% anatase and 25% rutile) in suspension; Reactor: glass bottle wrapped by aluminum foil; Two low pressure Hg lamps (primary output 254 nm and 365 nm) pH: 1.5, 3, 5.5, 7.5, 9, 11.5 and 13.5; O_2 or N_2-athmosphere [HA]: 0, 3 and 30 mg L^{-1}.	0.028 min^{-1} (UV 254 nm); 0.017 min^{-1} (UV 254 nm)^{f}; 0.0062 min^{-1} (UV 365 nm);	[51]
0.2 mg L^{-1}	0.2 g L^{-1} of TiO_2 (in suspension in a 0.1 mmol L^{-1} potassium nitrate solution; 10 W black light fluorescent lamps (365 nm); pH 5 and 7.	6.1×10^{-9} mol L^{-1} min^{-1} (pH 7); 1.1×10^{-7} mol L^{-1} min^{-1} (pH 5)	[52]
10 mg L^{-1}	0.1 g L^{-1} Graphene-TiO_2 (Degussa P25, 75% anatase and 25% rutile); Cylindrical pure quartz reactor; 8 low-pressure Hg lamp (24 W, primary output 254 nm); pH: 5.1, 6.8, 8.0 and 9.2.	0.0094 – 0.021 min^{-1} (79%^{g} and 99%^{h} BrO_3^- removal after 60 min)	[53]

$[BrO_3^-]_0$	Operational conditions	Efficiency	Ref.
0.2 mg L^{-1}	0.2 g L^{-1} TiO_2 (ST-21) in suspension in a KNO_3 or K_2SO_4 aqueous solution; Glass vessel reactor; Black light fluorescent lamps; Alumina loaded (wt. %): 0, 2.5, 7, 10, 20, 40; pH: 5.0, 5.5, 6.0, 6.5 and 7.0;	~ 0.016 min^{-1} (~ 65% BrO_3^- removal in 80 min) [i, j]	[54]
50 mg L^{-1}	0.6 g L^{-1} TiO_2 prepared from titanium isopropoxide through sol-gel method (suspension); Biannular pyrex glass reactor; 1000 W high-pressure mercury lamp; pH: 3, 7 and 10; T = 30 ºC;	~ 85% BrO_3^- removal in 80 min [i,k]	[55]
1000 mg L^{-1}	TiO_2-P90 from Degussa; Annular photoreactor; Medium-pressure mercury-vapor lamp (450 W); pH: ~ 2.5 and ~ 6.8 to 7; T = 25 ºC; $[BrO_3^-]$:$[CH_2O_2]$ molar ratio of 1:3.	0.330 cm^2/photons × 10^{18} (pH ~ 2.5) 0.0034 cm^2/photons × 10^{18} (pH ~ 6.8 to 7)	[56]

[a] 0.3 g TiO_2, [Methanol] = 20% (v/v), T = 20 ºC.
[b] 0.3 g TiO_2, [Methanol] = 20% (v/v), T = 20 ºC, [HA] = 5 mg L^{-1}.
[c] Surface water.
[d] Ground water.
[e] Deionised water.
[f] N_2-atmosphere.
[g] Tap water, 1% GR.
[h] Deionised water, 1% GR, pH 6.8.
[i] Data retrieved from the figures in the literature.
[j] 2.5% wt. alumina in a 0.1 mmol L^{-1} KNO_3 aqueous solution, pH 7.
[k] In the presence of oxygen, pH 7.

2.3.2.1 Photocatalyst dose

Increasing the catalyst mass improves the photocatalytic reaction rate, due to a higher catalyst surface area available, until it reaches the optimum dose of catalyst mainly due the attenuation of light inside the reaction medium [36, 57]. However, for immobilized catalyst systems, and depending on the illumination mechanism, i.e. front-side or back-side illumination (FSI or BSI), further increments in the catalyst mass can lead to constant or lower reaction rates, respectively. In the last case, since the catalyst film is being illuminated on the opposite side to the liquid-catalyst interface, higher film thicknesses can block the light from activating the catalyst near to the interface and the e^-/h^+ pairs will be generated further away from the liquid-catalyst boundary, being more susceptible to recombination [33, 36, 58-60].

2.3.2.2 *Initial contaminant concentration*

One of the main steps in heterogeneous photocatalysis is the adsorption of the reagents/pollutants into the catalyst surface, so higher degradation rates are achieved when the adsorption capacity increases. Nevertheless, the generation and migration of e^{-}/h^{+} pairs to the surface of the catalyst is also a limiting step in photocatalytic reactions. For solutions with a low concentration of pollutant, adsorption of the contaminant on the catalyst surface is the limiting step of the reaction [36, 61]. In these conditions, an increase on pollutant concentration enhances the photocatalytic reaction rate. When working with high concentrations of the pollutant, all the active sites on the catalyst surface will be occupied and further increments in its concentration will not favor the reaction rate. For this situation, the limiting step is the number of reactive species generated on the catalyst surface. In addition, a high pollutant concentration can saturate the catalyst surface, blocking the catalyst surface, restricting the activation of the catalyst by the UV light [19, 36]. Moreover, the adsorption of the generated intermediate products can also block the reactive sites in catalyst surface [36].

2.3.2.3 *Illumination source and intensity*

Photocatalysis depends directly on a light source, whether it is UV or visible light, to activate the catalyst and generate the e^{-}/h^{+} pairs, which will take part on the reduction/oxidation reaction of the desired compound [62]. The e^{-}/h^{+} recombination is a recurrent problem in photocatalytic reactions, so it is absolutely essential to prevent such phenomena. An increase in the illumination intensity will enhance the probability of catalyst activation and re-excitation of recombined e^{-}/h^{+} pairs [63]. Moreover, the wavelength range of the light source will also influence the reaction rate since, in order to activate the catalyst and generate the e^{-}/h^{+} pairs, it is necessary a minimum threshold corresponding to the band gap energy of the photocatalyst [36]. Different light sources may be chosen, such as halogen lamps, mercury lamps, light emitting diodes, UV lamps, xenon-lamps, among others. The appropriate light source and intensity must be chosen in order to improve the reaction rate and reduce energy consumption [41].

2.3.2.4 *Solution pH*

Photocatalytic reactions in aqueous solutions are strongly dependent on the pH of the solution since it affects the: i) catalyst surface charge; ii) adsorption/desorption of the pollutants/products; iii) position of conduction and valence bands; iv) amount of $HO^{\bullet}$ produced; v) change of the pollutant molecules; and vi) redox potential of the contaminants [36, 41, 64]. The surface chemistry of the catalyst, associated with the pH point of zero charge (pH_{PZC}), will determine the reaction between the donors and acceptors of electrons. That is, when solution $pH > pH_{PZC}$, the catalyst surface is negatively charged (Eq. (10)) and occurs electrostatic repulsion of anionic compounds, but when solution $pH < pH_{PZC}$, the surface is positively charged (Eq. (11)) and anionic compounds are attracted, favoring the degradation of the pollutant [36, 41]. For TiO_2, the pH value (acidic or alkaline) of the solution can protonate or deprotonate the surface, according to [65, 66]:

$$\mathrm{TiOH} + \mathrm{OH}^- \leftrightarrow \mathrm{TiO}^- + \mathrm{H_2O} \tag{10}$$

$$\mathrm{TiOH} + \mathrm{H}^+ \leftrightarrow \mathrm{TiOH_2}^+ \tag{11}$$

The pH_{PZC} is given by the negative logarithm of the first and second acid dissociation constants, as follows [36, 66]:

$$\mathrm{pH_{PZC}} = \frac{1}{2}(\mathrm{pK^s_{a1}} + \mathrm{pK^s_{a2}}) \tag{12}$$

For example, it has been reported for Degussa TiO_2 – P25 a $pK_{a1}{}^s = 2.4$ and $pK_{a2}{}^s = 8.0$, which results in a $pH_{PZC} = 6.25$ [66].

2.3.2.5 *Temperature*

In photocatalytic systems the activation of the photocatalyst is achieved by photonic adsorption, thus not requiring heating [64]. The increment on solution temperature favors the collision of the molecules with the catalyst surface, enhancing the reaction kinetics [41, 67]. However, when the temperature is very high ($T > 80$ ºC) the recombination of the e^-/h^+ pairs is promoted and the desorption of adsorbed molecules is enhanced, thus decreasing the reaction rate [41, 68]. On the other hand, lower temperatures ($T < 0$ ºC) favor the adsorption of the molecules through a spontaneous exothermic process, but desorption can be very slow and becomes the rate-limiting step of the reaction [36, 64]. A temperature range between 20 ºC and 80 ºC has been reported as the optimum for photocatalytic reactions [64].

2.3.2.6 *Dissolved oxygen*

Dissolved oxygen (DO) is an electron acceptor, therefore can act as a scavenger of the photoexcited e^- in the conduction band, preventing the recombination of e^-/h^+ pairs [42]. In addition, DO can also: i) contribute to the formation of highly reactive oxygen species (e.g. superoxide radical $O^{\bullet -}$ - Eq.(6), hydrogen peroxide - Eq.(13), and other subsequent species like $HO_2{}^{\bullet -}$ - Eq.(7)) [69]; ii) be directly involved in photocatalytic reactions; and iii) participate in the stabilization of radical intermediates [64].

$$\mathrm{O_2} + 2\mathrm{e}^- + 2\mathrm{H}^+ \rightarrow \mathrm{H_2O_2} \tag{13}$$

So, photocatalytic oxidation reactions are promoted in the presence of DO in solution, which is supplied using an aeration system, such as mechanical agitation or compressed air diffusion, and/or the electrooxidation of the H_2O molecule in the anode (Eq.(14)) [41].

$$2\mathrm{H_2O} \rightarrow \mathrm{O_2} + 4\mathrm{H}^+ + 4\mathrm{e}^- \tag{14}$$

However, when it comes to photocatalytic reduction processes, DO can block the adsorption of the pollutants into the catalyst surface since both reduction reactions occur in the same active sites. The scavenging of electrons in photocatalytic reduction reactions will reduce the amount of reactive species able to react with the pollutants and reduce them to an innocuous form, therefore interfering on the overall process efficiency.

2.3.2.7 Inorganic compounds

When photocatalysis is applied on the treatment of real waters, it is expected the presence of some ubiquitous compounds like inorganic ions, being necessary to understand their role in the photocatalytic process. Both inorganic anions (e.g. PO_4^{3-}, SO_4^{2-}, HCO_3^-, Cl^-) and cations (e.g. Fe^{2+}, Cu^{2+}) have been reported to influence photocatalysis, since they can compete for the active sites in the catalyst surface [65, 70-74]. Under acidic conditions ($pH < pH_{PZC}$), due to electrostatic attraction between the positively charged catalyst surface and the negatively charged ions, anions can easily adsorb to the catalyst surface, blocking the active sites [74].

2.3.2.8 Natural organic matter

Natural organic matter (NOM) is naturally present in surface and underground waters and may contain different compounds like: i) humic acids (HAs), which usually constitute the majority of the NOM in some waters and are insoluble in waters with pH < 2; ii) fulvic acids (FAs), soluble in the entire pH range; and iii) humin, an insoluble component of soil organic matter at both acidic and alkaline pH [75, 76].

Photocatalysis depends on the absorption of photons to generate highly reactive species able to degrade the pollutants. Organic substances, such as NOM, can absorb or scatter the photons emitted by the light source and reduce the amount of radiation that reaches the surface of the catalyst [77]. Therefore, lower amounts of e^-/h^+ pairs are generated. Moreover, those big molecules can adsorb on the catalyst surface, blocking the active sites. In turn, organic matter has also been reported to react with h^+ and $HO^\bullet$, exhibiting reaction rates constants in the order of 10^8 to 10^{10} M^{-1} s^{-1}, which could increase the reduction reaction rates since it prevents the re-oxidation of the Br^- ions by $HO^\bullet$ radicals and h^+ [78].

2.4 PHOTOCATALYTIC REACTORS

2.4.1 Photoreactors limitations

2.4.1.1 Photon transfer limitations

In photocatalytic processes, the first step is the light transport to the catalyst, in order to activate the semiconductor material by the incident radiation and produce e^-/h^+ pairs to initiate redox reactions on its surface [34]. Reactor design is a determinant factor for an efficient photon transport through the reaction medium, especially when it comes to scale-up, since the incident light has to pass through: i) a transparent wall; and ii) a medium, liquid or gaseous, that contains the reagents and other components that might absorb or scatter the radiation. Illumination efficiency also depends on the irradiation source (solar or artificial light), and it can cause restrictions in the reactor configuration. Hence, its design must be an integrated process [34, 79, 80]. It is also very important to guarantee a homogeneous distribution of the incident radiation on the catalyst surface, considering that a minimum amount of energy is required to activate the catalyst [34, 81].

Solar light is a costless and sustainable energy source. However, the solar-driven technologies demand high investment costs related to the collectors needed for the solar photons capture. Besides that, sunlight has several issues associated with its intermittency, intensity variation and with the fact that some catalysts can only use a small percentage of the solar spectrum. For instance, TiO_2 only uses 5% of the solar spectrum, corresponding to the UV radiation ($\lambda \leq 400$ nm) that reaches the Earth surface [33, 34, 36, 79]. As an alternative, artificial light can be used more flexibly and adapted to the reactor design.

Higher lighting efficiency can be achieved by using micro or nanoscale illumination [34]. Light emitting diodes (LEDs) are miniaturized light sources that arise as an alternative to classic lamps due to its robustness, long lasting, small size, availability in different wavelengths, efficiency and non-toxicity [34, 79, 82]. Combined with microreactors, microscale illumination provides a large illuminated catalyst surface per unit of reactor volume and its short irradiation path diminishes the barriers associated with photon transport to the catalyst surface and allows spatial uniformity of irradiance [83]. Furthermore, the catalyst surface illumination mechanism (FSI or BSI), can affect the reaction efficiency. In a BSI mechanism, increments on the catalyst film thickness improves the reaction rate until it reaches a maximum value, and then an additional increase on the film thickness leads to lower reaction rates since the charge carriers are generated far from the catalyst-liquid interface, enhancing the electron/hole recombination. On the other hand, in a FSI mechanism, increasing the catalyst film thickness enhances the reduction rate until it reaches the optimum value. Then, the reaction rate remains constant since after a certain catalyst film thickness the diffusional length of the charge carriers to the catalyst–liquid interface does not change. [58]. For this reason, photon transfer limitations could also be surpassed by the use of FSI mechanism.

2.4.1.2 Mass transfer limitations

When it comes to reactions on a solid-liquid interface, mass transfer is also an issue to take into consideration. It can be divided into external and internal mass transfer. External mass transfer includes the diffusion of the reagents from the bulk solution to the liquid-catalyst boundary, which is highly influenced by the degree of mixing inside the reactor. Internal mass transfer is related with the inter-particle diffusion of the reagents within the catalyst film to the active surface sites, where they can adsorb and eventually react, and it is mainly depended on the film porosity [34, 59].

Overcoming mass transfer limitations can be achieved by intensifying reactor designs that promote a large illuminated catalyst surface area per unit of reactor volume. Some of the reactors types are slurry systems, spinning disc reactors, monolithic reactors and microreactors [34]. Microreactors are one of the most promising reactor types due to its: i) high surface-to-volume ratio, which improves the mass and heat transfer; ii) short molecular diffusion path; and iii) fast mixing, even under laminar flow [34, 83]. External and internal mass transfer limitations can be also minimized by using turbulent flow regimes (high Reynolds number), promoting a higher degree of mixture of the bulk solution [34]. However, laminar flow regime reduces the friction between fluid and catalyst surface, preventing catalyst detachment, and the energy for liquid pump operation is diminished, saving costs.

2.4.2 Micro and mili-photoreactors

Nowadays, the use of immobilized catalyst configurations instead of a dispersed catalyst powder in photocatalytic processes is preferable since it avoids an additional step for catalyst separation from the solution. However, one of the major problems associated with it is the scale-up of such reactors, due to lower ratios of illuminated surface area per unit of reactor volume which leads to mass transfer limitations [84]. Therefore, the incorporation of micro- or even mili-structured photoreactors can minimize the limitations associated with the scale-up as they allow higher surface-to-volume ratios [85].

Microreactors major advantages are their high surface areas, excellent heat transfer properties, high reaction efficiencies, smaller molecular diffusion paths and high degree of mixing under laminar regime [83, 85, 86]. Also, the numbering-up concept in microreactors allows maintaining the optimal performance of the reactors by increasing the number of reactors instead of increasing its size. The numbering-up may occur by replicating the internal main functional elements of the reactor or by replicating the whole experimental set-up. This allows treating higher volumes without occupying very large areas for the experimental installation, reducing the associated costs [87].

Static mixers (SMs) incorporation in many industrial processes is increasing, mainly due to its good mixing and heat transference properties. SMs have the ability to divide and redistribute the streamlines using the energy of the flowing fluid [88]. A static continuous flow mixer, based on the NETmix technology, is constituted by a network of channels and chambers (Figure 2.3) that were modeled as perfect segregation plug flow devices connected with perfectly mixed stirred tanks. The high degree of mixing under laminar flow is one of the major advantages of using this mili-photoreactor [89, 90]. Therefore, its application to photocatalytic reactions can reduce mass transfer limitations and improve the overall process.

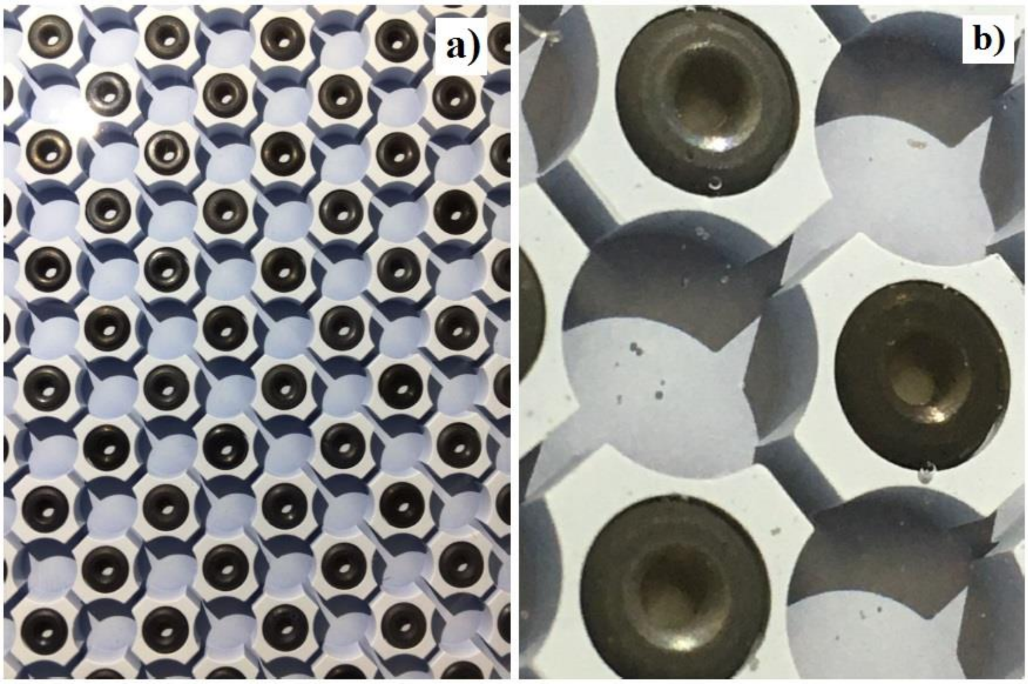

Figure 2. 3 – NETmix photoreactor: a) network of channels and chambers; b) detailed chamber and respective channels.

3 MATERIALS AND METHODS

3.1 CHEMICALS AND MATERIALS

The BrO_3^- stock solution (1000 mg L^{-1}), used throughout this work, was prepared by dissolving sodium bromate ($NaBrO_3$) salt, used as received, in ultrapure water (UPW). Table 3.1 displays the main characteristics of the commercial salt. BrO_3^- aqueous solutions were prepared before each experiment by diluting the required volume of the stock solution in UPW to obtain the desired concentration. All the synthetic solutions, including standards used on the calibration of analytical equipment, were prepared using ultrapure water (UPW) obtained from a Millipore Direct-Q® (18.2 MΩ cm at 25 ºC) water purification system. The entire laboratorial material used was cleaned with UPW before each use. Pure water (PW), used to dilute the alkaline detergent during the catalyst's supports cleaning procedure, was obtained through a reverse osmosis system from Panice®.

Table 3. 1 – Sodium bromate physicochemical properties.

Physicochemical properties	
Chemical name	Sodium bromate
Molecular structure	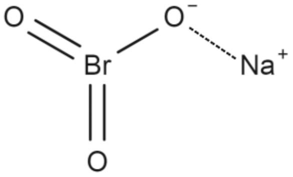
Molecular formula	$NaBrO_3$
Molecular weight (g mol^{-1})	150.90
Purity	>99%
Supplier	Merck

Iron (III) oxide (Fe_2O_3) nanopowder (particle size <50 nm, density of 5.24 g cm^{-3}, surface area: 50–245 m^2 g^{-1}, molecular weight (MW): 159.69 g mol^{-1}) was supplied from Sigma-Aldrich® and used as obtained. Titanium dioxide, Aeroxide® TiO_2 P25 powder (purity: > 99.5% wt., average primary particles size of 21 nm, density of ca. 4 g cm^3, specific surface area (BET): 50 ± 15 m^2 g^{-1}, crystal phases: 80% wt. anatase, 20% wt. rutile) was purchased from Evonik and used as received.

All the other chemicals used in this work are summarily described in Table 3.2.

Table 3. 2 – Physicochemical properties of the chemicals used in this work.

Chemical	Molecular formula	Molecular weight (g mol^{-1})	Purity / Concentration	Density (g cm^{-3})	Supplier	Purpose
Surfactant Triton® X–100	t-Oct-C_6H_4-$(OCH_2CH_2)_nOH$, n = 9–10	625 (average)	----	1.07	Sigma-Aldrich®	Preparation of catalyst suspensions
Bromate standard	BrO_3^-	127.901	(1000 ± 4) mg L^{-1}	1.00	Sigma-Aldrich®	Standard for ion chromatography
Bromide standard	Br^-	79.904	(1000 ± 4) mg L^{-1}	0.997–1.001	Sigma-Aldrich®	Standard for ion chromatography
Formate standard	CHO_2^-	45.017	1000 mg L^{-1}	0.999	Fluka® Analytical	Standard for ion chromatography
Potassium hydroxide	KOH	56.11	1.0 N	----	Alfa Aesar	Eluent for ion chromatography
Sodium hydroxide	NaOH	39.997	≥ 99% (w/w)	1.03	Labkem	pH buffer
Sulfuric acid	H_2SO_4	98.07	> 95% (w/w)	1.83	Fisher Scientific	pH buffer
Hydrochloric acid	HCl	36.46	37% (w/w)	1.18	Fisher Scientific	pH buffer
Formic acid	CH_2O_2	46.025	99.5% (w/w)	1.22	VWR Chemicals	Organic SA
Acetic acid	$C_2H_4O_2$	60.05	99.83%	1.048	Fisher Scientific	Determination of total dissolved iron concentration
Ascorbic acid	$C_6H_8O_6$	176.13	99.83%	1.65	Fisher Scientific	Determination of total dissolved iron concentration
Ammonium acetate	$C_2H_7NO_2$	77.08	99.6% (w/w)	1.17	Fisher Scientific	Determination of total dissolved iron concentration
1,10-Phenanthroline 1-hydrate	$C_{12}H_8N_2.H_2O$	198.23	≥ 99% (w/w)	----	Panreac	Determination of total dissolved iron concentration
Ethanol	C_2H_6O	46.07	99.99% (w/w)	0.789	Fisher Scientific	Preparation of Fe_2O_3 catalyst suspensions
Acetone	C_3H_6O	58.08	----	0.79	VWR Chemicals	Cleaning borosilicate glass slabs before catalyst depositions
Derquim LM 01	----	----	----	----	Panreac	Alkaline detergent to wash the laboratorial material and catalyst supports

3.1.1 Fresh water sample from a Water Treatment Plant

In order to evaluate the influence of a natural water matrix, a water sample pre-treated by a sequential ozonation-flocculation-filtration process was collected from a Water Treatment Plant (WTP) located near Porto, Portugal. Since the fresh water (FW) did not contain BrO_3^-, as could be seen in Table 3.3, it was spiked with 200 μg L^{-1} of BrO_3^- prior its use.

Table 3. 3 – Physicochemical characterization of the FW from a WTP.

Parameter (units)	Fresh Water Sample
Color	n.d. [a]
Odor	n.d. [a]
pH	7.36
Temperature (ºC)	25
Conductivity (μS cm^{-1})	283
Alkalinity (mg $CaCO_3$ L^{-1})	51
Turbidity (NTU)	0.25
Total dissolved carbon – TDC (mg L^{-1})	19.5
Dissolved inorganic carbon – DIC (mg L^{-1})	16.0
Dissolved organic carbon – DOC (mg L^{-1})	3.5
Total dissolved iron, TDI (mg L^{-1})	< 0.13 [b]
Total suspended solids – TSS (mg L^{-1})	< 2
Volatile suspended solids – VSS (mg L^{-1})	< 2
Nitrate – N-NO_3^- (mg L^{-1})	0.9
Sulfate – SO_4^{2-} (mg L^{-1})	27.1
Bromate – BrO_3^- (μg L^{-1})	<3.7 [c]
Bromide – Br^- (μg L^{-1})	24.2
Chloride – Cl^- (mg L^{-1})	14.2

[a] n.d. – not detected

[b] quantification limit value

[c] detection limit value

3.2 PHOTOREACTOR EXPERIMENTAL SETUP

The mili-photoreactor, based on the NETmix technology, has been fully described elsewhere [89-91]. It consists of a network of cylindrical chambers interconnected through a series of rectangular channels, whose characteristics are given in Table 3.4. This configuration allows a high degree of mixing under laminar regime. The NETmix photoreactor has two stainless steel distributors (see Figure 3.2): i) one with an inlet injection point and eight outlet points connected to the eight inlet points of the photoreactor (which are equally distributed on the top and on bottom of the reactor); and ii) other with one outlet point and eight inlet points that are connected with the eight outlet points of the reactor, located at the end of the network. Two different configurations of the mili-photoreactor were used: i) an acrylic structure containing a stainless steel slab (SSS) imprinted with a network of channels and chambers where the catalyst was deposited (10-20 mL of a 2% wt. TiO_2–P25 aqueous suspension, which corresponds to 193-381 mg), and then covered with a borosilicate slab (BS) without catalyst, being possible to analyze the mechanism of FSI (catalyst illuminated surface area per unit of reactor volume of 989 m^2 m^{-3}); and ii) an acrylic base imprinted with the network of channels and chambers and covered with a BS coated with 10-40 mg of catalyst, thereby analyzing the mechanism of BSI (catalyst illuminated surface area per unit of reactor volume of 333 m^2 m^{-3}). The bottom and upper slabs were sealed together by mechanical compression and O-rings.

Two different radiation sources, placed on top of the BS, were used and they comprised: i) 9 UVA–LEDs (270 mW, λ_{peak} = 365 nm); and ii) 18 UVA-LEDs (1400 mW, λ_{peak} = 365 nm).

The experimental setup (see Figure 3.1 and 3.2) consists of: i) a cylindrical glass vessel (capacity of 1.8 L) with a jacket, connected to a thermostatic bath to keep the solution temperature on the desired values; ii) a gear pump (ISMATEC BVP-Z Standard) operating at a flow rate of 75 L min^{-1} to recirculate the solution; iii) magnetic stirrer (Fisher Scientific FB 15011) to homogenize the solution inside the glass vessel; iv) pH electrode with temperature sensor (Hanna Instruments HI-2020 edge® hybrid multiparameter pH/temperature meter); and v) dissolved oxygen probe (Thermo Scientific™ Orion™ 3-Star benchtop dissolved oxygen meter). All the system units were connected by polytetrafluoroethylene (PTFE) tubing. A photonic flux of 0.61 ± 0.09 W was determined by Marinho et al. [92] in a 2-nitrobenzaldehyde (25 mM) actinometry for 9 UVA-LEDs (270 mW, λ_{peak} = 365 nm). Furthermore, in a unpublished work from the investigation group (data not showed), a photonic flux of 2.67 W for 18 UVA-LEDs (1400 mW, λ_{peak} = 365 nm) was determined.

Table 3. 4 – Summary of the NETmix photoreactor design dimensions.

NETmix photoreactor dimensions	
Window	
Length (cm)	13.7
Width (cm)	7.7
Chambers	
Diameter (mm)	6.5
Depth (mm)	3
Channels	
Length (mm)	2
Width (mm)	1
Depth (mm)	3
Borosilicate glass slab	
Thickness (mm)	4
Area (cm^2)	135
Total illuminated area (cm^2)	5.6
Total illuminated volume (cm^3)	16.7

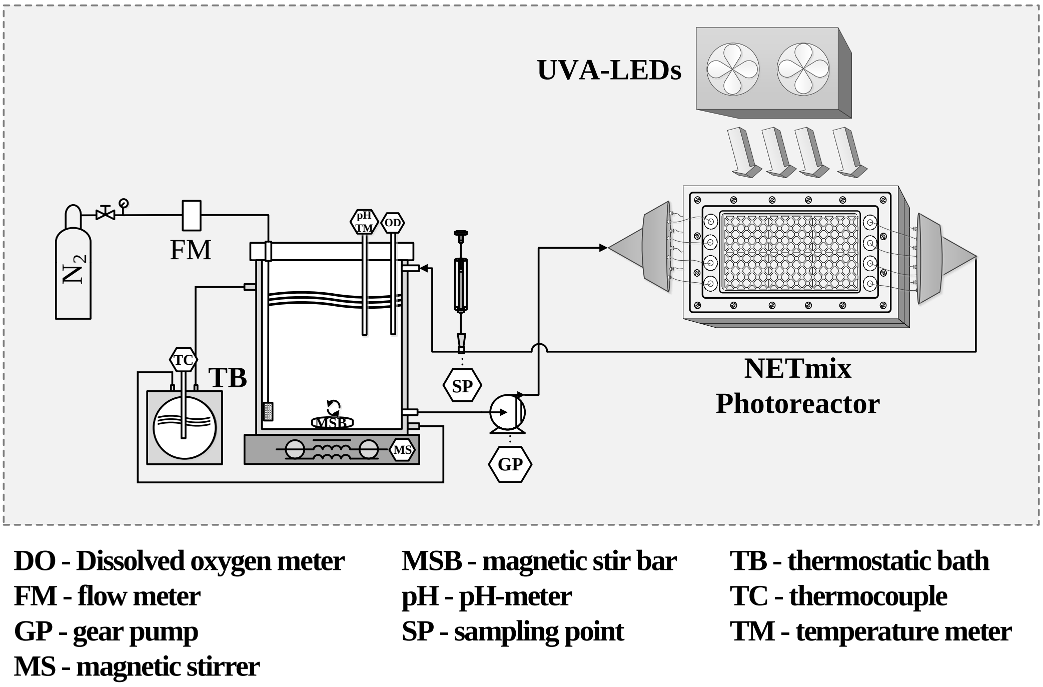
UVA-LEDs
N2
FM
pH TM
OD
TC
TB
MSB
MS
SP
GP
NETmix Photoreactor
DO - Dissolved oxygen meter
FM - flow meter
GP - gear pump
MS - magnetic stirrer
MSB - magnetic stir bar
pH - pH-meter
SP - sampling point
TB - thermostatic bath
TC - thermocouple
TM - temperature meter

Figure 3. 1 – Schematic representation of the experimental installation setup.

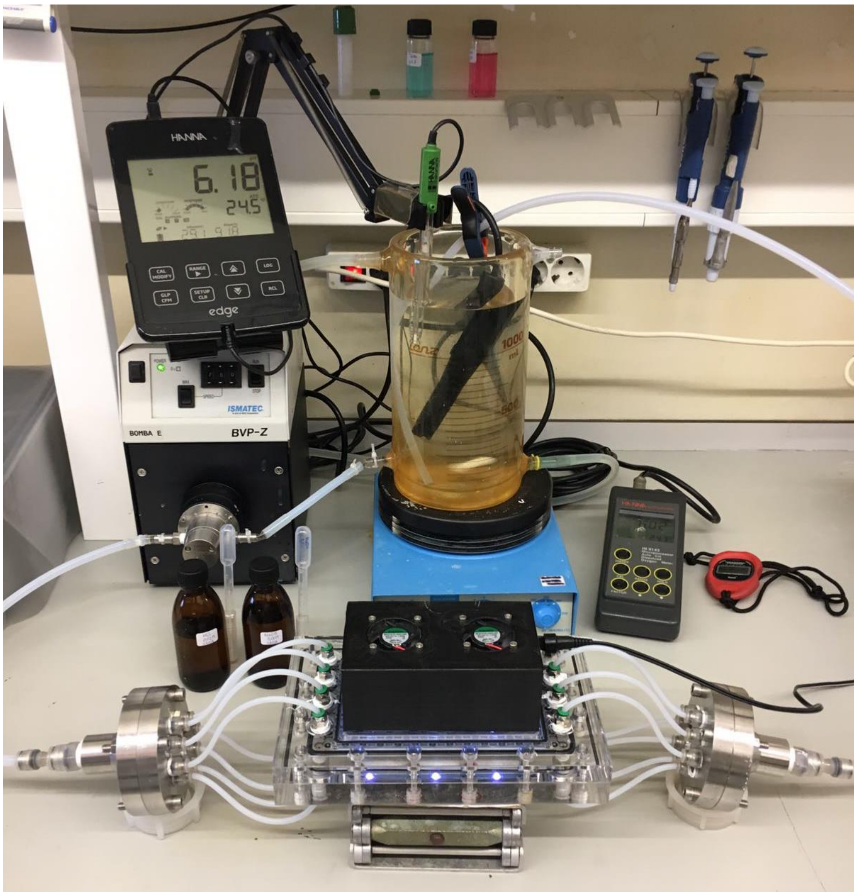

Figure 3. 2 – Photograph of the experimental apparatus.

3.3 PREPARATION OF CATALYST FILMS

Borosilicate glass slab (BS) and stainless steel slab (SSS) were used as catalyst support. Prior to catalyst deposition, BS was: i) thoroughly cleaned with alkaline detergent, diluted in PW, in an ultrasonic cleaning unit (Elmasonic S 120 (H) from Elma at 37 kHz) for 15 minutes; ii) washed with UPW; iii) cleaned with acetone; iv) rinsed with UPW; and v) dried in an oven. SSS was prepared before catalyst deposition by: i) cleaning with alkaline detergent, diluted in PW, in an ultrasonic cleaning unit for 30 minutes; ii) rinsed with UPW; and iii) drying in an oven.

Both Fe_2O_3 (0.1 mol L^{-1}) and TiO_2-P25 (2% wt.) catalyst aqueous suspensions were prepared in UPW, with the addition of 1 drop of Triton® X-100 per 100 mL of aqueous suspension. Before deposition, the catalyst suspension was sonicated in an ultrasonic unit for 15 minutes in order to disperse the catalyst particles and avoid agglomerations.

Spray deposition method was used to deposit the catalyst aqueous suspension over both support media. The spray system (Figure 3.3) was constituted by an airbrush (DEXTER DX-1839) connected to an air compressor (Wuto TC-20 series). Before deposition (Figure 3.4 a)), the BS was weighted in an analytical balance and then placed over a heating plate ($T = 200$ ºC) during the catalyst deposition (10, 20 and 40 mg) (Figure 3.4 b)). Afterwards, the BS was removed from the heating place and allowed to cool in air. Then, it was weighted to determine if the desired mass of catalyst had already been achieved and, if not, the process was repeated until the desired catalyst mass was reached. At the end, the BS was placed in an oven to remove the moisture and, after that, it was weighted in order to determine the exact mass of catalyst deposited. On the other hand, the deposition on the SSS was performed by measuring the deposited volume of the catalyst aqueous suspension, since the slab in too heavy to determine the catalyst mass by weight difference. Therefore, the SSS was placed over a heating plate ($T = 150$ ºC) and different volumes of the catalyst aqueous suspension (10, 15 and 20 mL) were deposited. At the end, both slabs were allowed to cool in the air before being assembled in the photoreactor (Figure 3.4 c) and d)).

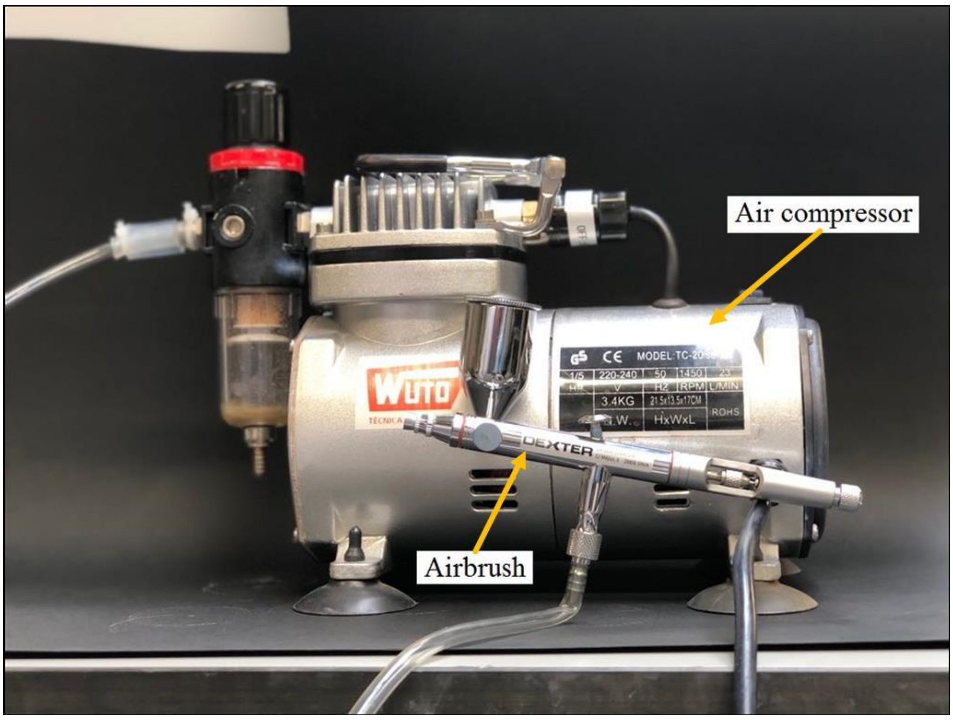
Air compressor
Airbrush

Figure 3. 3 – Spray deposition system.

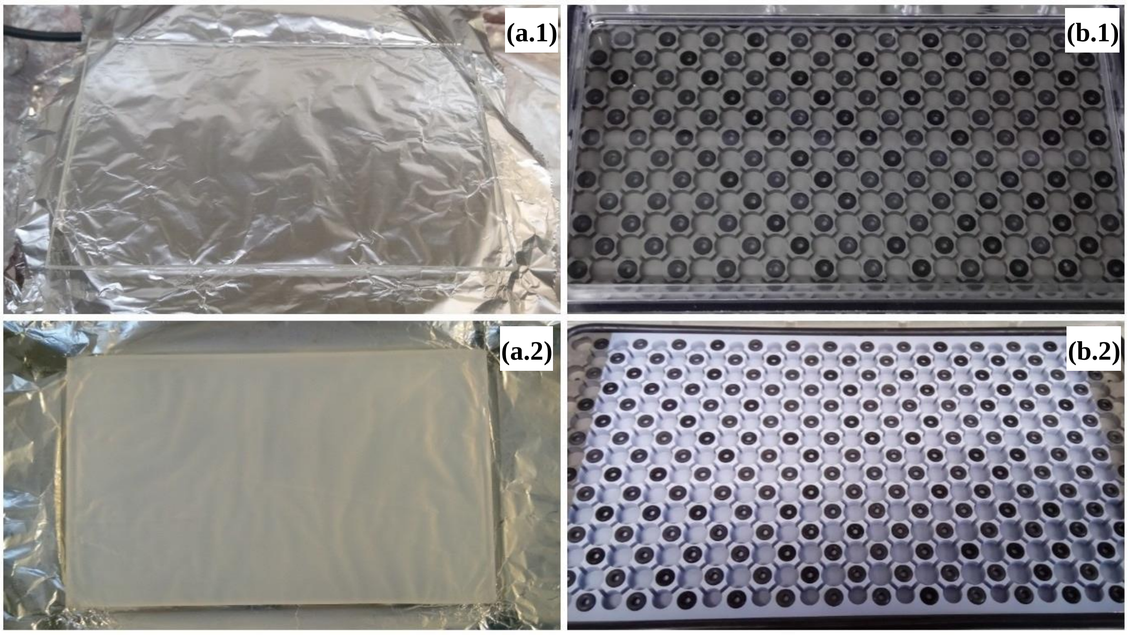

Figure 3. 4 – Photograph of the (a) BS and (b) SSS: (.1) before and (.2) after the TiO_2-P25 aqueous suspension deposition.

3.4 PHOTOCATALYTIC EXPERIMENTS PROCEDURE

Experiments were conducted with UPW and FW spiked with BrO_3^- to obtain a concentration of 200 µg L^{-1}. In order to evaluate the isolated influence of carbonates, sulfate and humic acids on the BrO_3^- photoreduction reaction, UP was also spiked with the same amount of dissolved inorganic carbon, sulfate and dissolved organic carbon (using humic acids as carbon source) encountered on the FW (see Table 3.3).

The experimental procedure consisted of the following steps: i) 1.5 L of a 200 µg L^{-1} BrO_3^- solution (1.56 µM) was added to the jacketed glass vessel, connected to the thermostatic bath in order to maintain the solution temperature at the intended value (15, 20, 25 and 30 ºC); ii) the solution pH was adjusted to the desired value (5.5, 6.5 and 7.5); iii) the recirculation pump was turned on (at 75 L min^{-1}) and the solution was recirculated for 5 minutes in the dark for homogenization. When DO levels lower than 0.1 mg L^{-1} were required, nitrogen (N_2) was also injected into the solution and the glass vessel was sealed with Parafilm® M in order to avoid the entry of oxygen. For the reactions with CH_2O_2 as SA, a given volume of the CH_2O_2 stock solution was added to the BrO_3^- solution, aiming a $[BrO_3^-]$:$[CH_2O_2]$ molar ratio of 1:3, right before the reaction started. Then, the initial sample was collected immediately after the reaction was initiated (t_0) by turning on the UVA-LEDs. During the reaction, the pH was adjusted with acid or alkaline buffers to maintain the solution pH in the required value. Samples were collected at predefined times, during a 2- or 3-hour reaction period, and filtered using a 0.20 µm nylon membrane filter (VWR International), to quantify BrO_3^- and Br^- concentrations by ion chromatography (IC).

3.5 ANALYTICAL METHODS

Table 3.5 presents all the analytical determinations performed during this study.

Table 3. 5 – Analytical methods.

Parameter	Methodology
BrO_3^{-} [a] Br^{-} [a] CHO_2^{-} [a] $N{-}NO_3^{-}$ [a] SO_4^{2-} [a] Cl^{-} [a]	Bromate, bromide, formate, nitrate, sulfate and chloride ions concentration were determined using a Thermo Scientific Dionex™ ICS-2100 Ion Chromatography System equipped with a Dionex™ IonPac™ AG19 guard column (2 × 50 mm) + Dionex™ IonPac™ AS19 analytical column (2 × 250 mm) and a Dionex™ AERS™ 500 Carbonate Electrolytically Regenerated Suppressor (2mm) in an Auto Suppression Recycle Mode. The operational conditions were the following: i) applied current to the suppressor of 15 mA; ii) column temperature of 30 ºC; iii) isocratic elution of a 20 mM KOH eluent at a flow rate of 0.30 mL min^{-1}; and iv) injection volume of 5 µL;
Temperature/pH	Temperature and pH were measured using a Hanna Instruments HI-2020 edge® hybrid multiparameter pH/temperature meter.
DO	Dissolved oxygen (DO) was measured using a Hanna Instruments HI-9143 portable dissolved oxygen meter or a Thermo Scientific™ Orion™ 3-Star benchtop dissolved oxygen meter.
Conductivity	Conductivity was obtained from a Hanna Instruments HI-9828 multiparameter portable meter.
Color	Color was determined according to the method 2120 B of Standard Methods for the Examination of Water and Wastewater [93].
Odor	Odor was determined according to the method 2150 B of Standard Methods for the Examination of Water and Wastewater [93].
Alkalinity	Alkalinity was determined according to the method 2320 B of Standard Methods for the Examination of Water and Wastewater [93].
Turbidity	Turbidity was determined using a Hanna Instruments HI88703 turbidimeter
Total dissolved iron	Total dissolved iron (Fe^{2+} and Fe^{3+}) concentration was determined according to the ISO 6332 [94] in the beginning and at the end of the experiments with Fe_2O_3 using a colorimetric method with 1,10-Phenanthroline, measuring the absorbance at 510 nm using a VWR UV-6300 Double Beam Spectrophotometer.
TDC [a] DIC [a] DOC [a]	Total dissolved carbon (TDC) and dissolved inorganic carbon (DIC) were measured using a Shimadzu TOC-V_{CSN} analyzer. Dissolved organic carbon (DOC) was obtained by the difference, i.e.: DOC = TDC – DIC.
TSS	Total suspended solids (TSS) content was determined according to the method 2540 D of Standard Methods for the Examination of Water and Wastewater [93], by filtrating the sample through a glass-fiber filter (GF/C) and drying the retained residue at 105 ºC until a constant weight was reached.
VSS	Volatile suspended solids (VSS) content was determined according to the method 2540 D of Standard Methods for the Examination of Water and Wastewater [93], by igniting at 550 ºC the residue obtained from the TSS determination, until constant weight.

[a] Samples were filtrated before analysis using 25 mm filters with 0.20 µm nylon membrane from VWR International.

3.6 KINETIC MODELS

BrO_3^- photocatalytic reduction processes for different operational parameters was evaluated by fitting a mathematic model to the experimental data, in order to obtain the kinetic constants of the reaction. A pseudo-first-order kinetic model was adjusted to the data by a nonlinear regression method using Fig.P software for Windows from Biosoft, minimizing the sum of the squared deviations between the experimental data and the predicted values. The pseudo-first-order kinetic model is represented by Eq. (15):

$$C = C_0 e^{-kt} \tag{15}$$

where, C is the BrO_3^- concentration at time t, C_0 is the initial BrO_3^- concentration and k is the pseudo-first-order kinetic constant.

The goodness of the kinetic model fitting was evaluated considering the (i) relative standard deviation, (ii) residual variance (S^2_R) and (iii) coefficient of determination (R^2).

4 RESULTS AND DISCUSSION

All the reactions were performed using solutions with an initial BrO_3^- concentration of 1.56 μM , as described in chapter 3. A flow rate (Q) of 75 L h^{-1}, corresponding to a Reynolds number (Re) of 834 (laminar flow), was adopted for all experiments performed since it was the optimum value reported by Marinho et al. [95]. The authors described that an increase in Re up to 830 increased the degree of mixing and improved the mass transfer of the pollutants in the bulk solution to the catalyst surface. Furthermore, Laranjeira et al. [89] determined that for $Re > 150$ (critical value), the flow in the NETmix photoreactor was enough to induce an intense mixing inside the chambers of the photoreactor. A temperature of 25 ºC was chosen as it is a close value to the ambient temperature. The reaction efficiency was assessed by measuring the decay in BrO_3^- concentration over time through ion chromatography. Br^- concentration was also assessed to verify that BrO_3^- was reduced to Br^-.

4.1 PRELIMINARY RESULTS

Before starting the experiments, some preliminary tests were performed in order to understand some operational details that might be affecting the photocatalytic process and interfering with the validity of the obtained results. All of the preliminary tests were performed using the NETmix photoreactor with an acrylic base, imprinted with channels and chambers, and with the catalyst deposited in the BS. Initially, the experiments were performed using an acidic pH value, around pH 3, since it was selected by several authors [50, 74, 96] as the optimal pH for BrO_3^- reduction.

Table 4.1 presents the operational conditions and kinetic parameters obtained for all the preliminary tests performed.

4.1.1 Influence of pH using iron oxide (Fe_2O_3) as photocatalyst

To evaluate the influence of pH on BrO_3^- reduction reaction rates, using Fe_2O_3 photocatalyst, a thin film of 20 mg was coated onto the BS (since it was determined by Marinho et al. [92] as the optimal TiO_2-P25 mass for Cr(VI) reduction under UVA-LEDs illumination) and experiments at pH 3 and at the natural solution pH (i.e. without control at the beginning and during reaction, pH ~ [5.6 – 5.8]) were performed. Figure 4.1 presents the results obtained for the different experimental conditions, showing both BrO_3^- decay and Br^- formation. The respective reaction rates are summarized in Table 4.1.

Table 4. 1 – Operational conditions and pseudo-first-order kinetic constants for bromate reduction (k), calculated for the preliminary tests performed, along with the corresponding coefficient of determination (R^2) and residual variance (S^2_R).

PRELIMINARY RESULTS										
Experiment [a]	**Catalyst**	**$pH_{av.}$** [b]	**Light source**	**$m_{deposited}$ (mg)**	**DO (μM)**	**$[BrO_3^-]$:$[CH_2O_2]$ ratio**	**Time (min)**	**k (× 10^{-3} min^{-1})**	**R^2**	**S^2_R (μM^2)**
Influence of pH using iron oxide (Fe_2O_3) as photocatalyst										
4.1.1	Fe_2O_3	3.08	LEDs 270 mW	20	[232 – 263]	----	0 – 180	3.0 ± 0.2	0.993	3.7×10^{-4}
4.1.2	Fe_2O_3	3.08	No light	20	[232 – 263]	----	0 – 180	2.7 ± 0.2	0.990	4.4×10^{-4}
4.1.3	Fe_2O_3	3.04	No light	0	[232 – 263]	----	0 – 180	2.6 ± 0.1	0.995	2.3×10^{-4}
4.1.4	Fe_2O_3	5.92 [c]	No light	20	[232 – 263]	----	0 – 180	[d]	[d]	[d]
4.1.5	Fe_2O_3	5.49 [c]	LEDs 270 mW	20	[232 – 263]	----	0 – 180	[d]	[d]	[d]
Influence of DO and formic acid using titanium dioxide (TiO_2-P25) as photocatalyst										
4.2.1	TiO_2–P25	5.52	LEDs 270 mW	20	[232 – 263]	----	0 – 120	11 ± 1	0.994	1.3×10^{-3}
4.2.2	TiO_2–P25	5.54	LEDs 270 mW	20	[232 – 263]	----	0 – 120	16 ± 1	0.998	5.8×10^{-4}
4.2.3	TiO_2–P25	5.63	LEDs 270 mW	20	<3.1	----	0 – 120	10.2 ± 0.4	0.999	1.7×10^{-4}
4.2.4	TiO_2–P25	5.55	LEDs 270 mW	20	<3.1	----	0 – 120	17 ± 2	0.990	2.7×10^{-3}
4.2.5	TiO_2–P25	5.53	LEDs 270 mW	20	[232 – 263]	1:3	0 – 120	11 ± 1	0.992	1.6×10^{-3}
4.2.6	TiO_2–P25	5.54	LEDs 270 mW	20	[232 – 263]	1:3	0 – 120	17 ± 2	0.994	1.7×10^{-3}
4.2.7	TiO_2–P25	5.55	LEDs 270 mW	20	<3.1	1:3	0 – 120	9.8 ± 0.5	0.998	3.2×10^{-4}
4.2.8	TiO_2–P25	5.55	LEDs 270 mW	20	<3.1	1:3	0 – 120	14 ± 2	0.990	2.5×10^{-3}

[a] Conditions: $[BrO_3^-]_0 = 1.56$ μM; Fe_2O_3 photocatalyst; $Q = 75$ L h^{-1}; $T = 25$ °C; $V_i = 1500$ mL.

[b] Average of the pH values measured during the reaction.

[c] Solution pH; no pH adjustment performed during the reaction.

[d] Not adjustable to a pseudo-first-order kinetic model.

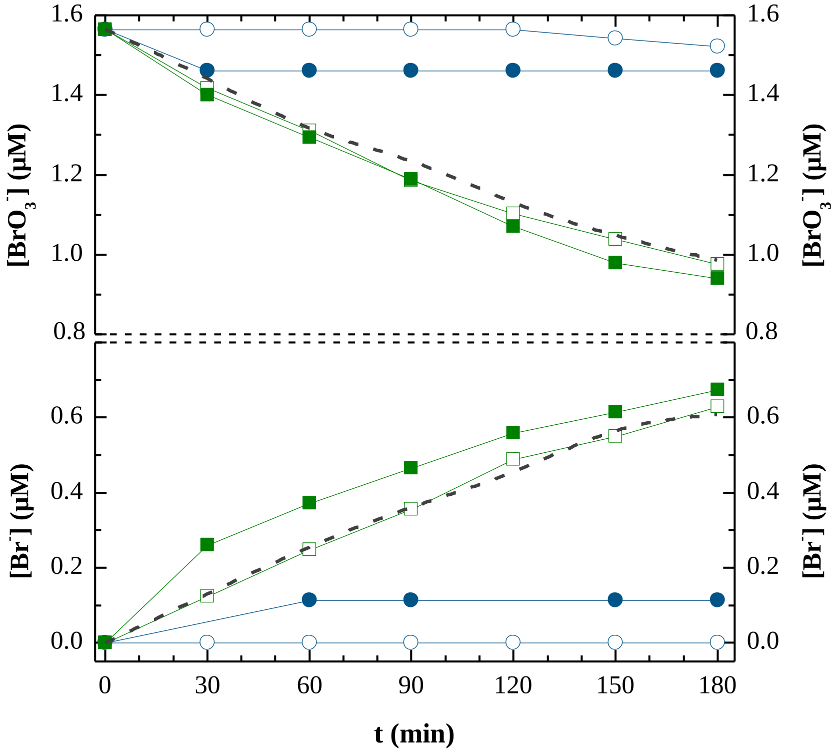

Figure 4. 1 – Influence of pH on BrO_3^- reduction mediated by Fe_2O_3 photocatalyst coated onto the BS. Open symbols: 20 mg Fe_2O_2, no light. Solid symbols: 20 mg Fe_2O_2, UVA-LEDs. No symbol (dashed line): no catalyst, no light. pH 3 (□, ■, - - -), solution pH (○, ●). Experimental conditions: $[BrO_3^-]_0 = 1.56$ µM, $Q = 75$ L h^{-1}, $T = 25$ ºC, [DO]: 232-263 µM.

Initially, a reaction at pH 3 with light was performed, resulting in a BrO_3^- reduction of 39.9% after 3 hours. To verify that adsorption of BrO_3^- on the catalyst surface was not occurring, a reaction in the same conditions but in the dark was performed, and it was verified that BrO_3^- concentration was decaying as well, allowing to achieve a BrO_3^- removal of 37.6%, which is very close to the value obtained using UVA-LEDs. Given these results and considering that batch adsorption tests have shown no adsorption of both BrO_3^- and Br^- ions onto the Fe_2O_3 surface at pH 3 (data not shown), a reaction at this pH without catalyst or light was also performed, in order to evaluate if the photoreactor alone could be having some influence in the reaction. In fact, it was checked a BrO_3^- reduction of 37.0%, thus corroborating the influence of the reactor materials on the reduction reaction.

As the photoreactor is made of acrylic, more specifically of polymethyl methacrylate (PMMA), an acidic hydrolysis of this ester could be occurring. PMMA hydrolysis results in the formation of a carboxylic acid, the methacrylic acid, and an alcohol, the methanol, according to Eq. (16) [97].

$$CH_2{=}C(CH_3)COOCH_3 + H_2O \rightarrow CH_2{=}C(CH_3)COOH + CH_3OH \qquad (16)$$

When the PMMA is hydrolyzed, changes in the carbon oxidation state (COS) are happening, which might be associated with the BrO_3^- reduction since electrons are being transferred. That is, while in PMMA, the average COS is -4/5, in its hydrolysis' products, namely methacrylic acid and methanol, the average COS is -1/2 and -2, respectively. Therefore, when the PMMA is hydrolyzed, an oxidation and a reduction might be occurring simultaneously. Taking into consideration that the ester redox potential is negative (between -2.3 and -1.4 V [98]) and BrO_3^- has a higher redox potential, the electrons generated in the oxidation reaction of the PMMA might preferably reduce the BrO_3^- molecule, thus, explaining the removal efficiencies obtained in the absence of light and photocatalyst at pH 3.

To reinforce this hypothesis and verify if this phenomenon still occurred at less acidic conditions, an experiment at a higher pH was performed. Accordingly, a reaction at the natural solution pH (without adjusting, $pH_{average} = 5.92$), with Fe_2O_3 and in the dark was performed, and only a 2.7% decay of BrO_3^- in a 3-hour reaction period was verified, which supports the hypothesis of the acidic hydrolysis of PMMA. So, it was decided that further reactions must all be performed at higher pH values.

Since at pH 3, the BrO_3^- reduction rate without catalyst is very close to the values obtained using Fe_2O_3 (with or without radiation), as it is showed in Table 4.1 and Figure 4.1, it was concluded that this catalyst was not working at low pH values. To understand the efficiency of the reaction using Fe_2O_3 as photocatalyst, at higher pH values, a reaction at the natural solution pH with UVA-LEDs radiation was also performed but the removal was only 6.6% in the same reaction period. Such weak performance could be associated with the short bandgap energy of this photocatalyst, which favors the recombination of the photogenerated e^-/h^+ pairs [43, 44]. For this reason, it was decided to test a different photocatalyst, with a higher bandgap energy, to prevent the recombination and improve the photocatalytic reaction. Therefore, TiO_2-P25 was chosen for all further experiments. Furthermore, since a total or nearly total reduction of BrO_3^- into Br^- was being achieved in all the experiments, the Br^- formation results will not be showed from now on.

4.1.2 Influence of dissolved oxygen content and addition of a sacrificial agent using TiO_2-P25 as photocatalyst

Several experiments were performed using TiO_2-P25 in different conditions: i) with DO and without addition of a SA; ii) without DO and without addition of a SA; iii) with DO and adding a SA; and iv) without DO and adding a SA. A pH of 5.5 was adopted for such reactions since it was an intermediate value between pH 3 and the pH of a fresh water (ca. 7.5), and it was selected by Zhang et al. [51] as the optimal value for BrO_3^- reduction using TiO_2-P25 as photocatalyst. As mentioned before, the SA can be an organic compound, such as a carboxylic acid, that is used as a scavenger of h^+ or $HO^\bullet$, in order to enhance photocatalytic reduction reactions [38]. So, CH_2O_2

was chosen as a SA, once according to Tan et al. [99], it has also demonstrated to be a good SA in the photocatalytic reduction of selenium anions using TiO_2 as photocatalyst and UV radiation. Formic acid concentration was selected according to the stoichiometry of the reaction, which corresponded to a $[BrO_3^-]$:$[CH_2O_2]$ molar ratio of 1:3 [56]. To evaluate the parameters mentioned earlier, a mass of 20 mg of a 2% wt. TiO_2-P25 aqueous suspension was deposited on the BS. A replicate of each reaction was performed to evaluate the replicability of the results. Figure 4.2 (a – d) compares the first and second reactions for each operational condition evaluated and Figure 4.2 (e – f) compares all the first and second reactions, respectively.

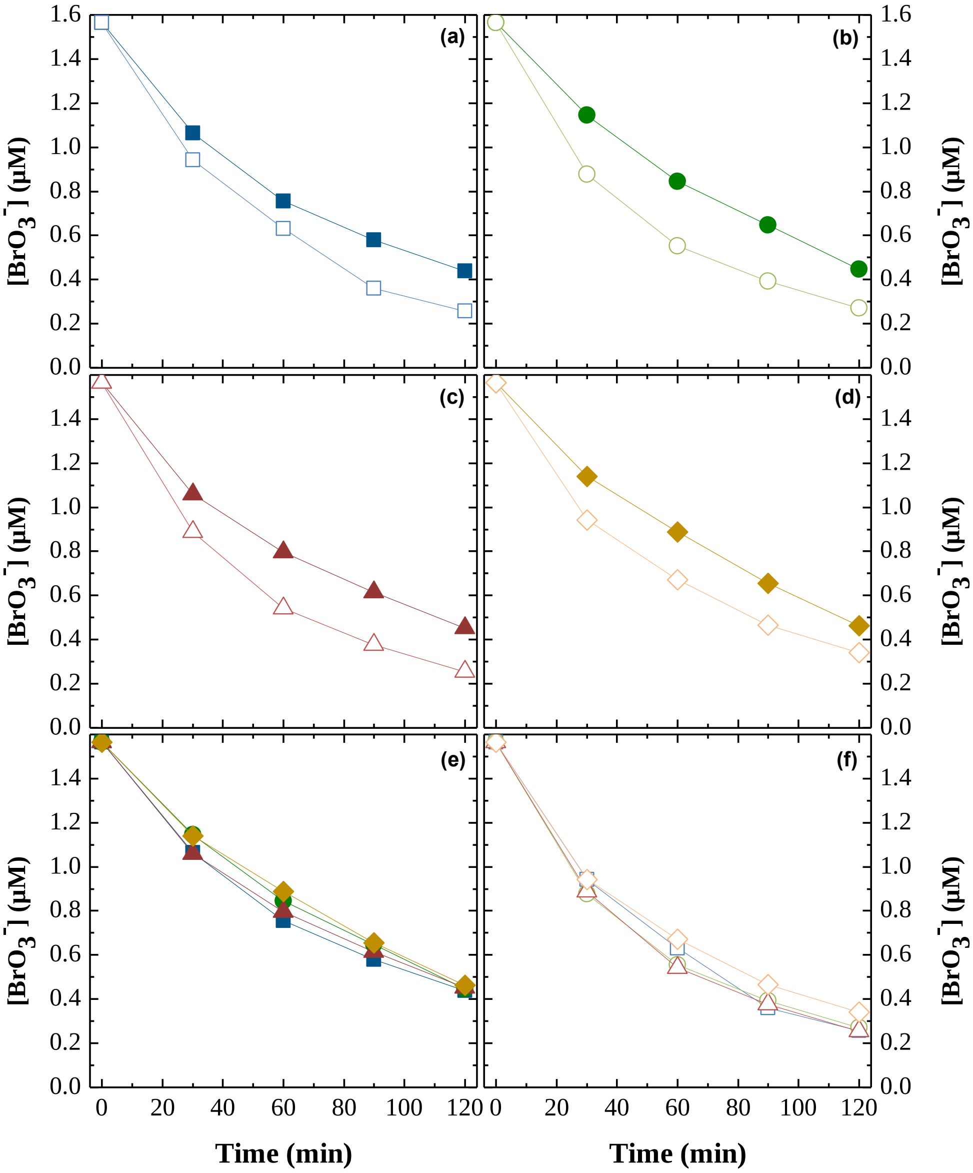

Figure 4. 2 – Influence of DO content and addition of CH_2O_2 as a SA on the BrO_3^- reduction by TiO_2-P25 photocatalyst deposited on the BS. Solid symbols: (e) first reactions. Open symbols: (f) second reactions. (a) With DO, without CH_2O_2 (■, □); (b) without DO, without CH_2O_2 (●, ○); (c) with DO, with CH_2O_2 (▲, △); (d) without DO, with CH_2O_2 (◆, ◇). Experimental conditions: $[BrO_3^-] = 1.56$ μM, pH 5.5, $Q = 75$ L h^{-1}, $T = 25$ ºC, UVA-LEDs 270 mW, 20 mg of TiO_2-P25.

As it is showed in Figure 4.2 (a – d), the BrO_3^- decay was visibly higher in the second reaction for each experimental condition. It is worth to mention that each operational condition was assessed in the same day, with the first reaction performed early in the morning and the second reaction performed around midday. Moreover, the reactions were performed in an uncontrolled environment, so the influence of some environmental conditions might be reflected in the results. It was verified that all the second reactions coincided with the hottest period of the day (midday), where the ambient temperature reached high values, between 30 and 35 ºC, in contrast with the morning reactions that were performed at an ambient temperature around 20 or 25 ºC. Such fact could be related with the performance of the LEDs used as illumination source. According to the Stefan-Boltzmann's law (Eq. (17)), the irradiated power per unit of area (I) of a body is proportional to the fourth power of its temperature (T), suggesting that an increment in room temperature could lead to an augmentation of the LEDs temperature, which could increase the irradiated power [100].

$$I = \varepsilon \sigma T^4 \tag{17}$$

where, I is the irradiated power per unit of area (W m^{-2}), ε is the emissivity of the body, σ is the Stefan-Boltzmann constant (5.672×10^{-8} W m^{-2} K^{-4}) and T is the temperature of the body (K). This could explain the differences in the results performed in the morning, where the ambient temperature was lower, with the results of the experiments performed during midday. However, further tests should be conducted in order to confirm the origin of such differences.

Therefore, it was concluded that all the reactions needed to be performed in a controlled environment that could maintain a constant ambient temperature, minimizing the external fluctuations and allowing a proper comparison between the experiments. So, the experimental setup was relocated to another laboratory where air-conditioning was installed, thus being possible to control the room temperature.

In addition, from Figure 4.2 and Table 4.1, it was possible to verify that there was no significant difference between all the first and second reactions, indicating that neither the presence of oxygen nor the presence of a SA had influence on the BrO_3^- photocatalytic reduction, as it will be explored in the next chapters. Furthermore, contrary to Fe_2O_3, TiO_2 showed good catalytic activity, reaching to removal efficiencies higher than 70% with pseudo-first-order kinetic constants between $(9.8 \pm 0.5) \times 10^{-3}$ and $(17 \pm 2) \times 10^{-3}$ min^{-1}.

4.2 BOROSILICATE GLASS SLAB EXPERIMENTS

4.2.1 Influence of pH, dissolved oxygen content, sacrificial agent addition and catalyst film reusability

In a controlled environment, fluctuations of the ambient parameters are reduced. So, the results were expected to be reproducible. For this reason, the replicability of the results was evaluated while varying the pH of the solution. The concentration of H^+ or HO^- ions in solution, controlled by the pH, will have an effect on the photocatalyst surface (Eq. (10) and (11)), which could interfere in the adsorption of the contaminants and, consequently, affect the photocatalytic reaction. Therefore, two different pH values were tested (6.5 and 5.5) using TiO_2-P25 deposited on the BS (Figure 4.3).

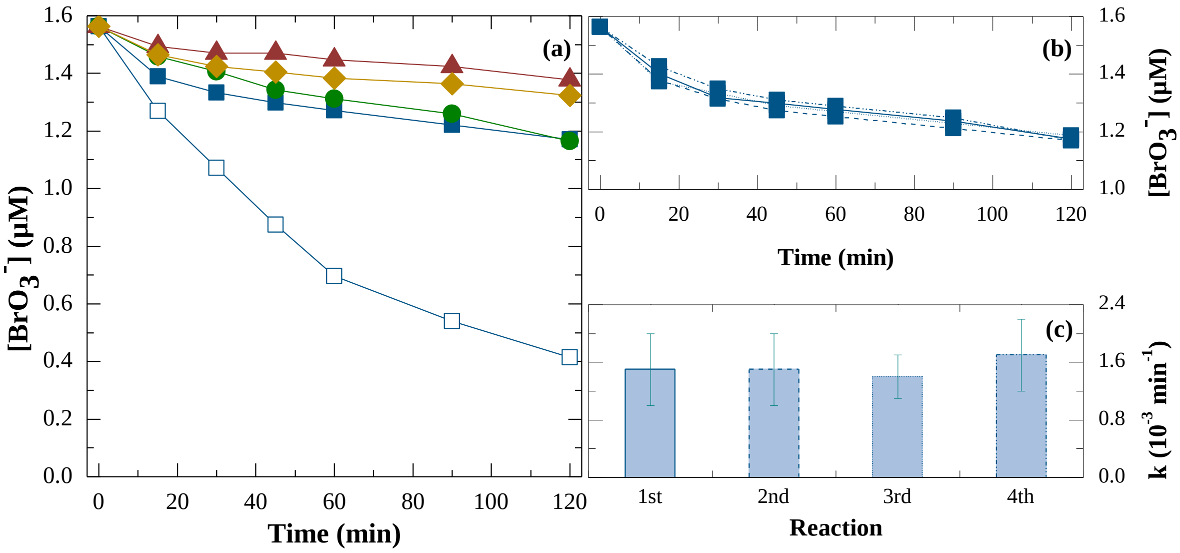

Figure 4. 3 – (a) Influence of pH, DO content and CH_2O_2 addition on the BrO_3^- reduction by TiO_2-P25 photocatalyst deposited on the BS. (b), (c) Replicates: 1st (———), 2nd (- - - - -), 3rd (· · · · ·), 4th (· · – · ·). Solid symbols: pH 6.5. Open symbols: pH 5.5. With DO, without CH_2O_2 (■, □); without DO, without CH_2O_2 (●); with DO, with CH_2O_2 (▲); without DO, with CH_2O_2 (◆). Experimental conditions: $[BrO_3^-] = 1.56$ µM, $Q = 75$ L h^{-1}, $T = 25$ °C, UVA-LEDs 270 mW, 20 mg of TiO_2-P25.

Four replicates at pH 6.5 were performed, three in the same day and a final one in the 12th use of the catalyst film (Figure 4.3 (b) and (c)), and it was observed that the kinetic constants were very similar, so it is possible to conclude with a 95% certainty that the results were replicable. At pH 6.5, a BrO_3^- removal of 25.2% in a 2-hour reaction period was obtained. When comparing with a further reaction performed at pH 5.5, a 7.8-fold increase in the kinetic constant (Table 7) was observed (BrO_3^- reduction of 73.5% after 2 hours) (Figure 4.3 (a)). Since pH_{PZC} of TiO_2-P25 is around 6.4 [101, 102], when the solution has a pH near to this value, the surface of TiO_2 has a neutral net charge (positive charges are in equilibrium with negative charges), which could cause electrostatic repulsion of anionic substances by the negative charges on the catalyst surface. On the other hand, as it was described earlier, when the solution pH is lower than pH_{PZC} (Eq. (10)), the TiO_2 surface becomes positively charged (positive charges predominate on its surface) and negatively charged compounds will be more attracted to its surface. This is of high importance since it will favor the adsorption of the pollutants on the catalyst surface and, thus, promote the contact between them and the reactive species [51].

Furthermore, for BrO_3^- reduction reaction to occur, 6 H^+ per BrO_3^- molecule are necessary (as shown in Eq. (2)) [51]. So, decreasing the pH increases the H^+ concentration in the solution which improves the reaction rate.

Zhang et al. [51] studied a large range of pH (1.5, 3, 5.5, 7.5, 9, 11.5 and 13.5) and reported in their experiments a higher BrO_3^- removal at pH 5.5 using TiO_2-P25 as photocatalyst, with a decrease in the efficiency when working at strong acidic or alkaline conditions. Moreover, they associated the decrease in efficiency at higher pH values with the decreasing of active sites for BrO_3^- adsorption. Marks et al. [56] also reported that, for several oxoanions photocatalytic reduction, including BrO_3^-, the decrease of pH improved the reaction rates. A 7.6-fold decrease on BrO_3^- kinetic constants was observed by Lin et al. [50] when the pH increased from 3 to 7, which is also agreement with the results here obtained.

Another important parameter, when applying photocatalytic reduction processes for pollutants removal, is DO since oxygen is an e^- acceptor and might compete with pollutants for the photogenerated electrons on the surface of the catalyst [42, 51]. To assess the oxygen influence, experiments were carried out with BrO_3^- synthetic solutions at pH 6.5, using 20 mg TiO_2-P25 deposited on the BS, with DO concentrations: (i) in a range of 232 – 263 μM, achieved only by the equilibrium with the atmosphere (no O_2 or air addition); and (ii) below 3.1 μM (detection limit of the DO probe), by injecting N_2 into the solution. It is important to point out that it was not possible to remove some air or N_2 bubbles inside the photoreactor that tended to accumulate near to the BS. This could impair the bromate mass transfer to the catalyst deposited on the BS.

Table 4. 2 – Operational conditions and pseudo-first-order kinetic constants for bromate reduction (k), calculated for the borosilicate glass slab experiments, along with the corresponding coefficient of determination (R^2) and residual variance (S^2_R).

BOROSILICATE GLASS SLAB

Experiment [a]	**pH$_{av.}$** [b]	**Light source**	**$m_{deposited}$ (mg)**	**DO (μM)**	**[BrO_3^-]:[CH_2O_2] molar ratio**	**Time (min)**	**k (× 10^{-3} min^{-1})**	**R^2**	**S^2_R (μM^2)**
Replicates									
4.3.1 – 1st replicate	6.40	LEDs 270 mW	20	[232 – 263]	----	0 – 120	1.5 ± 0.5 [c]	0.943	4.2×10^{-4}
4.3.2 – 2nd replicate	6.45	LEDs 270 mW	20	[232 – 263]	----	0 – 120	1.5 ± 0.5 [c]	0.949	3.5×10^{-4}
4.3.3 – 3rd replicate	6.45	LEDs 270 mW	20	[232 – 263]	----	0 – 120	1.4 ± 0.3 [c]	0.976	1.4×10^{-4}
4.3.4 – 4th replicate	6.39	LEDs 270 mW	20	[232 – 263]	----	0 – 120	1.7 ± 0.5 [c]	0.954	4.4×10^{-4}
Influence of pH, DO content and CH_2O_2 addition									
4.3.5 – with DO, no CH_2O_2	5.46	LEDs 270 mW	20	[232 – 263]	----	0 – 120	12.3 ± 0.9	0.992	1.3×10^{-3}
4.3.6 – with DO, no CH_2O_2	6.42	LEDs 270 mW	20	[232 – 263]	----	0 – 120	1.6 ± 0.2 [c, d]	0.981	1.4×10^{-4}
4.3.7 – without DO, no CH_2O_2	6.63	LEDs 270 mW	20	<3.1	----	0 – 120	2.0 ± 0.1 [c]	0.997	3.3×10^{-5}
4.3.8 – with DO, with CH_2O_2	6.38	LEDs 270 mW	20	[232 – 263]	1:3	0 – 120	0.7 ± 0.2 [c]	0.970	6.4×10^{-5}
4.3.9 – without DO, with CH_2O_2	6.42	LEDs 270 mW	20	<3.1	1:3	0 – 120	0.9 ± 0.2 [c]	0.961	1.1×10^{-4}
Influence of the catalyst film thickness									
4.4.1 – 10 mg	5.51	LEDs 270 mW	10	[232 – 263]	----	0 – 120	6.3 ± 0.6	0.982	1.3×10^{-3}
4.4.2 – 20 mg	5.46	LEDs 270 mW	20	[232 – 263]	----	0 – 120	12.3 ± 0.9	0.992	1.3×10^{-3}
4.4.3 – 40 mg	5.53	LEDs 270 mW	40	[232 – 263]	----	0 – 120	17 ± 1	0.996	8.5×10^{-4}

[a] Conditions: $[BrO_3^-]_0$ = 1.56 μM; TiO_2-P25 photocatalyst; Q = 75 L h^{-1}; T = 25 ºC; V_i = 1500 mL.

[b] Average of the pH values measured during the reaction.

[c] The pseudo-first-order kinetic constants were determined in the time interval from 15 to 120 min, without considering the first point (t = 0 min).

[d] Determined using the average of the replicates.

As it is observed from Table 4.2, the BrO_3^- removal was only slightly improved when N_2 was added to the solution at pH 6.5, with an increase of the kinetic constant of 1.3 times. Since both BrO_3^- and O_2 reduction reactions take place at the same locations, at higher solution pH the active sites for anions adsorption on the TiO_2 surface are reduced and the competition between BrO_3^- and O_2 could be higher. Therefore, when the DO content is reduced, fewer oxygen molecules will compete with BrO_3^- for the adsorption on the limited active sites of the catalyst and an improvement in the reaction rate is possible to occur. At lower pH values, this is less likely to occur since there are much more active sites on the surface of the catalyst for the adsorption of BrO_3^-, and the competition between BrO_3^- and O_2 might not be considerable. In the preliminary results (Figure 4.2), it was possible to conclude with 95% confidence that, at pH 5.5 using TiO_2-P25 as photocatalyst, the efficiencies did not suffer a considerable variation by the removal of DO from the solution.

Xie and Shang [103] reported a 35% decrease on the BrO_3^- removal when increasing the [DO] from 8 to 18 mg L^{-1}, however, when the DO content decreased from 8 to ca. 0 mg L^{-1}, only an 8% improvement was observed. Moreover, Wang et al. [104] verified that at pH 2.5 using TiO_2 as photocatalyst, the reduction of Cr(IV) in a N_2-purged system did not suffer an improvement, which means that at acidic pH values, the thermodynamic driving forces for O_2 and Cr(IV) reduction are similar. Other authors have reported a decrease in the photocatalytic reduction of BrO_3^- using TiO_2 [51], or in the amount of Cr(VI) photoreduced using ZnO as catalyst [105], when purging the DO content from the solution, which could indicate that the presence of oxygen might have other role in solution besides being just an e^- acceptor.

Therefore, it was concluded from this study that the removal of DO from the solution did not induce a considerable improvement on the reduction of BrO_3^- using TiO_2 as photocatalyst deposited onto the BS.

Relatively to the influence of the SA addition, some organic compounds can act as an $h^+/HO^\bullet$ scavenger, avoiding the e^-/h^+ recombination and producing strong reductive species. Therefore, the photocatalytic reduction of a substance/pollutant can occur: i) directly, by reacting with the e^- in the CB; or ii) indirectly, by the reaction between the pollutants and highly reductive species, generated by the oxidation of organic compounds in the VB. Carboxylic acids, such as formic acid (CH_2O_2), can be used as a SA since their reaction with $h^+/HO^\bullet$ could form the CO_2 radical ($E^o(CO_2/{}^\bullet CO_2^-) = \sim -2.0$ V), as follows [38, 106]:

$$CH_2O_2 + HO^\bullet \rightarrow CO_2^{\bullet-} \tag{18}$$

Two reactions at pH 6.5, adding formic acid in the $[BrO_3^-]:[CH_2O_2]$ molar ratio of 1:3 (stoichiometric ratio), were performed, one with N_2 injection, to purge the DO, and the other without removing the oxygen. As it is observed in Figure 4.3 (a), the addition of CH_2O_2 as SA caused a decrease on the reaction efficiency, especially when [DO] was in the range of 232 – 263 μM. From the results in Table 4.2, it is possible to verify that the reaction rate decreased 2.2 times with the addition of CH_2O_2, in the presence of DO. The same was also verified in the reactions performed with injection of N_2, where a 2.3 decrease in the reaction rate was obtained by adding CH_2O_2. It was observed that purging the DO from the solution, prior to the addition of the SA, resulted in a smaller decrease of the reaction rate since there were less O_2 molecules competing for the active sites, contrary to what happens in the reaction with O_2 and CH_2O_2, where both will be competing for the adsorption sites on the catalyst surface.

Tan et al. [99] used different organic compounds (formic acid, methanol, ethanol, acetic acid, salicylic acid and sucrose) as SA for the TiO_2-driven photocatalytic reduction of selenium ions and verified that the fastest reduction rates were achieved using CH_2O_2 (at pH 3, with N_2 injection). They suggested that the good performance of CH_2O_2 was related with the fact that this organic molecule is relatively small and, at the solution pH in which the reactions were performed, CH_2O_2 could be ionized ($pK_a = 3.75$) into formate ions (CHO_2^-). This anion would be more predisposed to adsorb on the positively charged TiO_2 surface, which was proved by the higher CH_2O_2 adsorption (0.73 mg C g^{-1} TiO_2) on the TiO_2 surface when selenium ions were present in solution. Higher adsorption of CH_2O_2 promotes the contact between the organic substance and the h^+ or $HO^\bullet$, which ensures the scavenging of these oxidizing species and might promote the formation of strong reducing species. Furthermore, they also obtained higher selenium reductions in the presence of CH_2O_2 when the DO was purged from the system by addition of N_2, which they found to be related with the CH_2O_2 capability to react with the oxygen in the TiO_2 matrix. Hérissan et al. [107] performed the photocatalytic reduction of nitrate in the presence of CH_2O_2, using TiO_2 as photocatalyst and a $[NO_3^-]$:$[CH_2O_2]$ molar ratio of 1:5 (to assure that CH_2O_2 was not the limiting agent as the molar ratio based on the stoichiometry of the reaction was 1:4). They verified that higher concentrations of CH_2O_2 did not improve the efficiency of the reaction since there was a higher competition for the adsorption sites between CH_2O^- and NO_3^-. These authors also verified that the presence of DO in solution was not desirable since O_2 molecules compete with NO_3^- for the e^- on the TiO_2 surface. Wang et al. [104] carried out a series of experiments for the photocatalytic reduction of Cr(VI), using different photocatalysts (TiO_2, ZnO and ZnS) and with the addition of CH_2O_2 (20 mM) as a SA. They observed that for TiO_2 and ZnO, the increase of solution pH resulted in lower removal efficiencies (ca. 46% decrease when the pH increased from 2.5 to 6), which they assumed to be related to the decrease of positive charges on the TiO_2 surface with the increase of pH. At $pH > 6$, the larger amount of negative charges resulted in greater electrostatic repulsion between the TiO_2 surface and both Cr(VI) ions and $COO^{\bullet-}$ radicals (pK_a $[HCOO^\bullet/COO^{\bullet-}] = 1.4$), which interfered with the adsorption of those molecules onto the catalyst surface and, consequently, with the photocatalytic reaction. The authors have also found that with the increase of pH, more $COO^{\bullet-}$ molecules would be repulsed by TiO_2 into the bulk solution and be free to reduce the pollutants. However, this increase in free radicals was not reflected on the reaction rates, which means that the reaction mainly occurs through direct reaction with the e^- on the surface of the catalyst and not by reaction with the free $COO^{\bullet-}$ radicals.

Since this work was performed at pH 6.5, which is close to the pH_{PZC} = 6.4 of TiO_2-P25 [101, 102], the surface of TiO_2 would be very close to neutrality, with fewer positive charges when compared with lower pH values, and the adsorption of BrO_3^- onto its surface could be reduced. Moreover, a $[BrO_3^-]$:$[CH_2O_2]$ molar ratio of 1:3 could saturate the catalyst surface due to the high amount of CH_2O_2 molecules in solution and then reduce the efficiency of the photocatalytic process by blocking the active sites for BrO_3^- adsorption. In the presence of high DO concentrations, the competition between BrO_3^- and O_2 for e^- was even greater. In this case, BrO_3^- removal efficiencies were lower than when DO was purged from solution, since in the latter the competition would not be considerable and more e^- would be available for the BrO_3^- reduction. However, in both cases, the addition of a SA had a negative effect on the reaction rate.

During the reactions with the addition of CH_2O_2, the molar ratio of $[BrO_3^-]$:$[CH_2O_2]$ was not maintained constant, which allowed to observe the SA consumption behaviour during the reaction. Therefore, CH_2O_2 was found to be consumed relatively fast during the beginning of the reaction (when the ratio between BrO_3^- and CH_2O_2 was superior), and then the consumption starts slowing down (data not shown). This fast depletion of CH_2O_2 in solution can be related with its shorter reaction pathway, during which e^- can be generated, which diminishes the reducing power of CH_2O_2 when compared to other SAs [108].

For these reasons, one can conclude that the addition of CH_2O_2 in a $[BrO_3^-]$:$[CH_2O_2]$ molar ratio of 1:3 did not enhance the photocatalytic reduction, in fact, it actually worsens the reduction of BrO_3^-. So, it was decided to perform further experiments without the addition of a SA. In the future, different CH_2O_2 concentrations and different SAs shall be used, since they might have a different behaviour in BrO_3^- solutions.

4.2.2 Influence of catalyst film thickness

Lastly, the influence of the catalyst film thickness was assessed by depositing 10, 20 and 40 mg of catalyst on the BS (Figure 4.4). As before, a 2% wt. TiO_2-P25 aqueous suspension was used, as described in section 3.3. The reactions were performed at pH 5.5 since, as it was mentioned earlier, better reaction rates were obtained. For all the film thicknesses evaluated, three replicates were conducted and the average was used for comparison. The experimental conditions and the pseudo-first-order kinetic constants obtained for each film thickness are presented in Table 4.2.

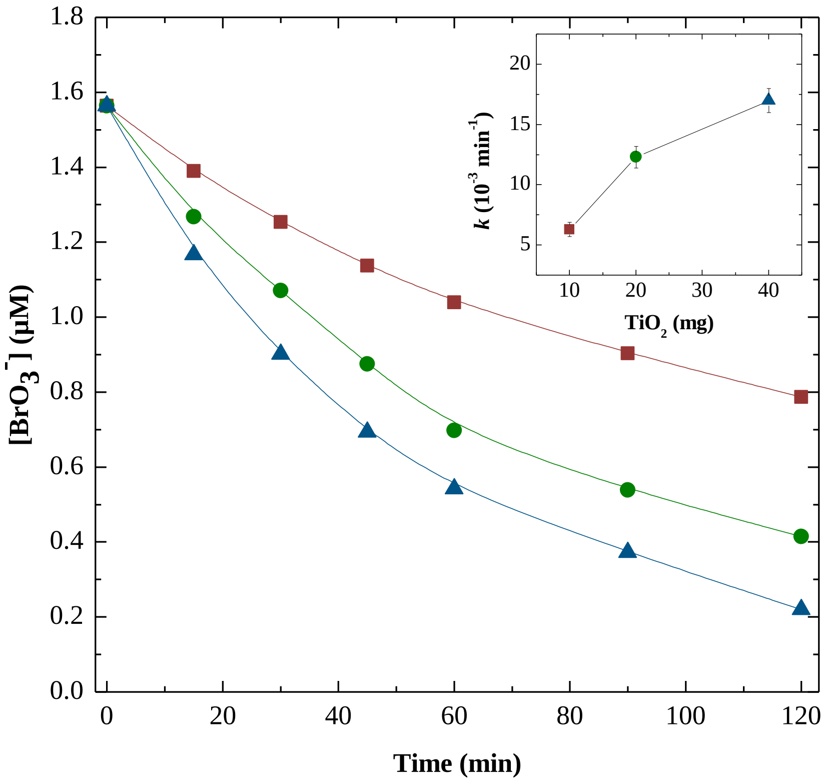

Figure 4. 4 – Influence of catalyst film thickness on the BrO_3^- reduction by TiO_2-P25 photocatalyst deposited on the BS. Mass of catalyst: 10 mg (■); 20 mg (●); 40 mg (▲). Experimental conditions: $[BrO_3^-]$ = 1.56 μM, pH 5.5, Q = 75 L h^{-1}, T = 25 ºC, [DO]: 232-263 μM, UVA-LEDs 270 mW.

In the experiments performed with 10 mg of TiO_2-P25 (film thickness of 0.19 μm) deposited on the BS, only 49.7% of BrO_3^- was reduced after 2-hour irradiation. When doubling the mass of catalyst to 20 mg (film thickness of 0.37 μm), a 73.5% BrO_3^- removal efficiency was achieved, corresponding to a 2-fold increase on the kinetic constants (Table 4.2), which is in accordance with the 2-fold increase of the film thickness. However, an increase of the catalyst mass to 40 mg (film thickness of 0.74 μm), only improved 1.4 times the reaction rate, which corresponded to 85.9% BrO_3^- removal efficiency. Overall, a 2.8-fold increase on the reduction rate was observed with the increment of catalyst amount from 10 to 40 mg. This behavior suggests that the optimum TiO_2 dose should be near to 40 mg, corresponding to a film density of 0.30 mg cm^{-2} (considering A_{BS} = 135 cm^2).

When the catalyst is deposited on the BS, a BSI mechanism is present, which means that the e^-/h^+ pairs will be generated on the opposite site of the liquid-catalyst interface where the pollutants are adsorbed. As it is expected for a BSI mechanism, the reaction rate reaches a maximum value and an additional increase on the catalyst film thickness lead to lower reaction rates since the charge carriers are generated far from the catalyst-liquid interface, enhancing the electron/hole recombination [58]. In order to overcome these limitations, the catalyst should be deposited in the channels and chambers of the photoreactor, allowing a FSI mechanism, as it will be further demonstrated in this chapter.

In these experiments, it was not possible to observe the decay of the reactions rates. In the future, additional experiments with a superior (> 0.74 μm) and inferior film thickness (between 0.37 and 0.74 μm) should be conducted in order to verify this phenomenon and to ensure the optimum catalyst film thickness.

4.3 STAINLESS STEEL SLAB EXPERIMENTS

As it was mentioned before, there are several limitations in photocatalytic processes that may affect the reduction reactions of the pollutants in solution. A series of experiments were conducted with a SSS as catalyst support on the NETmix photoreactor, since this reactor design allowed to overcome some limitations mentioned in chapter 2.4.1. Therefore, a 2% wt. TiO_2-P25 aqueous suspension was used for the spray deposition of the catalyst on the channels and chambers of the NETmix photoreactor.

4.3.1 Influence of solution pH and dissolved oxygen content

Even though the optimal pH in the BS was 5.5, it is still important to assess the influence of this parameter when the catalyst is deposited onto the SSS, since this reactor configuration allows a higher catalyst surface area per reactor volume, which enhances the efficiency of the reaction. Hence, three pH values (5.5, 6.5 and 7.5) were evaluated, as it is shown in Figure 4.5, in order to get as close as possible to the pH of a fresh water in a WTP (see Table 3) but still obtaining good efficiencies. The operational parameters and the pseudo-first-order kinetic constants are represented in Table 4.3.

As was verified for the BS experiments, the BrO_3^- reduction rates using the SSS as catalyst support decreased with the increase of pH, which was related with the depletion of positive charges when approaching the pH_{PZC} of TiO_2-P25 (ca. 6.4 [101, 102]), and with the fact that above PZC the TiO_2 surface is negatively charged and electrostatic repulsions occur between the catalyst surface and the negatively charged BrO_3^- molecules [36, 41, 64].

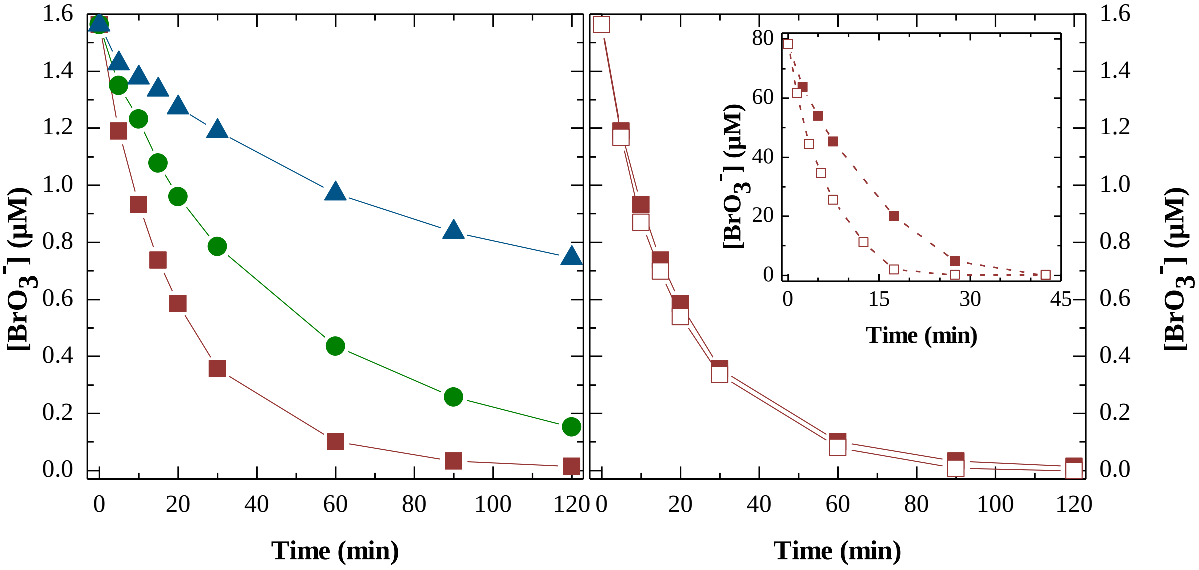

Figure 4. 5 – Influence of pH and DO content on the BrO_3^- reduction by TiO_2-P25 photocatalyst deposited on the SSS. Reactor: NETmix photoreactor (———); Batch photoreactor (- - - - -). Solid symbols: [DO]: 232-263 μM (without N_2 injection). Open symbols: [DO] < 3.1 μM (with N_2 injection). Solution pH: 5.5 (■, □), 6.5 (●), 7.5 (▲). Experimental conditions: $[BrO_3^-]$ = 1.56 μM, Q = 75 L h^{-1}, T = 25 ºC, UVA-LEDs 270 mW, 15 mL of a 2% wt. TiO_2-P25 aqueous suspension.

BrO_3^- removal at pH 5.5 was ca. 99% in a 2-hour period, but when the solution pH was increased to 6.5 and 7.5, the BrO_3^- decay was 90.3% and 52.4%, respectively. As it is represented in Table 4.3, the increment of pH from 5.5 to 6.5 resulted in a 55% drop on the BrO_3^- reaction rate and a further increase from pH 6.5 to 7.5 led to a 73% reduction on the BrO_3^- photoreduction rate. Overall, an 8.3-fold decrease on the BrO_3^- reaction rate occurred when the pH was changed from 5.5 to 7.5. Using as an example a WTP in the Region of Porto (Portugal), a chemically treated fresh water from that treatment plant has a pH around 7.4 (see Table 3), which implies that if a photocatalytic reduction process for BrO_3^- removal is proposed to be incorporated in the treatment line, it would be necessary a preliminary acidification step to allow the pH correction to values near 6.5. Besides, a further pH correction step can be also required to achieve values near 7.0. So, it is very important to study the application of a photocatalytic process to a fresh water treatment at different pH values, in order to determine the highest pH possible for the treatment without significantly losing efficiency, which it will be done in the section 4.3.4.

Table 4. 3 – Operational conditions and pseudo-first-order kinetic constants for bromate reduction (k), calculated for the stainless steel slab experiments performed, along with the corresponding coefficient of determination (R^2) and residual variance (S^2_R).

STAINLESS STEEL SLAB									
Experiment	**pH$_{av.}$**[b]	**Light source**	**$V_{deposited}$ (mL)**	**$m_{deposited}$**[c] **(mg)**	**DO (μM)**	**Time (min)**	**k (× 10^{-3} min^{-1})**	**R^2**	**S^2_R (μM^2)**
Influence of solution pH									
4.5.1 – pH 5.5[a]	5.52	UVA-LEDs 270 mW	15	286.7	[232 – 263]	0 – 120	50 ± 2	0.999	2.3×10^{-4}
4.5.2 – pH 6.5[a]	6.44	UVA-LEDs 270 mW	15	285.8	[232 – 263]	0 – 120	22 ± 2	0.995	1.3×10^{-3}
4.5.3 – pH 7.5[a]	7.37	UVA-LEDs 270 mW	15	285.8	[232 – 263]	0 – 120	6.0 ± 0.7[d]	0.990	7.5×10^{-4}
Influence of the DO content									
4.5.4 – DO presence[a]	5.52	UVA-LEDs 270 mW	15	285.8	[232 – 263]	0 – 120	50 ± 2	0.999	2.3×10^{-4}
4.5.5 – DO absence[a]	5.54	UVA-LEDs 270 mW	15	285.8	<3.1	0 – 120	54 ± 2	0.999	4.2×10^{-4}
4.5.6 – Batch[e]	5.55	150 W mercury vapor lamp[f]	----	[g]	[232 – 263]	0 – 42.5	80 ± 9	0.995	5.0
4.5.7 – Batch[e]	5.50	150 W mercury vapor lamp[f]	----	[g]	<3.1	0 – 42.5	156 ± 9	0.997	2.0
Influence of the catalyst film thickness									
4.6.1 – 10 mL[a]	5.52	UVA-LEDs 270 mW	10	192.5	[232 – 263]	0 – 120	40 ± 4	0.992	2.3×10^{-3}
4.6.2 – 15 mL[a]	5.52	UVA-LEDs 270 mW	15	286.7	[232 – 263]	0 – 120	50 ± 2	0.999	2.3×10^{-4}
4.6.3 – 20 mL[a]	5.51	UVA-LEDs 270 mW	20	381.2	[232 – 263]	0 – 120	50 ± 2	0.998	5.7×10^{-4}
Influence of radiation intensity									
4.6.4 – LEDs 270 mW[a]	5.52	UVA-LEDs 270 mW	15	286.7	[232 – 263]	0 – 120	50 ± 2	0.999	2.3×10^{-4}
4.6.5 – LEDs 1400 mW[a]	5.52	UVA-LEDs 1400 mW	15	285.8	[232 – 263]	0 – 120	61 ± 5	0.995	1.6×10^{-3}
4.6.6 – LEDs 270 mW[a]	5.51	UVA-LEDs 270 mW	20	381.2	[232 – 263]	0 – 120	50 ± 2	0.998	5.7×10^{-4}
4.6.7 – LEDs 1400 mW[a]	5.52	UVA-LEDs 1400 mW	20	381.2	[232 – 263]	0 – 120	61 ± 4	0.995	1.3×10^{-3}
Influence of the photoreactor, photolysis and adsorption of BrO_3^-									
4.6.8[a]	5.54	No light	15	286.7	[232 – 263]	0 – 120	[h]	[h]	[h]
4.6.9[a]	5.57	No light	0	0	[232 – 263]	0 – 120	[h]	[h]	[h]
4.6.10[a]	5.53	UVA-LEDs 270 mW	0	0	[232 – 263]	0 – 120	[h]	[h]	[h]

STAINLESS STEEL SLAB									
Experiment	**$pH_{av.}$ [b]**	**Light source**	**$V_{deposited}$ (mL)**	**$m_{deposited}$ [c] (mg)**	**DO (μM)**	**Time (min)**	**k ($\times 10^{-3}$ min^{-1})**	**R^2**	**S^2_R (μM^2)**
Influence of the Temperature									
4.7.1 – 15 ºC [i]	5.50	UVA-LEDs 270 mW	15	287.6	[232 – 263]	0 – 120	41 ± 3	0.994	1.7×10^{-3}
4.7.2 – 20 ºC [i]	5.51	UVA-LEDs 270 mW	15	287.6	[232 – 263]	0 – 120	42 ± 4	0.993	1.9×10^{-3}
4.7.3 – 25 ºC [i]	5.52	UVA-LEDs 270 mW	15	286.7	[232 – 263]	0 – 120	50 ± 2	0.999	2.3×10^{-4}
4.7.4 – 30 ºC [i]	5.51	UVA-LEDs 270 mW	15	287.6	[232 – 263]	0 – 120	50 ± 4	0.994	1.8×10^{-3}
Influence of the fresh water matrix									
4.8.1 – SW pH 5.5 [a]	5.52	UVA-LEDs 270 mW	15	286.7	[232 – 263]	0 – 120	50 ± 2	0.999	2.3×10^{-4}
4.8.2 – SW pH 6.5 [a]	6.44	UVA-LEDs 270 mW	15	285.8	[232 – 263]	0 – 120	22 ± 2	0.995	1.3×10^{-3}
4.8.3 – SW pH 7.5 [a]	7.37	UVA-LEDs 270 mW	15	285.8	[232 – 263]	0 – 120	6.0 ± 0.7 [d]	0.990	7.5×10^{-4}
4.8.4 – FW pH 5.5 [a]	5.52	UVA-LEDs 270 mW	15	287.6	[232 – 263]	0 – 120	23 ± 1	0.999	3.1×10^{-4}
4.8.5 – FW pH 6.5 [a]	6.53	UVA-LEDs 270 mW	15	287.6	[232 – 263]	0 – 120	8.9 ± 0.4	0.996	4.5×10^{-4}
4.8.6 – FW pH 7.5 [a]	7.40	UVA-LEDs 270 mW	15	287.6	[232 – 263]	0 – 120	4.0 ± 0.1	0.997	1.2×10^{-4}

[a] Conditions: $[BrO_3^-]_0 = 1.56$ μM; TiO_2-P25 photocatalyst; $Q = 75$ L h^{-1}; $T = 25$ ºC; $V_i = 1500$ mL.

[b] Average of the pH values measured during the reaction.

[c] Taking into account the mass loss (< 5%).

[d] Determined using the average of the replicates

[e] $[BrO_3^-]_0 = 78$ μM; TiO_2-P25 photocatalyst; $T = 25$ ºC; $V = 800$ mL.

[f] UV-Immersion lamp (150 W): medium-pressure mercury vapor lamp with an emission spectrum in the UV range above 190 nm.

[g] 100 mg L^{-1} of TiO_2-P25 in suspension.

[h] Not adjustable to a pseudo-first-order kinetic model.

[i] Conditions: $[BrO_3^-]_0 = 1.56$ μM; TiO_2-P25 photocatalyst; $Q = 75$ L h^{-1}; $V_i = 1500$ mL.

As mentioned earlier for the BS experiments, it was observed some bubbles (air or N_2) inside the photoreactor that could not be purged from the system and that tended to accumulate on top, near to the BS. While these bubbles could cause some mass transfer limitations when the catalyst was deposited on the BS, when the catalyst is deposited on the channels and chambers of the NETmix photoreactor their interference should be less significant. Therefore, it was also assessed the influence of the DO content using TiO_2 as photocatalyst supported on the SSS. To this end, an experiment at pH 5.5 with injection of N_2 into the BrO_3^- solution (until reaching a DO concentration below 3.1 μM) was performed and then compared with a reaction at pH 5.5 with [DO] within a range of 232 – 263 μM.

From Figure 4.5, it was possible to observe that purging the oxygen from the solution did not have a considerable effect on the reaction rate, which is proven by the 1.1-fold (~ 8%) increase on the BrO_3^- reaction rate when [DO] < 3.1 μM. This value was not in accordance with the experimental results obtained in a batch photoreactor, where a 2-fold increase of the kinetic constant was observed when the DO was purged from the system. Since the NETmix photoreactor has a lot of inlets points, some air might be entering the system and preventing the DO concentration to reach values close to zero μM.

Since the detection limit of the DO probe is 3.1 μM, it was not possible to guarantee the complete absence of DO. Furthermore, as the detection limit is almost the double of the initial concentration of BrO_3^- in solution, a competition between oxygen and BrO_3^- for the adsorption sites on the catalyst surface may still occur with the injection of N_2. Hence, the injection of N_2 for the DO removal from the solution did not have a significant influence on the BrO_3^- reduction, whether the catalyst was deposited on the BS or on the SSS of the NETmix photoreactor.

4.3.2 Influence of the catalyst film thickness and illumination intensity

In chapter 2.3.2.1. it was mentioned that increments on the catalyst mass improves the photocatalytic reaction, due to higher catalyst surface area available for degradation of the pollutants, until it reaches an optimum dose of catalyst [58]. Therefore, in order to evaluate the catalyst film thickness, different volumes of a 2% wt. TiO_2-P25 aqueous suspension were deposited on the SSS and the BrO_3^- decay was assessed (Figure 4.6): i) 10 mL (film thickness of 1.78 μm); ii) 15 mL (film thickness of 2.65 μm); and iii) 20 mL (film thickness of 3.53 μm). Three replicates of each film thickness were performed and the average was used for comparison.

Prior to these experiments, a reaction without catalyst and without light was performed, in order to verify if the composition of the photoreactor had an effect on the BrO_3^- removal and, then, the same experiment but with light (UVA-LEDs 270mW) was conducted to evaluate if BrO_3^- photolysis could occur. For both reactions, a slight BrO_3^- decay (< 2.5%) was observed, which revealed that BrO_3^- did not reacted with the light or with the photoreactor material. Furthermore, a reaction in the dark with 15 mL of TiO_2 deposited on the SSS also shown a negligible adsorption (2.5 %) of BrO_3^-. Hence, it is possible to conclude that the photoreactor material did not have an influence on the BrO_3^- removal and that this compound was not removed by photolysis or adsorption on the TiO_2 surface.

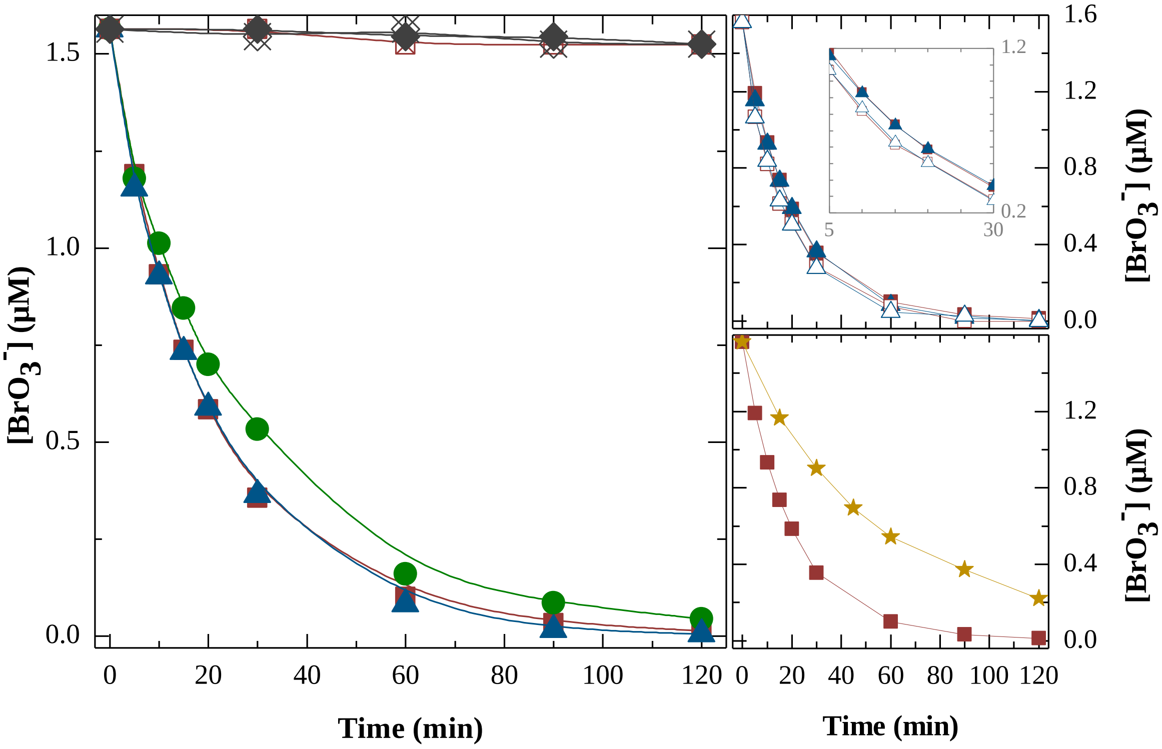

Figure 4. 6 – Influence of the catalyst film thickness and illumination intensity on the BrO_3^- reduction by TiO_2-P25 photocatalyst deposited on the SSS and comparison with the BS (★) best result (40 mg of TiO_2, pH 5.5, $[BrO_3^-] = 1.56$ μM, $Q = 75$ L h^{-1}, $T = 25$ °C, [DO]: 232-263 μM, without CH_2O_2). Solid symbols: with catalyst, UVA-LEDs 270 mW. Open symbols: with catalyst, UVA-LEDs 1400 mW. Crossed symbols: no light. TiO_2-P25 deposited on the SSS: 0 mL (◆, ※), 10 mL (●), 15 mL (■, □, ☒), 20 mL (▲, △). Experimental conditions: $[BrO_3^-] = 1.56$ μM, pH 5.5, $Q = 75$ L h^{-1}, $T = 25$ °C, [DO]: 232-263 μM.

The catalyst film thickness experiments revealed that a TiO_2-P25 mass of 286.7 mg (15 mL of a 2% wt. TiO_2-P25 aqueous suspension deposited on the SSS) corresponded to the best film thickness (2.65 μm), with a 99.1% BrO_3^- removal in a 2-hour reaction time. An increment on the film thickness from 1.78 to 2.65 μm (film density from 0.7 to 1.1 mg cm^{-2}) led to a 1.3-fold increase on the reduction rate (Table 4.3). However, when the film thickness was increased from 2.65 μm to 3.53 μm (film density from 1.1 to 1.4 mg cm^{-2}), almost no improvement on the reaction rate was observed (~ 1%). This is in good agreement with the results reported in the literature [34, 58, 59] for a FSI mechanism, since after a certain catalyst film thickness the diffusional length of the charge carriers to the catalyst–liquid interface does not change. This performance means that the optimal value is 286.7 mg (15 mL) of TiO_2-P25, which corresponds to a film density of 1.1 mg cm^{-2}. Furthermore, the TiO_2 films deposited on the SSS by the spray technique showed good adherence and stability after 13 consecutive reactions.

Comparing the FSI with the BSI mechanism (film thicknesses of 2.65 and 0.74 μm, respectively) under the best conditions, one can conclude that the photocatalyst reactivity in combination with the photoreactor was improved 2.9 times, from 41 to 118 μmol BrO_3^- $m^{-3}{}_{\text{illuminated volume}}$ s^{-1}. For this reactor configuration (FSI mechanism), a catalyst surface illuminated area per reactor volume of 989 m^2 m^{-3} was obtained. Comparing with the BSI mechanism, which only allowed 333 m^2 m^{-3}, the FSI mechanism resulted in a 3-fold increase on the catalyst surface area per reactor volume, which is in concordance with the 2.9-fold increase on the photocatalyst reactivity when FSI was used.

The influence of the illumination intensity was also evaluated by comparing two UVA-LEDs (365 nm) sources, one with an output power of 270 mW and other with 1400 mW, for the optimal conditions obtained so far, using two catalyst film thicknesses: 15 and 20 mL of TiO_2-P25. By analyzing Figure 4.6, the BrO_3^- decay did not seem to have suffered a substantial increase with a 5.2-fold increment of the LEDs output power. However, when determining the pseudo-first-order kinetic constants (Table 4.3), it was possible to observe a 1.23-fold and a 1.21-fold increase on the reaction rate, using a SSS deposited with 15 and 20 mL of TiO_2-P25, respectively, irradiated with UVA-LEDs 1400 mW. An enlargement of the section of the graph, where these differences are more visible, is represented in Figure 4.6.

The illumination of a determined catalyst film thickness with a more powerful light source enhances the probability of more activated sites being generated on the surface of the TiO_2 and promotes the re-excitation of the recombined e^-/h^+ pairs [63]. Venkatachalam et al. [109] studied the effect of illumination intensity, in a range from 16 to 64 W, on the degradation of 4-chlorophenol by TiO_2 nanoparticles doped with Zr^{4+} and verified that increasing the light intensity led to an increase on the degradation of this compound. The authors concluded that higher illumination intensities increase the probability of excitation of the catalyst particles and re-excitation of recombined electrons. Therefore, the increment on the reaction rates (Figure 4.6) verified for the increase in the irradiation intensity is in accordance with the literature. Nevertheless, for the reactions with the UVA-LEDs 1400 mW, raising the catalyst film thickness from 2.65 μm to 3.53 μm still did not have an effect on the BrO_3^- reduction rates.

Since the increment of the reaction rate was much lower when compared with the increment on the LEDs output power, it was decided to pursue the experiments using the LEDs with lower irradiance.

4.3.3 Influence of temperature

As mentioned in chapter 2.3.2.5, variations in temperature between 20 and 80 ºC are not expected to have a drastic effect on the reaction rates, since the apparent activation energy within this range is often very small [64]. Evgenidou et al. [110] studied the influence of temperature on dichlorvos (10 mg L^{-1}) degradation rate for both TiO_2 (100 mg L^{-1}, pH 6.2) and ZnO (500 mg L^{-1}, pH 7.4) photocatalysts and they verified a slight increase in the reaction rate with the increase of temperature. Likewise, the studies conducted by Chen and Ray [67] for the degradation of 4-nitrophenol (200 ppm) using TiO_2 photocatalyst (2 g L^{-1}) on a temperature range from 15 to 50 ºC revealed a linear increase of the reaction rate with the temperature. Both studies concluded that these results could be related to a higher collision frequency of molecules with the catalyst. They also referred that since the bandgap of the catalyst is too high to overcome by thermal excitation, the generation of the e^-/h^+ pairs is mainly achieved by irradiation.

Therefore, the influence of temperature variation in BrO_3^- removal was assessed by testing different values of temperature (15, 20, 25 and 30 ºC) on the best experimental conditions. Figure 4.7 represents the decay in BrO_3^- concentration, during a 2-hour reaction period, for the different temperatures assessed and shows the pseudo-first-order kinetic constants obtained for each temperature (see also Table 4.3).

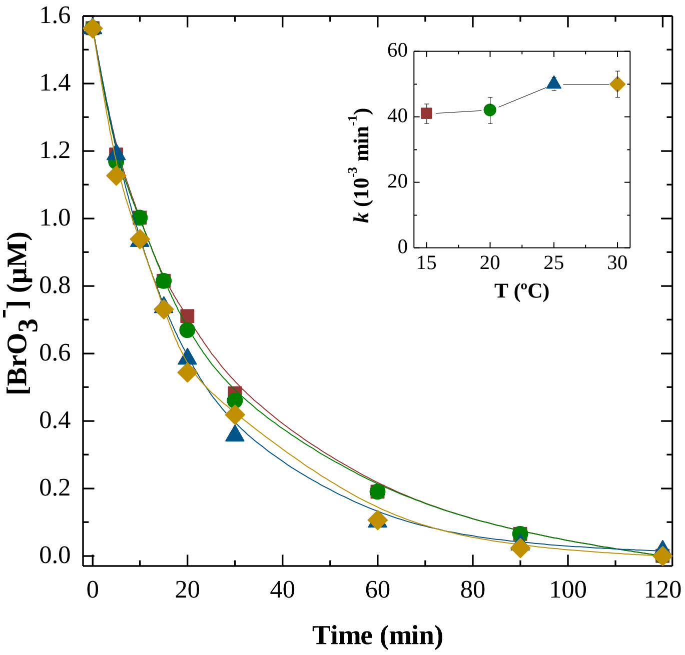

Figure 4. 7 – Influence of temperature on the BrO_3^- reduction by TiO_2-P25 photocatalyst deposited on the SSS. Temperature: 15 ºC (■); 20 ºC (●); 25 ºC (▲); 30 ºC (◆). Experimental conditions: [BrO_3^-] = 1.56 μM, pH 5.5, Q = 75 L h^{-1}, UVA-LEDs 270 mW, [DO]: 232-263 μM, 15 mL of a 2% wt. TiO_2-P25 aqueous suspension.

It was observed that there was no major difference in the reaction rates, except when the temperature was increased from 20 to 25 ºC where a 14.8% increase was attained. Taking into account the confidence interval for both kinetic constants (Table 4.3), the difference was negligible. Overall, one can conclude that small increments in temperature led to a minor increase on the reaction rate, as it was previously seen on the literature.

4.3.4 Influence of a fresh water matrix

The previous experiments demonstrated good results for the application of heterogeneous photocatalysis for BrO_3^- reduction on a synthetic water (UPW spiked with BrO_3^-). However, it is important to access the applicability of such process to fresh water matrices from a WTP that have been chemically treated. In this case, it is necessary to consider the physicochemical properties of the water, since some of their natural characteristics may affect the photocatalytic reduction of the target compound, such as the inorganic (PO_4^{3-}, SO_4^{2-}, CO_3^{2-}/HCO_3^-, Cl^-) and organic matter (humic and fulvic acids) content [20, 42].

Several experiments with a fresh water sample (FW), physic and chemically treated in a WTP through an ozonation + flocculation + filtration process (physicochemical characteristics described in chapter 3.1.1), were conducted at pH 5.5, 6.5 and 7.5, and compared with the results for the synthetic water. Except for pH, the best operational conditions obtained for the experiments with the BrO_3^- synthetic solutions were used (15 mL of a 2% wt. TiO_2-P25 suspension deposited on the SSS, $[BrO_3^-] = 1.56$ µM, $Q = 75$ L h^{-1}, $T = 25$ ºC, UVA-LEDs 270 mW, [DO]: 232-263 µM). Figure 4.8 and Table 4.3 present the results for the SW (analysed on chapter 4.3.1) and FW experiments.

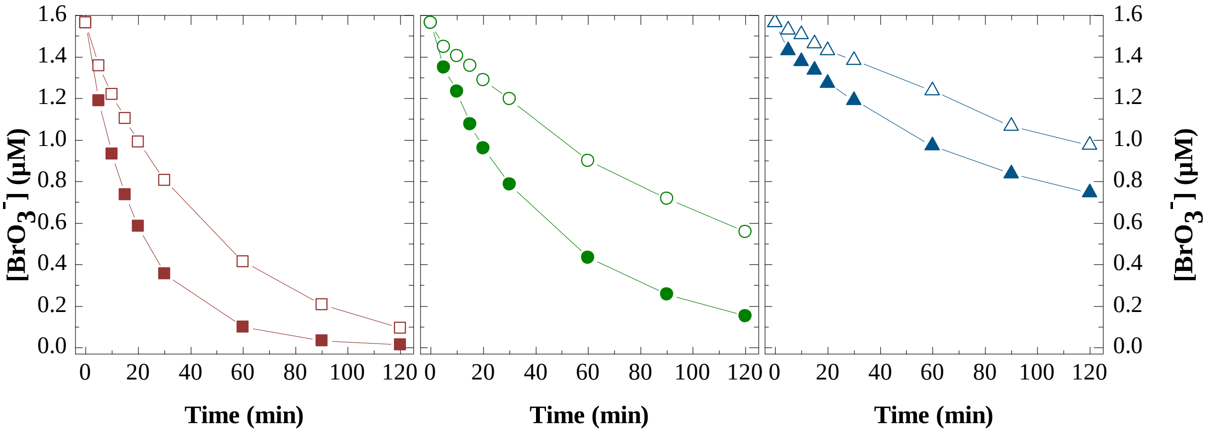

Figure 4. 8 – Influence of the fresh water matrix on the BrO_3^- reduction by TiO_2-P25 photocatalyst deposited on the SSS. Solid symbols: synthetic water. Open symbols: chemically treated fresh water. pH: 5.5 (■, □); 6.5 (●, ○); 7.5 (▲, △). Experimental conditions: $[BrO_3^-]$ = 1.56 µM, $Q = 75$ L h^{-1}, $T = 25$ ºC, UVA-LEDs 270 mW, [DO]: 232-263 µM, 15 mL of a 2% wt. TiO_2-P25 aqueous suspension.

As expected, according to the results obtained for the SW, the FW experiments at pH 5.5 (94% BrO_3^- removal) revealed a higher BrO_3^- reduction rate in a 2-hour reaction period, followed by pH 6.5 (64% BrO_3^- removal) and lastly for pH 7.5 (38% BrO_3^- removal). As shown in Table 4.3, an increment on the pH of the fresh water samples from 5.5 to 6.5 led to a 2.6-fold decrease of the reaction rate and a further increment from pH 6.5 to 7.5 resulted in a 2.2-fold decrease of the reaction rate. When compared with SW, the results for drinking water samples showed a lower BrO_3^- reduction rate for all the pH values tested, more specifically a decrease of: i) 54.5% at pH 5.5; ii) 60.4% at pH 6.5; and iii) 33.1% at pH 7.5, which suggests that the FW matrix had a negative effect on the reaction rate.

Natural organic matter (NOM), such as humic (HA) or fulvic (FA) acids, present in drinking water samples can act as a SA agent of reactive species, such as h^+ or $HO^\bullet$, avoiding the re-oxidation of Br^- into BrO_3^- and minimizing the e^-/h^+ recombination. However, NOM in the solution or adsorbed on the catalyst surface can block light, decreasing the number of photons absorbed by the photoactive sites [20, 77]. In this case, the constituents of NOM are most likely the main contributors for the observed slower reaction rates using FW when compared to synthetic water. In addition, some typical inorganic ions (PO_4^{3-}, SO_4^{2-}, CO_3^{2-}/HCO_3^-, Cl^-) that are naturally present in water can interfere with the BrO_3^- removal, blocking the catalyst surface [111]. On the other hand, these ions can act as a radical scavenger (e.g. $HO^\bullet$ scavenging by carbonate and bicarbonate ions [73]), which could improve the reaction efficiency by preventing the re-oxidation of Br^- ions.

Ji et al. [70] performed the photocatalytic oxidation of atenolol by TiO_2 aqueous suspensions and investigated the influence of natural water constituents (HCO_3^- and HAs) and river water matrix. Their studies revealed that HAs presence decreased substantially the reaction rates, especially at higher concentrations, which was possibly related with the adsorption of HAs onto the TiO_2 surface and blockage of active sites, competition for the reactive species (such as $HO^\bullet$ radicals) and light screening and inner filter effects. On the other hand, HCO_3^- was expected to have a detrimental effect on atenolol degradation since they can act as a $HO^\bullet$ scavenger, but the presence of HCO_3^- actually improved the reaction rates due to the production of $CO_3^{\bullet-}$ radicals that have a longer lifetime than $HO^\bullet$ and could diffuse into the bulk solution and react with the pollutant. These authors have also reported a decrease of the reaction rates when comparing the river water experiments with the reactions performed with UPW, which could be related with the saturation of the TiO_2 surface with ions (CO_3^{2-}, HCO_3^-, Cl^-, etc.) naturally present in the river water and that would block atenolol from adsorbing on the catalyst surface. These results demonstrated that $HO^\bullet$ radical scavenging, which in our study could have a positive effect on the reaction rates, can be masked through the saturation of the catalyst surface with other ions or with NOM. Zhang et al. [51] also investigated the influence of HA (3 mg L^{-1} and 30 mg L^{-1}) on BrO_3^- (0.1 mmol L^{-1}) reduction by TiO_2 suspensions and UV (254 nm) irradiation. They found that at lower HA concentrations, the removal of BrO_3^- was enhanced by 11%, which could be due to the scavenging of $HO^\bullet$ radicals. However, at higher HA concentrations, the reaction rate suffered a severe decrease possibly due to the saturation of the TiO_2 surface with HA, which could interfere with the adsorption of BrO_3^- on the active sites. Furthermore, high concentrations of HA can block the transference of light which could also interfere with the photon absorption by the catalyst particles and, consequently, with the generation of e^-/h^+ pairs. The HA concentration of 3 mg L^{-1} (0.25 mmol C L^{-1}) used by these authors was 2.5 times higher than the BrO_3^- amount in solution and the competition for the adsorption sites on the surface of the catalyst might be negligible. However, in the FW experiments conducted in this dissertation, the [DOC] of 3.5 mg L^{-1} (0.29 mmol C L^{-1}) was 187 times superior to the BrO_3^- concentration (1.56 μmol L^{-1}), which could generate a very high competition for the adsorption sites and decrease the reaction efficiency.

Therefore, the less efficient results obtained for the FW experiments might be related with the presence of organic matter and inorganic ions that could be interfering with the adsorption of BrO_3^- on the TiO_2 surface. The physicochemical characterization (Table 3.3) of the fresh water sample revealed a concentration of $[SO_4^{2-}]$ = 0.28 mmol L^{-1}, $[Cl^-]$ = 0.40 mmol L^{-1}, [DIC] = 1.3 mmol C L^{-1}, which are in much higher concentrations than $[BrO_3^-]_0$ = 1.56 μmol L^{-1}, and could result in an intense competition for the adsorption sites on the TiO_2 surface. Also, the organic matter content in the FW ([DOC] = 0.29 mmol C L^{-1}) was considerably high, which could be saturating the TiO_2 surface and blocking the light from reaching the catalyst particles. To better understand the influence of such parameters, some reactions with sulfate (pH 5.5; $[SO_4^{2-}]$ = 0.28 mmol L^{-1}), bicarbonate (pH 6.5 and with a concentration correspondent o the [DIC] present in the FW at pH 6.5, i.e. 0.8 mmol C L^{-1}) and humic acids (pH 5.5; [HA] = 0.29 mmol C L^{-1}) were performed (data not shown). It was verified a 50.1%, 63.8% and 48.2% decrease on the BrO_3^- reduction rate for the reactions with the addition of SO_4^{2-}, HCO_3^- and HAs, respectively. Such results revealed that at much higher concentrations than BrO_3^-, inorganic ions could be competing for the adsorption sites at the surface of the catalyst and impeding the adsorption of BrO_3^- and, consequently, decreasing the efficiency of the reaction. Likewise, the presence of HAs in high concentrations can be saturating the TiO_2 surface and block the BrO_3^- molecules from adsorbing and reacting with the reducing species, and could also be screening the incident light and reducing the amount of photons that reach the catalyst surface and photoexcite the TiO_2 particles.

These experiments showed promising results for the application of a heterogeneous photocatalytic process for BrO_3^- reduction on chemically treated fresh waters since a concentration bellow 10 μg L^{-1} was achieved under 2-hour reaction time. It is worth mention that a pH correction step would be necessary (lower pH values resulted in better reduction rates) to enhance the removal of this pollutant.

5 CONCLUSIONS

The TiO_2-driven photocatalytic reduction of BrO_3^- using the NETmix mili-photoreactor irradiated by UVA-LEDs was successfully accomplished. Preliminary results demonstrated that: i) highly acidic pH values (~3.0) had an effect on the acrylic structure of the NETmix photoreactor, resulting in its acidic hydrolysis, thus promoting indirect BrO_3^- reduction; ii) for higher pH values (~5.5), contrary to TiO_2, Fe_2O_3 did not prove to be a good photocatalyst, exhibiting very low reaction rates; and iii) high ambient temperatures affected the LEDs performance, by increasing the irradiated power, so a controlled environment was necessary to perform the experiments. TiO_2–P25 was deposited on a BS and on a SSS through spray deposition technique, thereby studying the BSI and FSI mechanisms, respectively. Moreover, the catalyst films showed good adherence and stability after at least 13 consecutive reactions.

For the BS experiments, it was concluded that: i) the BrO_3^- reaction rate increased 7.8 times with a decrease of pH from 6.5 to 5.5, since below pH_{PZC} the surface of TiO_2 is positively charged and improves the adsorption of BrO_3^-; ii) DO levels below 3.1 μM at pH 6.5 slightly improved the kinetic constant by 1.3 times, possibly due to smaller competition between O_2 and BrO_3^- molecules for e^-, but did not improve the reaction at pH 5.5; iii) the use of CH_2O_2 as a SA ($[BrO_3^-]:[CH_2O_2]$ molar ratio of 1:3) had a negative effect at pH 6.5 on BrO_3^- reduction, either in the presence or absence of high amounts of DO, decreasing the reaction rate by ca. 2.3 times, which could be related with higher competition between CHO_2^- and BrO_3^- for the adsorption sites; and iv) increasing the catalyst film thickness improves the reaction rate until the maximum value is reached, which should be around 0.74 μm (40 mg of TiO_2-P25).

On the other hand, the experiments conducted with a thin film of catalyst deposited onto the channels and chambers of the SSS, corresponding to a FSI mechanism, proved to be the best photoreactor configuration due to an increase on the catalyst surface area per reactor volume, from 333 m^2/m^3 to 989 m^2/m^3, when compared to BSI. Such as in the BS, higher reaction rates were obtained at lower pH values (pH 5.5 > pH 6.5 > pH 7.5), since above the pH_{PZC} of TiO_2-P25 the surface is negatively charged and electrostatic repulsions can occur between the catalyst surface and the BrO_3^- molecules. Purging the DO from the solution showed a negligible effect on BrO_3^- reduction, which was not in accordance with the 2-fold increase of the kinetic constant obtained in a batch photoreactor, possibly due to the numerous inlet points on the NETmix photoreactor, which might let some air into the system and preventing the DO concentration to reach values close to zero. An increase on the catalyst film thickness from 1.78 μm to 2.65 μm led to a 1.3-fold increase on the reduction rate and a further increase to 3.53 μm did not improve on the reaction rate, which is in good agreement with a FSI mechanism. Therefore, the optimal catalyst film thickness proved to be 2.65 μm (15 mL of 2% wt. TiO_2-P25 suspension). Comparing the FSI with the BSI mechanism, under the best conditions, one can conclude that the photocatalyst reactivity in combination with the photoreactor was improved 2.9 times, which is in good agreement with the 3-fold on the catalyst surface area per reactor volume. Increasing the UVA-LEDs output power slightly improved the photocatalytic reaction, but the increment on the reaction rate was much lower than the increment on the LEDs output power, which is not cost-effective. Also, temperature variation (15-30ºC) had a negligible effect on the reduction reaction rate. Under the best conditions (SSS, pH 5.5, 15 mL of a TiO_2 suspension, 25 ºC, absence of SA and [DO] = 232 – 263 µM), the fresh water matrix affected negatively the reaction when compared with the results obtained for the synthetic one. The presence of both inorganic and organic matter in FW, such as SO_4^{2-}, HCO_3^- and HAs, at much higher concentrations than BrO_3^-, can have a detrimental effect on the reaction efficiency since they can compete for the active sites on the catalyst surface and the presence of HAs can also block the incident radiation, thus reducing the photogenerated e^-/h^+ pairs.

Under the best conditions, promising results were obtained for the application of a heterogeneous TiO_2 photocatalytic process to a chemically treated fresh water from a WTP, since a concentration bellow 10 µg L^{-1} (guideline value) was achieved under 2-hour reaction time. Nevertheless, a pH correction step may be also needed to enhance the BrO_3^- reduction rates.

6 LIMITATIONS AND FUTURE WORK

In order to validate the hypothesis of acidic hydrolysis of the acrylic polymer (i.e. PMMA) used in the NETmix manufacturing, additional experiments at different pH values should be performed using a solution of pristine PMMA in a chemically inactive reactor.

Since the addition of a [BrO_3^-]:[CH_2O_2] molar ratio of 1:3 did not improve the reaction rate, lower ratios could be tested to assess if the competition between BrO_3^- and CH_2O_2 was less significant at those ratios. A higher concentration of CH_2O_2 could also be tested to understand the behavior of the reaction rate at higher [BrO_3^-]:[CH_2O_2] molar ratios. Moreover, different SAs, like methanol, ethanol, citric acid, tartaric acid or oxalic acid, could also be tested to increase our knowledge about the influence of other compounds in the reduction of BrO_3^-.

The morphological properties of the TiO_2-P25 thin films is also an important parameter to evaluate. So, in order to assess the homogeneity (distribution of the particles), actual film thickness, and particles shape and size, scanning electron microscopy (SEM) should be performed. To better understand the influence of the FW matrix on the TiO_2 films surface and complement the SEM analysis, additional studies based on energy dispersive X-ray spectroscopy (EDX), X-ray photoelectron spectroscopy (XPS) and Fourier Transform infrared spectroscopy (FTIR) could also be carried out.

Finally, since inorganic ions are naturally present in fresh waters and sulfate and bicarbonates proved to have a negative influence on the BrO_3^- photocatalytic reduction, some experiments with other inorganic ions (e.g. NO_3^-, Cl^-, PO_4^{3-}) should also be performed. The effect of other types of NOM, like fulvic acids, could also be assessed.

7 REFERENCES

[1] United Nations, Transforming our world: The 2030 Agenda for Sustainable Development, 2015, pp. 35.

[2] WWAP (United Nations World Water Assessment Programme), The United Nations World Water Development Report 2017. Wastewater: The Untapped Resource., UNESCO, Paris, 2017.

[3] UN-Water, Towards a Worldwide Assessment of Freshwater Quality: A UN-Water Analytical Brief, Switzerland, 2016.

[4] J.C. Cardoso, G.G. Bessegato, M.V. Boldrin Zanoni, Efficiency comparison of ozonation, photolysis, photocatalysis and photoelectrocatalysis methods in real textile wastewater decolorization, Water Research, 98 (2016) 39-46.

[5] A.R. Ribeiro, O.C. Nunes, M.F.R. Pereira, A.M.T. Silva, An overview on the advanced oxidation processes applied for the treatment of water pollutants defined in the recently launched Directive 2013/39/EU, Environment International, 75 (2015) 33-51.

[6] J.R. Bolton, K.G. Bircher, W. Tumas, C.A. Tolman, Figures-of-merit for the technical development and application of advanced oxidation technologies for both electric- and solar-driven systems (IUPAC Technical Report), Pure and Applied Chemistry, 73 (2001) 627.

[7] X. Yu, D. Cabooter, R. Dewil, Effects of process variables and kinetics on the degradation of 2,4-dichlorophenol using advanced reduction processes (ARP), Journal of Hazardous Materials, 357 (2018) 81-88.

[8] R. Butler, A. Godley, L. Lytton, E. Cartmell, Bromate Environmental Contamination: Review of Impact and Possible Treatment, Critical Reviews in Environmental Science and Technology, 35 (2005) 193-217.

[9] U. von Gunten, Y. Oliveras, Advanced Oxidation of Bromide-Containing Waters: Bromate Formation Mechanisms, Environmental Science & Technology, 32 (1998) 63-70.

[10] F. Soltermann, C. Abegglen, M. Tschui, S. Stahel, U. von Gunten, Options and limitations for bromate control during ozonation of wastewater, Water Research, 116 (2017) 76-85.

[11] World Health Organization, Guidelines for drinking-water quality: 4th edition, incorporating the 1st addendum, Geneva, 2017, pp. 631.

[12] World Health Organization, Bromate in Drinking-water, Background document for development of WHO Guidelines for Drinking-water Quality, World Health Organization, Geneva, 2005.

[13] International Union of Pure and Applied Chemistry, Alkali Metal Halates, Ammonium Iodate and Iodic Acid, in: H.S. Miyamoto, M. (Ed.) IUPAC Solubility Data Series, Pergamon Press, 1987.

[14] A. Mills, A. Belghazi, D. Rodman, Bromate removal from drinking water by semiconductor photocatalysis, Water Research, 30 (1996) 1973-1978.

[15] International Agency for Research on Cancer, Some Chemicals that Cause Tumours of the Kidney or Urinary Bladder in Rodents and Some Other Substances, IARC Monographs on the Evaluation of Carcinogenic Risks to Humans, International Agency for Research on Cancer, Lyon, France, 1999.

[16] Environmental Protection Agency, Federal Register Volume 71, Issue 2 (January 4, 2006), Office of the Federal Register, National Archives and Records Administration, Washington, D.C., 2006, pp. 387-493.

[17] Council of the European Union, Council Directive 98/83/EC of 3 November 1998 on the quality of water intended for human consumption, in: Official Journal of the European Communities (Ed.)Brussels, 1998, pp. 32 - 54.

[18] United States Environmental Protection Agency, Information on the Integrated Risk Information System (IRIS) Chemical Assessment Summary: Bromate; CASRN 15541-45-4, United States Environmental Protection Agency, 2001, pp. 27.

[19] G. Wen, C. Qiang, Y. Feng, T. Huang, J. Ma, Bromate formation during the oxidation of bromide-containing water by ozone/peroxymonosulfate process: Influencing factors and mechanisms, Chemical Engineering Journal, 352 (2018) 316-324.

[20] Q. Xiao, S. Yu, L. Li, T. Wang, X. Liao, Y. Ye, An overview of advanced reduction processes for bromate removal from drinking water: Reducing agents, activation methods, applications and mechanisms, Journal of Hazardous Materials, 324 (2017) 230-240.

[21] F. Ali, J.A. Khan, N.S. Shah, M. Sayed, H.M. Khan, Carbamazepine degradation by UV and UV-assisted AOPs: Kinetics, mechanism and toxicity investigations, Process Safety and Environmental Protection, 117 (2018) 307-314.

[22] Y. Deng, R. Zhao, Advanced Oxidation Processes (AOPs) in Wastewater Treatment, Current Pollution Reports, 1 (2015) 167-176.

[23] D.A. Armstrong, R.E. Huie, W.H. Koppenol, S.V. Lymar, G. Merényi, P. Neta, B. Ruscic, D.M. Stanbury, S. Steenken, P. Wardman, Standard electrode potentials involving radicals in aqueous solution: inorganic radicals (IUPAC Technical Report), Pure and Applied Chemistry, 87 (2015) 1139.

[24] J. Hoigné, Inter-calibration of OH radical sources and water quality parameters, Water Science and Technology, 35 (1997) 1-8.

[25] F.C. Moreira, R.A.R. Boaventura, E. Brillas, V.J.P. Vilar, Electrochemical advanced oxidation processes: A review on their application to synthetic and real wastewaters, Applied Catalysis B: Environmental, 202 (2017) 217-261.

[26] M. Trojanowicz, A. Bojanowska-Czajka, I. Bartosiewicz, K. Kulisa, Advanced Oxidation/Reduction Processes treatment for aqueous perfluorooctanoate (PFOA) and perfluorooctanesulfonate (PFOS) – A review of recent advances, Chemical Engineering Journal, 336 (2018) 170-199.

[27] B.P. Vellanki, B. Batchelor, A. Abdel-Wahab, Advanced Reduction Processes: A New Class of Treatment Processes, Environmental Engineering Science, 30 (2013) 264-271.

[28] X. Liu, T. Zhang, Y. Shao, Aqueous Bromate Reduction by UV Activation of Sulfite, CLEAN – Soil, Air, Water, 42 (2014) 1370-1375.

[29] B. Jung, R. Nicola, B. Batchelor, A. Abdel-Wahab, Effect of low- and medium-pressure Hg UV irradiation on bromate removal in advanced reduction process, Chemosphere, 117 (2014) 663-672.

[30] V.S.V. Botlaguduru, B. Batchelor, A. Abdel-Wahab, Application of UV–sulfite advanced reduction process to bromate removal, Journal of Water Process Engineering, 5 (2015) 76-82.

[31] A.N. Soon, B.H. Hameed, Heterogeneous catalytic treatment of synthetic dyes in aqueous media using Fenton and photo-assisted Fenton process, Desalination, 269 (2011) 1-16.

[32] M.E. Simonsen, Chapter 4 - Heterogeneous Photocatalysis, in: E.G. Søgaard (Ed.) Chemistry of Advanced Environmental Purification Processes of Water, Elsevier, Amsterdam, 2014, pp. 135-170.

[33] J.-M. Herrmann, Heterogeneous photocatalysis: fundamentals and applications to the removal of various types of aqueous pollutants, Catalysis Today, 53 (1999) 115-129.

[34] T. Van Gerven, G. Mul, J. Moulijn, A. Stankiewicz, A review of intensification of photocatalytic processes, Chemical Engineering and Processing: Process Intensification, 46 (2007) 781-789.

[35] R. Ameta, M.S. Solanki, S. Benjamin, S.C. Ameta, Chapter 6 - Photocatalysis, in: S.C. Ameta, R. Ameta (Eds.) Advanced Oxidation Processes for Waste Water Treatment, Academic Press2018, pp. 135-175.

[36] O. Carp, C.L. Huisman, A. Reller, Photoinduced reactivity of titanium dioxide, Progress in Solid State Chemistry, 32 (2004) 33-177.

[37] G.G. Bessegato, T.T. Guaraldo, J.F. Brito, M.F. Brugnera, M.V.B. Zanoni, Achievements and Trends in Photoelectrocatalysis: from Environmental to Energy Applications, Electrocatalysis, 6 (2015) 415–441.

[38] M.I. Litter, N. Quicia, J.M. Meichtrya, A. M. Senna, Photocatalysis: Applications, in: D.D. Dionysiou, G.L. Puma, J. Ye, J. Schneider, D. Bahnemann (Eds.), The Royal Society of Chemistry, Cambridge, United Kingdom, 2016, pp. P001-380.

[39] A. Mills, S. Le Hunte, An overview of semiconductor photocatalysis, Journal of Photochemistry and Photobiology A: Chemistry, 108 (1997) 1-35.

[40] P. Vanýsek, Electrochemical series, in: W. M. Haynes (Ed.) Handbook of Chemistry and Physics, CRC Press, Boca Raton, FL, 2012.

[41] R. Daghrir, P. Drogui, D. Robert, Photoelectrocatalytic technologies for environmental applications, Journal of Photochemistry and Photobiology A: Chemistry, 238 (2012) 41-52.

[42] M.N. Chong, B. Jin, C.W.K. Chow, C. Saint, Recent developments in photocatalytic water treatment technology: A review, Water Research, 44 (2010) 2997-3027.

[43] M. Mishra, D.-M. Chun, α-Fe2O3 as a photocatalytic material: A review, Applied Catalysis A: General, 498 (2015) 126-141.

[44] P. Xu, G.M. Zeng, D.L. Huang, C.L. Feng, S. Hu, M.H. Zhao, C. Lai, Z. Wei, C. Huang, G.X. Xie, Z.F. Liu, Use of iron oxide nanomaterials in wastewater treatment: A review, Science of The Total Environment, 424 (2012) 1-10.

[45] K. Sivula, F. Le Formal, M. Grätzel, Solar water splitting: Progress using hematite (α-Fe 2O3) photoelectrodes, ChemSusChem, 4 (2011) 432-449.

[46] O. Akhavan, R. Azimirad, Photocatalytic property of Fe2O3 nanograin chains coated by TiO2 nanolayer in visible light irradiation, Applied Catalysis A: General, 369 (2009) 77-82.

[47] L. Andronic, D. Perniu, A. Duta, Synergistic effect between TiO2 sol–gel and Degussa P25 in dye photodegradation, 2013.

[48] T. Ohno, K. Sarukawa, K. Tokieda, M. Matsumura, Morphology of a TiO2 Photocatalyst (Degussa, P-25) Consisting of Anatase and Rutile Crystalline Phases, Journal of Catalysis, 203 (2001) 82-86.

[49] J.M. Herrmann, Heterogeneous photocatalysis: state of the art and present applications In honor of Pr. R.L. Burwell Jr. (1912–2003), Former Head of Ipatieff Laboratories, Northwestern University, Evanston (Ill), Topics in Catalysis, 34 (2005) 49-65.

[50] K.-Y.A. Lin, C.-H. Lin, S.-Y. Chen, H. Yang, Enhanced photocatalytic reduction of concentrated bromate in the presence of alcohols, Chemical Engineering Journal, 303 (2016) 596-603.

[51] X. Zhang, T. Zhang, J. Ng, J.H. Pan, D.D. Sun, Transformation of Bromine Species in TiO2 Photocatalytic System, Environmental Science & Technology, 44 (2010) 439-444.

[52] H. Noguchi, A. Nakajima, T. Watanabe, K. Hashimoto, Design of a Photocatalyst for Bromate Decomposition: Surface Modification of TiO2 by Pseudo-boehmite, Environmental Science & Technology, 37 (2003) 153-157.

[53] X. Huang, L. Wang, J. Zhou, N. Gao, Photocatalytic decomposition of bromate ion by the UV/P25-Graphene processes, Water Research, 57 (2014) 1-7.

[54] H. Noguchi, A. Nakajima, T. Watanabe, K. Hashimoto, Removal of bromate ion from water using TiO2 and alumina-loaded TiO2 photocatalysts, Water Science and Technology, 46 (2002) 27-31.

[55] S.-S. Hong, M.-S. Lee, J.-H. Kim, B.-H. Ahn, K.-T. Lim, G.-D. Lee, Photocatalytic Decomposition of Bromate over Titanium Dioxides Prepared Using Sol-Gel Method, Journal of Industrial and Engineering Chemistry, 8 (2002) 150-155.

[56] R. Marks, T. Yang, P. Westerhoff, K. Doudrick, Comparative analysis of the photocatalytic reduction of drinking water oxoanions using titanium dioxide, Water Research, 104 (2016) 11-19.

[57] Y.-H. Chen, K.-J. Tu, Thickness Dependent on Photocatalytic Activity of Hematite Thin Films, International Journal of Photoenergy, (2012).

[58] B.A. Marinho, R.O. Cristóvão, R. Djellabi, J.M. Loureiro, R.A.R. Boaventura, V.J.P. Vilar, Photocatalytic reduction of Cr(VI) over TiO2-coated cellulose acetate monolithic structures using solar light, Applied Catalysis B: Environmental, 203 (2017) 18-30.

[59] D. Chen, F. Li, A.K. Ray, External and internal mass transfer effect on photocatalytic degradation, Catalysis Today, 66 (2001) 475-485.

[60] C.-Y. Wu, Y.-L. Lee, Y.-S. Lo, C.-J. Lin, C.-H. Wu, Thickness-dependent photocatalytic performance of nanocrystalline TiO2 thin films prepared by sol–gel spin coating, Applied Surface Science, 280 (2013) 737-744.

[61] Y. Zhang, S. Jing, H. Liu, Reactivity and mechanism of bromate reduction from aqueous solution using Zn–Fe(II)–Al layered double hydroxides, Chemical Engineering Journal, 266 (2015) 21-27.

[62] Y. Zhang, X. Xiong, Y. Han, X. Zhang, F. Shen, S. Deng, H. Xiao, X. Yang, G. Yang, H. Peng, Photoelectrocatalytic degradation of recalcitrant organic pollutants using TiO2 film electrodes: An overview, Chemosphere, 88 (2012) 145-154.

[63] N. Wang, X. Li, Y. Wang, X. Quan, G. Chen, Evaluation of bias potential enhanced photocatalytic degradation of 4-chlorophenol with TiO2 nanotube fabricated by anodic oxidation method, Chemical Engineering Journal, 146 (2009) 30-35.

[64] S. Malato, P. Fernández-Ibáñez, M.I. Maldonado, J. Blanco, W. Gernjak, Decontamination and disinfection of water by solar photocatalysis: Recent overview and trends, Catalysis Today, 147 (2009) 1-59.

[65] A.-G. Rincón, C. Pulgarin, Effect of pH, inorganic ions, organic matter and H2O2 on E. coli K12 photocatalytic inactivation by TiO2: Implications in solar water disinfection, Applied Catalysis B: Environmental, 51 (2004) 283-302.

[66] C. Kormann, D.W. Bahnemann, M.R. Hoffmann, Photolysis of chloroform and other organic molecules in aqueous titanium dioxide suspensions, Environmental Science & Technology, 25 (1991) 494-500.

[67] D. Chen, A.K. Ray, Photodegradation kinetics of 4-nitrophenol in TiO2 suspension, Water Research, 32 (1998) 3223-3234.

[68] U.I. Gaya, A.H. Abdullah, Heterogeneous photocatalytic degradation of organic contaminants over titanium dioxide: A review of fundamentals, progress and problems, Journal of Photochemistry and Photobiology C: Photochemistry Reviews, 9 (2008) 1-12.

[69] Y. Wang, C.-s. Hong, Effect of hydrogen peroxide, periodate and persulfate on photocatalysis of 2-chlorobiphenyl in aqueous TiO2 suspensions, Water Research, 33 (1999) 2031-2036.

[70] Y. Ji, L. Zhou, C. Ferronato, X. Yang, A. Salvador, C. Zeng, J.-M. Chovelon, Photocatalytic degradation of atenolol in aqueous titanium dioxide suspensions: Kinetics, intermediates and degradation pathways, Journal of Photochemistry and Photobiology A: Chemistry, 254 (2013) 35-44.

[71] T. Tang, G. Lu, W. Wang, R. Wang, K. Huang, Z. Qiu, X. Tao, Z. Dang, Photocatalytic removal of organic phosphate esters by TiO2: Effect of inorganic ions and humic acid, Chemosphere, 206 (2018) 26-32.

[72] O. Ken-ichi, Y. Yasunori, T. Hiroki, T. Masashi, I. Akira, Heterogeneous Photocatalytic Decomposition of Phenol over TiO2 Powder, Bulletin of the Chemical Society of Japan, 58 (1985) 2015-2022.

[73] C. Guillard, H. Lachheb, A. Houas, M. Ksibi, E. Elaloui, J.-M. Herrmann, Influence of chemical structure of dyes, of pH and of inorganic salts on their photocatalytic degradation by TiO2 comparison of the efficiency of powder and supported TiO2, Journal of Photochemistry and Photobiology A: Chemistry, 158 (2003) 27-36.

[74] Z. Zhang, Y. Luo, Y. Guo, W. Shi, W. Wang, B. Zhang, R. Zhang, X. Bao, S. Wu, F. Cui, Pd and Pt nanoparticles supported on the mesoporous silica molecular sieve SBA-15 with enhanced activity and stability in catalytic bromate reduction, Chemical Engineering Journal, 344 (2018) 114-123.

[75] M. Sillanpää, M.C. Ncibi, A. Matilainen, Advanced oxidation processes for the removal of natural organic matter from drinking water sources: A comprehensive review, J. Environ. Manage., 208 (2018) 56-76.

[76] H. Särkkä, M. Vepsäläinen, M. Sillanpää, Natural organic matter (NOM) removal by electrochemical methods — A review, Journal of Electroanalytical Chemistry, 755 (2015) 100-108.

[77] J. Wenk, U. von Gunten, S. Canonica, Effect of Dissolved Organic Matter on the Transformation of Contaminants Induced by Excited Triplet States and the Hydroxyl Radical, Environmental Science & Technology, 45 (2011) 1334-1340.

[78] F.L. Rosario-Ortiz, S.P. Mezyk, D.F.R. Doud, S.A. Snyder, Quantitative Correlation of Absolute Hydroxyl Radical Rate Constants with Non-Isolated Effluent Organic Matter Bulk Properties in Water, Environmental Science & Technology, 42 (2008) 5924-5930.

[79] R. Lakerveld, G.S.J. Sturm, A.I. Stankiewicz, G.D. Stefanidis, Integrated design of microwave and photocatalytic reactors. Where are we now?, Current Opinion in Chemical Engineering, 5 (2014) 37-41.

[80] M.E. Leblebici, G.D. Stefanidis, T. Van Gerven, Comparison of photocatalytic space-time yields of 12 reactor designs for wastewater treatment, Chemical Engineering and Processing: Process Intensification, 97 (2015) 106-111.

[81] M. Motegh, J. Cen, P.W. Appel, J.R. van Ommen, M.T. Kreutzer, Photocatalytic-reactor efficiencies and simplified expressions to assess their relevance in kinetic experiments, Chemical Engineering Journal, 207-208 (2012) 607-615.

[82] E.E. Coyle, M. Oelgemoller, Micro-photochemistry: photochemistry in microstructured reactors. The new photochemistry of the future?, Photochem Photobiol Sci, 7 (2008) 1313-1322.

[83] N. Padoin, L. Andrade, J. Ângelo, A. Mendes, R.d.F.P.M. Moreira, C. Soares, Intensification of photocatalytic pollutant abatement in microchannel reactor using TiO2 and TiO2-graphene, AIChE J., 62 (2016) 2794-2802.

[84] A.K. Ray, A.A.C.M. Beenackers, Novel photocatalytic reactor for water purification, AIChE J., 44 (1998) 477-483.

[85] R. Gorges, S. Meyer, G. Kreisel, Photocatalysis in microreactors, Journal of Photochemistry and Photobiology A: Chemistry, 167 (2004) 95-99.

[86] Y. Matsushita, N. Ohba, S. Kumada, K. Sakeda, T. Suzuki, T. Ichimura, Photocatalytic reactions in microreactors, Chemical Engineering Journal, 135 (2008) S303-S308.

[87] M.N. Kashid, A. Gupta, A. Renken, L. Kiwi-Minsker, Numbering-up and mass transfer studies of liquid–liquid two-phase microstructured reactors, Chemical Engineering Journal, 158 (2010) 233-240.

[88] A. Ghanem, T. Lemenand, D. Della Valle, H. Peerhossaini, Static mixers: Mechanisms, applications, and characterization methods – A review, Chemical Engineering Research and Design, 92 (2014) 205-228.

[89] P.E. Laranjeira, A.A. Martins, J.C.B. Lopes, M.M. Dias, NETmix®, a new type of static mixer: Modeling, simulation, macromixing, and micromixing characterization, AIChE J., 55 (2009) 2226-2243.

[90] P.E. Laranjeira, A.A. Martins, M.I. Nunes, J.C.B. Lopes, M.M. Dias, NETmix®, a new type of static mixer: Experimental characterization and model validation, AIChE J., 57 (2011) 1020-1032.

[91] M.F. Costa, C.M. Fonte, M.M. Dias, J.C.B. Lopes, Heat transfer performance of NETmix—A novel micro-meso structured mixer and reactor, AIChE J., 63 (2017) 2496-2508.

[92] B.A. Marinho, R.O. Cristóvão, R. Djellabi, A. Caseiro, S.M. Miranda, J.M. Loureiro, R.A.R. Boaventura, M.M. Dias, J.C.B. Lopes, V.J.P. Vilar, Strategies to reduce mass and photons transfer limitations in heterogeneous photocatalytic processes: Hexavalent chromium reduction studies, J. Environ. Manage., 217 (2018) 555-564.

[93] A.D. Eaton, L.S. Clesceri, A.E. Greenberg, M.A.H. Franson, Standard methods for examination of water and waste water., American Public Health Association, Washington, DC, 1998.

[94] International Organization for Standardization, ISO 6332: Water Quality – Determination of Iron – Spectrometric Method Using 1,10-Phenanthroline, International Organization for Standardization,, Geneva, Switzerland, 1998.

[95] B.A. Marinho, R. Djellabi, R.O. Cristóvão, J.M. Loureiro, R.A.R. Boaventura, M.M. Dias, J.C.B. Lopes, V.J.P. Vilar, Intensification of heterogeneous TiO2 photocatalysis using an innovative micro–meso-structured-reactor for Cr(VI) reduction under simulated solar light, Chemical Engineering Journal, 318 (2017) 76-88.

[96] K.-Y.A. Lin, C.-H. Lin, H. Yang, Enhanced bromate reduction using zero-valent aluminum mediated by oxalic acid, Journal of Environmental Chemical Engineering, 5 (2017) 5085-5090.

[97] W.N. Ayre, S.P. Denyer, S.L. Evans, Ageing and moisture uptake in polymethyl methacrylate (PMMA) bone cements, Journal of the Mechanical Behavior of Biomedical Materials, 32 (2014) 76-88.

[98] H.G. Roth, N.A. Romero, D.A. Nicewicz, Experimental and Calculated Electrochemical Potentials of Common Organic Molecules for Applications to Single-Electron Redox Chemistry, Synlett, 27 (2016) 714-723.

[99] T. Tan, D. Beydoun, R. Amal, Effect of organic hole scavengers on the photocatalytic reduction of selenium ions, 2003.

[100] D. Annaratone, Engineering Heat Transfer, Springer, Milano, Italy, 2010.

[101] M. Kosmulski, The pH dependent surface charging and points of zero charge. VII. Update, Advances in Colloid and Interface Science, 251 (2018) 115-138.

[102] K. Doudrick, O. Monzón, A. Mangonon, K. Hristovski, P. Westerhoff, Nitrate Reduction in Water Using Commercial Titanium Dioxide Photocatalysts (P25, P90, and Hombikat UV100), Journal of Environmental Engineering, 138 (2012) 852-861.

[103] L. Xie, C. Shang, The effects of operational parameters and common anions on the reactivity of zero-valent iron in bromate reduction, Chemosphere, 66 (2007) 1652-1659.

[104] X. Wang, S.O. Pehkonen, A.K. Ray, Removal of Aqueous Cr(VI) by a Combination of Photocatalytic Reduction and Coprecipitation, Industrial & Engineering Chemistry Research, 43 (2004) 1665-1672.

[105] L.B. Khalil, W.E. Mourad, M.W. Rophael, Photocatalytic reduction of environmental pollutant Cr(VI) over some semiconductors under UV/visible light illumination, Applied Catalysis B: Environmental, 17 (1998) 267-273.

[106] A. Samad, S. Ahsan, I. Tateishi, M. Furukawa, H. Katsumata, T. Suzuki, S. Kaneco, Indirect photocatalytic reduction of arsenate to arsenite in aqueous solution with TiO2 in the presence of hole scavengers, Chinese Journal of Chemical Engineering, 26 (2018) 529-533.

[107] A. Hérissan, J.M. Meichtry, H. Remita, C. Colbeau-Justin, M.I. Litter, Reduction of nitrate by heterogeneous photocatalysis over pure and radiolytically modified TiO2 samples in the presence of formic acid, Catalysis Today, 281 (2017) 101-108.

[108] F. Mahlamvana, R.J. Kriek, Photocatalytic reduction of [RhCln(H2O)6−n]3−n (n=0–6) in a titanium dioxide suspension: The role of structurally different sacrificial reducing agents, Applied Catalysis B: Environmental, 162 (2015) 445-453.

[109] N. Venkatachalam, M. Palanichamy, B. Arabindoo, V. Murugesan, Enhanced photocatalytic degradation of 4-chlorophenol by Zr4+ doped nano TiO2, Journal of Molecular Catalysis A: Chemical, 266 (2007) 158-165.

[110] E. Evgenidou, K. Fytianos, I. Poulios, Semiconductor-sensitized photodegradation of dichlorvos in water using TiO2 and ZnO as catalysts, Applied Catalysis B: Environmental, 59 (2005) 81-89.

[111] W.-f. Chen, Z.-Y. Zhang, Q. Li, H.-Y. Wang, Adsorption of bromate and competition from oxyanions on cationic surfactant-modified granular activated carbon (GAC), Chemical Engineering Journal, 203 (2012) 319-325.